Properties of the many-nucleon system in the unitary-model-operator approach

(   )

28   12

Abstract

One of the fundamental problems in nuclear physics is to understand the nuclear structure and reactions based on the nuclear interactions. Such attempt has been advanced owing to the developments in the computational techniques, understanding of nuclear interactions, and nuclear many-body methods. In this thesis, our main focus is to solve the many-body Schrödinger equation with the unitary-model-operator approach (UMOA) and to discuss the ground-state properties from the nucleon-nucleon (NN) interactions.

By using the UMOA, we calculate ground-state energies and charge radii for the doubly magic nuclei, ^{4}He, ^{16}O, ^{40}Ca, and ^{56}Ni with the CD-Bonn potential. Then, there is the difficulty that our final results depend on the $\hbar\omega$, which is the parameter used to span our model space. Since the initial Hamiltonian does not include $\hbar\omega$, calculated observables should not depend on $\hbar\omega$. To investigate and reduce the $\hbar\omega$-dependence in the UMOA results, we introduce the one-body correlation operator to the UMOA for the first time. Using the softened NN interactions, we examine the applicability of the new UMOA framework through calculations for ^{4}He and oxygen isotopes and comparison with the results in the other *ab initio* calculations.

We calculate ground-state energies and radii of the shell closed nuclei from ^{4}He to ^{218}Pb in the new UMOA framework. As shown in the recent *ab initio* calculations, our ground-state energies become larger and our radii become smaller than the experimental data as the mass number increases. Looking closely at the calculation results, however, we find that the observables coming from the proton-neutron asymmetry could be independent of resolution scale of NN interactions. At least, this is confirmed in the asymmetry term of liquid drop model and neutron skin thickness. Interestingly, our neutron skin thickness results are consistent with the experimental trend and recent CCM result.

As reported in the recent theoretical works, it is needed to introduce the three-nucleon interaction to the UMOA. For this reason, finally, we demonstrate the extension of the UMOA framework and calculate the ground-state energies of ^{4}He. The UMOA results show the good agreement with the result in the other *ab initio* calculation.

Table of Contents

Chapter 1

Introduction

Nuclear physics is the field of physics to study properties of the quantum many-body system associated with constituent particles interacting through the strong force. Since the discovery of the radioactivity in the end of 1800's, studies in nuclear physics have been done mainly by the investigation of the stable nuclei whose life time is quite long. From such research, the cornerstones such as the saturation property of nuclei and magic number have been established. Owing to the recent progress in experimental techniques and facilities such as RIBF at RIKEN, a new era of nuclear physics has begun. By the observations of rare isotopes which do not exist in nature, new phenomena have been revealed, for instance, the halo structure in the loosely bound system [1] and shell evolution [2]. These developments will be important in the study for astrophysical issues such as the nucleosynthesis, supernova explosions, and neutron stars. In such a situation, the progress in the theoretical approaches is required, which hold the predictive power. For this purpose, one can begin with the fundamental theory of the strong interaction, which is known as the quantum chromodynamics (QCD) described in terms of quarks and gluons. Due to the non-perturbative property of the QCD at the low-energy regime, one has to employ the numerical methods such as the lattice QCD (LQCD) to investigate the low-energy nuclear structure. However, it has not been possible to understand the low-energy nuclear structure directly from the LQCD yet, because of computational limitations. In order to investigate properties of finite nuclei, so far, we have to reduce the degree of freedom from quarks to protons and neutrons, so called the nucleon.

There are two major obstacles when one investigates a nucleus starting from nucleons degrees of freedom. First, the nuclear interactions acting among nucleons have to be determined. Second, we have to solve the quantum many-body problem associated with the nuclear interactions.

1.1   Nuclear Interaction

The study for the nuclear interaction has a long history. The mechanism of the nuclear interaction was firstly proposed by Yukawa [3]. He discussed the nucleon-nucleon (NN) interaction as the exchange of the massive particle which was discovered in 1947 and is well known as the pion in the present day. After the discovery of the pion, the long-range part ($r \gtrsim 2$ fm; r is the distance between two

nucleons) of the nuclear interaction became well established from the *NN* scattering of high angular-momentum states [4,5] and from the deuteron properties [6]. As the next step, the two-pion exchange was considered in 1950's. However, none could not reproduce well the experimental data by the one- and two-pion exchange interaction. With the discovery of the heavy mesons in 1960's, the one-boson-exchange model was developed [7] and the situation was changed better. In addition, a lot of efforts have been made for the construction of the nuclear interactions.

Nowadays, the sophisticated *NN* interactions, such as Argonne v18 (AV18) [8] and charge-dependent Bonn (CD-Bonn) [9] interactions, have been developed and can reproduce well the *NN* scattering data and deuteron properties. Due to the contributions of the scalar, pseud-scalar, vector, and axial-vector mesons, the *NN* interactions can have very complicated structure. Namely, realistic *NN* interactions strongly depend on the quantum state of *NN* system such as the spin, the isospin, the orbital angular momentum, and the total angular momentum. This complexity of the underlying interaction is one of the features in nuclear physics. Besides modern phenomenological interactions, nuclear interactions can be derived based on the chiral effective field theory (EFT) [10, 11]. In the chiral EFT framework, nuclear interactions can be obtained by the perturbative expansion of the effective Lagrangian. Moreover, many-body interactions can be derived systematically and can hold the hierarchy because of the power counting. This is one of the advantages in the interactions based on the chiral EFT. As shown in the recent studies [12, 13], the importance of the three-nucleon (3*N*) interaction has been recognized. For this reason, the nuclear interactions based on the chiral EFT have been employed in the recent *ab initio* calculations. The current standard choice is to keep *NN* interaction at next-to-next-to-next-to leading order (N^{3}LO) and 3*N* interaction at N^{2}LO.

As discussed in Sec. 2.1, it is known that the realistic *NN* interactions show the strong repulsion at short distance. This means the strong coupling between low- and high-momentum regions. Due to the strong repulsion, the difficulties arise, for example, breaking down of the perturbation expansion and slow convergence in numerical calculations. To tame the strong short-range correlations, the *G*-matrix theory was introduced by Brückner and his collaborators [14]. The *G*-matrix is the two-body interaction constructed by summing up the ladder diagrams passing through the high-momentum intermediate states. The overview of the *G*-matrix theory can be found, for example, in Ref. [15]. Strictly speaking, the *G*-matrix cannot be categorized as the effective interaction. As demonstrated in Ref. [16], the *G*-matrix does not ensure the decoupling between the low- and high-momentum regions.

Recently, the new prescription has been invented based on renormalization group techniques. In these frameworks, it is ensured to suppress the coupling between low- and high-momentum regions. As a result, the acceleration of the convergence in numerical calculations is observed (see Sec. 2.2 for details) and softened interactions are applicable to the heavy nuclei.

1.2 *Ab Initio* **Calculations**

Our main problem is to solve the many-body Schrödinger equation:

$$H|\Psi_k\rangle = E_k|\Psi_k\rangle, \tag{1.1}$$

with the Hamiltonian H, and the kth eigenstate $|\Psi_k\rangle$ and eigenvalue E_k. Since the energy scale of a nucleus is of the order of MeV and is much smaller than the nucleon mass ~ 1 GeV, the nuclear structure is usually discussed in the non-relativistic quantum mechanics. The non-relativistic Hamiltonian H is

$$H = \sum_{i<j}^{A} \frac{(\mathbf{p}_i - \mathbf{p}_j)^2}{2Am} + \sum_{i<j}^{A} V_{ij}^{NN} + \sum_{i<j<k}^{A} V_{ijk}^{NNN} + \cdots, \tag{1.2}$$

with the mass number A, the momentum of the ith nucleon $\mathbf{p}_i$, the nucleon mass m, the NN interaction V_{ij}^{NN}, the $3N$ interaction V_{ijk}^{NNN}, and so on.

To solve Eq. (1.1) based on the underlying interactions, one can choose the calculation methods according to mass region. For $A = 3$ or 4, one can apply the few-body methods such as the Faddeev equation [17] and Faddeev-Yakubovsky equation [18]. For the system with the $A \lesssim 20$, one can employ the no-core shell model (NCSM) [19], Green's function Monte Carlo [20], and nuclear lattice effective field theory [21]. As a very recent progress, the reaction processes which are important for the nucleosynthesis have also been studied in the NCSM framework [22].

For the system with $A \gtrsim 20$, one cannot exactly solve Eq. (1.1) due to current computational limitations. To investigate the heavier system, some approximations are inevitable. From the experimental evidence, the introduction of the mean field should be reasonable. Actually, the phenomenological Woods-Saxon potential is successful for the stable nuclei. To find the mean field consistent with the underlying interactions, one can employ the Hartree-Fock (HF) method. In Table 1.1, the HF ground-state energies calculated with the chiral NN interaction at N³LO [10] are exhibited. Although the HF method works well in the many-electron system, one can find that the HF method in the many-nucleon system clearly fails to reproduce even the ground-state energies. To gain the ground-state energy, one should take into account the many-body correlation which is not included in the HF method. For this purpose, one can employ, for example, the coupled-cluster method (CCM) [24], self-consistent Green's function method [25], in-medium similarity renormalization group approach [26],

Table 1.1: Ground-state energies for ⁴He, ¹⁶O and ⁴⁰Ca. The calculations are done with the chiral N³LO NN interaction [10] and by the Hartree-Fock (HF) method. The displayed results are obtained in the 13, 15, and 15 major-shell calculations for ⁴He, ¹⁶O, and ⁴⁰Ca, respectively. The experimental data are taken from Ref. [23]. All the energies are in units of MeV.

	⁴He	¹⁶O	⁴⁰Ca
HF calc.	0.18	24.06	82.81
Exp.	−28.30	−127.62	−342.05

and unitary-model-operator approach (UMOA) [27]. In these methods, the many-body correlations can be included order by order and can be truncated where the inclusion of the correlations is sufficient. From the comparison with the exact solutions, it is known that the inclusion of the two-body correlations is practically sufficient in most of cases. By truncating the higher order correlations, the mass region $A \simeq 100$ is reachable [28]. In the recent *ab initio* calculations, ground-state energies for oxygen isotopes are successful with the chiral $NN + 3N$ interactions [29–32], while, starting from the same interaction set, the systematic overbound is reported in calcium and nickel regions [28, 33, 34].

In this work, we employ the UMOA. The history of the UMOA is as follows. As shown in Table 1.1, HF or Brückner-HF calculations did not well reproduce the data in 1950's and 1960's. To consider the higher order correlations, the UMOA was invented based on the cluster expansion which is a decomposition according to the number of interacting particles [35]. In the UMOA, the ground-state properties of ^{16}O and ^{40}Ca were discussed with the phenomenological assumptions [36]. In 1986, Suzuki and Okamoto merged the former UMOA framework and the Hermite effective-interaction theory [37]. In such a framework, the UMOA was formulated to decouple the two-particle-two-hole (2p2h) excitations with the certain reference state. In other words, the UMOA was established as the in-medium Okubo-Lee-Suzuki method.

So far, the UMOA has been applied to investigate the medium-mass nuclei. Ground-state energies, charge radii and single-particle energies of ^{16}O and ^{40}Ca were calculated with realistic NN interactions, and the saturation property, the relation between the binding energy and density, of each nucleus was discussed [27, 37, 38]. Recently, the particle-basis (proton-neutron) formalism was introduced [39] due to the development of high-precision charge-dependent NN interactions. The results with this formalism are shown in Refs. [39, 40, 42, 43]. In this UMOA framework, however, there is difficulty that the calculated observables depend on $\hbar\omega$ which is a parameter characterising the single-particle basis spanning our model space. Note that the final results should not depend on $\hbar\omega$, because the initial Hamiltonian does not include $\hbar\omega$. To investigate and reduce the $\hbar\omega$-dependence of results, we extend the UMOA framework. Namely, in addition to the 2p2h, the 1p1h excitations are decoupled with the reference state.

Our main focus is the ground-state energies and radii of finite nuclei. The ground-state energies and radii are obvious and reflects the nuclear structure. In addition, both ground-state energies and radii are indispensable to discuss the saturation property of finite nuclei, which is the fundamental property of finite (stable) nuclei. Note that the saturation property is nucleus-independent behavior of the binding energy per nucleon (~ 8 MeV) and central density of a nucleus (~ 0.17 fm^{-3}). It is important to understand the saturation property based on the underlying interactions. Since our survey across the nuclear chart can be a clue to investigate the infinite nuclear matter system, this study can be important not only in nuclear physics but also in astrophysics. Especially, the nuclear equation of state (EOS) is an important issue in astrophysical objects such as neutron stars and supernovae. The EOS has mainly been investigated with mean-field theory. However, the EOS strongly depends on the choice of the effective-interaction models. It is worth starting from the *ab inito* calculations for finite nuclei. In the recent CCM works, the parameters of the EOS are discussed by calculating the neutron

skin thickness of ^{48}Ca nucleus [41]. Although the importance of the 3N interaction is reported in many recent works, we keep up to the *NN* interactions in this work. Since there are no systematic *ab initio* calculations for heavy nuclei, it is worth doing the UMOA calculation for nuclei across the nuclear chart even if one starts from only the *NN* interactions. Moreover, it is interesting whether the certain properties can be determined with only the *NN* interaction. In this work, we calculate the ground-state energies and radii for 35 closed shell nuclei from ^{4}He to ^{218}Pb.

The contents of this thesis are following. In chapter 2, the *NN* interactions employed in the actual calculations are discussed. Since the bare interactions are too hard to apply the UMOA calculations, the free-space Okubo-Lee-Suzuki method, $V_{\text{low k}}$ interaction, and SRG transformation are introduced. In chapter 3, the theoretical framework of the UMOA is introduced. The construction of the general A-body transformed Hamiltonian and its cluster expansion are shown. Then, the actual calculation procedures *method I* and *method II* are shown. In chapter 4, the numerical results with the *NN* interactions are shown. We show the results of ^{4}He, ^{16}O, ^{40}Ca, and ^{56}Ni with the *method I*, former UMOA framework, based on Refs. [42, 43]. These results strongly depend on $\hbar\omega$. To investigate and reduce the $\hbar\omega$-dependence of results, we newly introduce the one-body correlation operator to the UMOA. Through the calculations for ^{4}He and oxygen isotopes, one can confirm the applicability of the UMOA. We apply the UMOA to the shell closed nuclei from ^{4}He to ^{218}Pb and discuss the bulk properties of the many-nucleon system. Our ground-state energies and radii become overbound and smaller than the experimental data as the mass number increases. We find that the observables coming from the proton-neutron asymmetry can be insensitive to the choice of the resolution scale for the *NN* interaction and can be determined uniquely. Finally, the extension of the UMOA towards the inclusion of the 3N interaction is demonstrated. In chapter 5, the results in this work are summarized and a future perspective is given.

Chapter 2

NN Interactions for Numerical Calculations

The determination of the nuclear Hamiltonian (interactions) is one of the longstanding problems in the low-energy nuclear structure theory. Since a nucleon has internal degrees of freedom, the nuclear Hamiltonian can include the many-body interactions beyond the nucleon-nucleon (*NN*) level. All the interactions among nucleons can be, in principle, provided by solving the QCD which is well known as the fundamental theory for the system consisting of quarks and gluons. Due to the non-perturbative property of the QCD in the low-energy regime, however, it is difficult to derive the nuclear interactions from the QCD. Recently, a lot of efforts are made for the direct derivation of the nuclear interactions through the first principle calculations of QCD on the lattice [44]. So far, it is not possible to obtain the high-precision *NN* interaction from the lattice QCD calculations at the physical point yet.

In the current situation,the *NN* and three-nucleon (3*N*) interactions are available. As for the *NN* sector, we can use the various *NN* interactions which can reproduce the properties of *NN* system with high precision. In the sense of fitting to reproduce the observables of *NN* system, construction of the *NN* interaction can be established. The 3*N* interaction is one of the recent important issues in this field. Basically, the effect of the 3*N* interaction should be smaller than that of *NN* interaction and seems to be not significant. Owing to the recent developments of the experimental techniques, the experiments have been enabled for the extreme cases, i.e., the neutron-rich nuclei. As shown in Ref. [13], the effect of the 3*N* interaction becomes important for oxygen drip line. Although the effect of the 3*N* interactions is an important topic, our calculations, discussed in this thesis, are done with the *NN* interaction.

The *NN* interaction cannot be determined uniquely, because the interactions are not basically observables and can have non-local structure which provides the model dependence. The model dependence of the interactions cannot be removed by fitting at *NN* level. The low-momentum- ($V_{\text{low k}}$) and similarity-renormalization-group- (SRG) evolved interactions, introduced in Sec. 2.2, provide a kind of answer for this model dependence. These *NN* interactions are derived based on the renormalization group (RG) technique. By roughing the resolution scale in RG technique, such *NN* interactions show the universality. Since the RG technique induces the many-body interactions, however, the choice of the initial nuclear Hamiltonian still can be an important issue in the low-energy nuclear structure theory.

Since our calculations, in this thesis, are limited with nucleon-nucleon (*NN*) interactions, we show the features of realistic *NN* interactions which reproduce precisely the *NN* scattering phase shifts, as well as the deuteron properties. As discussed in Sec 2.1, such realistic *NN* interactions cannot be applied directly to the many-body calculation in many cases. To obtain the tractable *NN* interactions, the prescriptions are introduced based on the similarity transformation of the original *NN* interaction, as shown in Sec. 2.2.

2.1 Realistic *NN* interactions

Here, we mention the properties of the realistic *NN* interactions, which can reproduce the proton-proton and proton-neutron scattering phase shift data. There are a large numbers of the realistic *NN* interactions. In this work, we will mainly employ the Argonne V18 (AV18) [8] interaction, the charge-dependent Bonn (CD-Bonn) [9] interaction, and the chiral *NN* interaction up to next-to-next-to-next-to leading order (N^3LO) by Entem and Machleidt [10]. The constructions of such interactions are following.

- The AV18 interaction is written as a sum of an electro-magnetic part, a one-pion-exchange (OPE) part, and an intermediate- and short-range phenomenological part. The phenomenological part is regularized by the Woods-Saxon function. It does not have the momentum-dependence except for the operators such as $\mathbf{L}^2$, $\mathbf{L} \cdot \mathbf{S}$, and is given as a function of relative coordinate of two nucleons after the partial wave decomposition.

- The CD-Bonn interaction is based on the boson-exchange Feynman amplitude. The mesons with masses smaller than nucleon mass are considered, i.e. π, η, ρ, ω, and σ. The form factor is introduced to cut off the interaction at a short distance.

- The N^3LO interaction is derived from the chiral effective field theory (EFT). In the chiral EFT, the effective Lagrangian is written by the nucleon and pion. The N^3LO interactions are obtained by perturbative expansion up to next-to-next-to-next-to leading order. The short-range terms beyond the energy scale of pion are written by contact terms fitted by the experimental phase shift data in the *NN* scattering. There are several prescriptions to regularize the interaction at large momenta, see e.g. Refs. [10, 11]. The cutoff momentum $\Lambda = 500$ MeV/c is commonly used.

These interactions are constructed to reproduce the *NN* scattering phase shift data with high precision. For example, the proton-neutron (*pn*) scattering phase shifts calculated with such interactions are shown in Fig. 2.1 as the function of laboratory energy T_{lab}. The experimental data are reproduced well especially for lower partial waves. Note that the phase shift data used fitting are up to the order of 300 MeV, because the pion production threshold energy is roughly 300 MeV. The interaction-model dependence of the calculated phase shift values can appear beyond this energy.
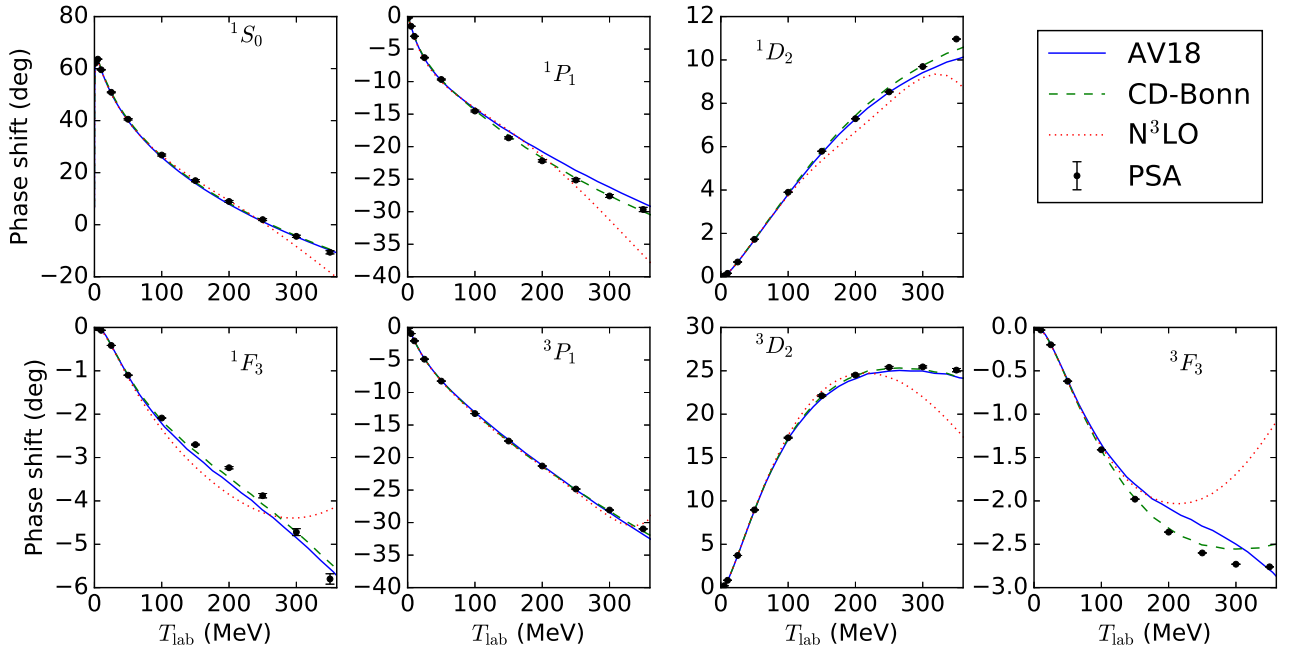
Figure 2.1: The *pn* phase shifts as functions of T_{lab}. The calculated phase shifts are from AV18 [8] (solid line), CD-Bonn [9] (dashed line), and N^{3}LO [10] (dotted line) interactions. The phase-shift analysis data are taken from Nijimengen phase shift analysis [45].

The calculated deuteron binding energies and *D*-state probabilities (P_D) are exhibited in Table 2.1. As shown in Table 2.1, the deuteron biding energy can be reproduced well. The P_D is defined by

$$P_D = \frac{\int dr r^2 \psi_D^2(r)}{\int dr r^2 [\psi_S^2(r) + \psi_D^2(r)]}, \tag{2.1}$$

with the *S*-wave and *D*-wave radial wave functions $\psi_S(r)$ and $\psi_D(r)$, respectively. Thus, P_D indicates the amount of mixing of *D*-state in the deuteron wave function and relates the strength of the tensor interaction which mixes the different orbital angular momentum states. Note that P_D is not an observable and depends on interaction models, because the wave function is not observable.

In Fig. 2.2, *NN* interactions for the *pn* $^1S_0$ channel are shown as functions of a relative distance of proton and neutron *r*. The CD-Bonn and chiral N^{3}LO interactions are defined as the non-local interac-

Table 2.1: The binding energies (B. E.) and *D*-state probability (P_D) of deuteron with the AV18 [8], CD-Bonn [9], and chiral N^{3}LO [10] interactions. Calculations are done with the relative momentum space.

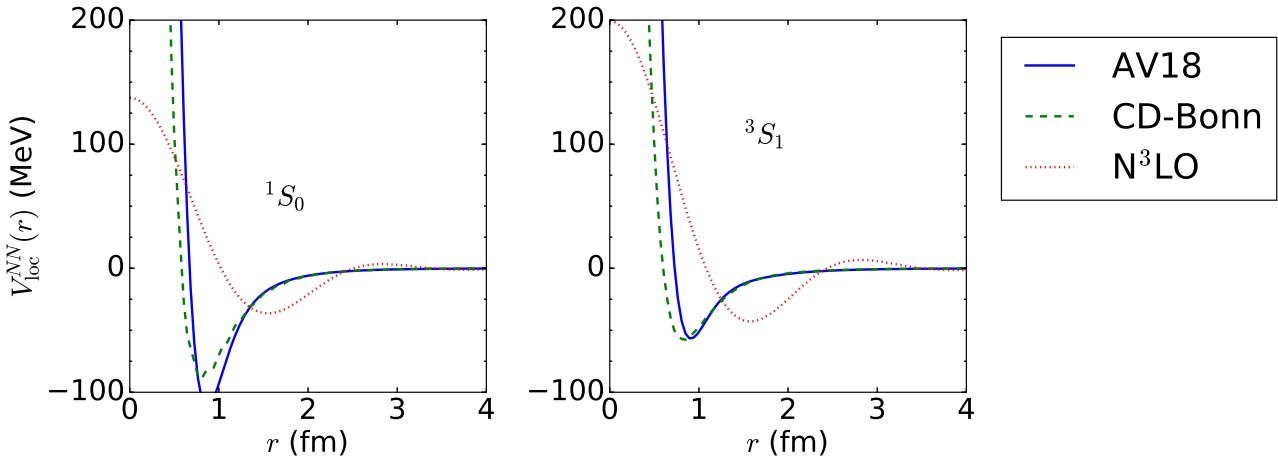|		AV18	CD-Bonn	N^{3}LO	Exp.
B. E.	(MeV)	2.224575	2.224575	2.22458	2.224575
P_D	(%)	5.76	4.85	4.51	

Figure 2.2: The local part of the *NN* interactions for *pn S*-wave channels of AV18 (solid curve) CD-Bonn (dashed curve), and N^{3}LO (dotted curve) interactions as functions of a relative coordinate of proton and neutron.

tions which depend on relative coordinates of both of the initial and final states, i.e. $V^{NN} = V^{NN}(r, r')$. We employ the local projection introduced in Ref. [46] to plot Fig. 2.2. As discussed in Ref. [46], the residual non-local part is perturbative and the dominant part of the *NN* interactions are illustrated in Fig. 2.2. As for the N^{3}LO interaction, we see the oscillation around $r \sim 3$ fm. The position of this oscillation corresponds to the cutoff momentum $\Lambda = 500$ MeV$/c$ for the N^{3}LO interaction. Since the treatment of the one-pion exchange is common in the realistic *NN* interactions, all the interactions shown in Fig. 2.2 are close to each other in the long-range region ($r \gtrsim 2$). The *NN* interaction for the *S* wave is attractive at middle range ($0.5 \lesssim r \lesssim 2$), and is repulsive at short range ($r \lesssim 0.5$) known as the repulsive core. In these regions, especially for N^{3}LO and other interactions, V^{NN}_{loc} largely depends on the interaction model. This difference means the uncertainties of our knowledge about the *NN* interactions and is discussed in Sec. 2.2. The existence of the repulsive core can be the problem in actual calculations. For instance, the perturbative expansion obviously break down, because the matrix element of V^{NN} becomes large. Also, the existence of the repulsive core demands the computational resource.

A further insight about the repulsive core can be obtained by looking the *NN* interactions represented in the momentum space. Fig. 2.3 shows the momentum space representation of AV18, CD-Bonn, and N^{3}LO interactions for *pn* $^1S_0$ channel. Since the short-range physics relates with the high-momentum region, we discuss the high-momentum component to discuss the short-range repulsion. Here, we divide the high- and low-momentum regions at $k \sim 2.0$ fm^{-1} which corresponds to energy 350 MeV in laboratory frame. Since the results of the phase-shift analysis are available below 350 MeV in the laboratory frame, various realistic *NN* interactions can reproduce the experimental results for *NN* system up to this energy scale. Beyond this energy, complicated high-energy physics becomes efficient. In this sense, the high- and low-momentum regimes are defined here. Then, the
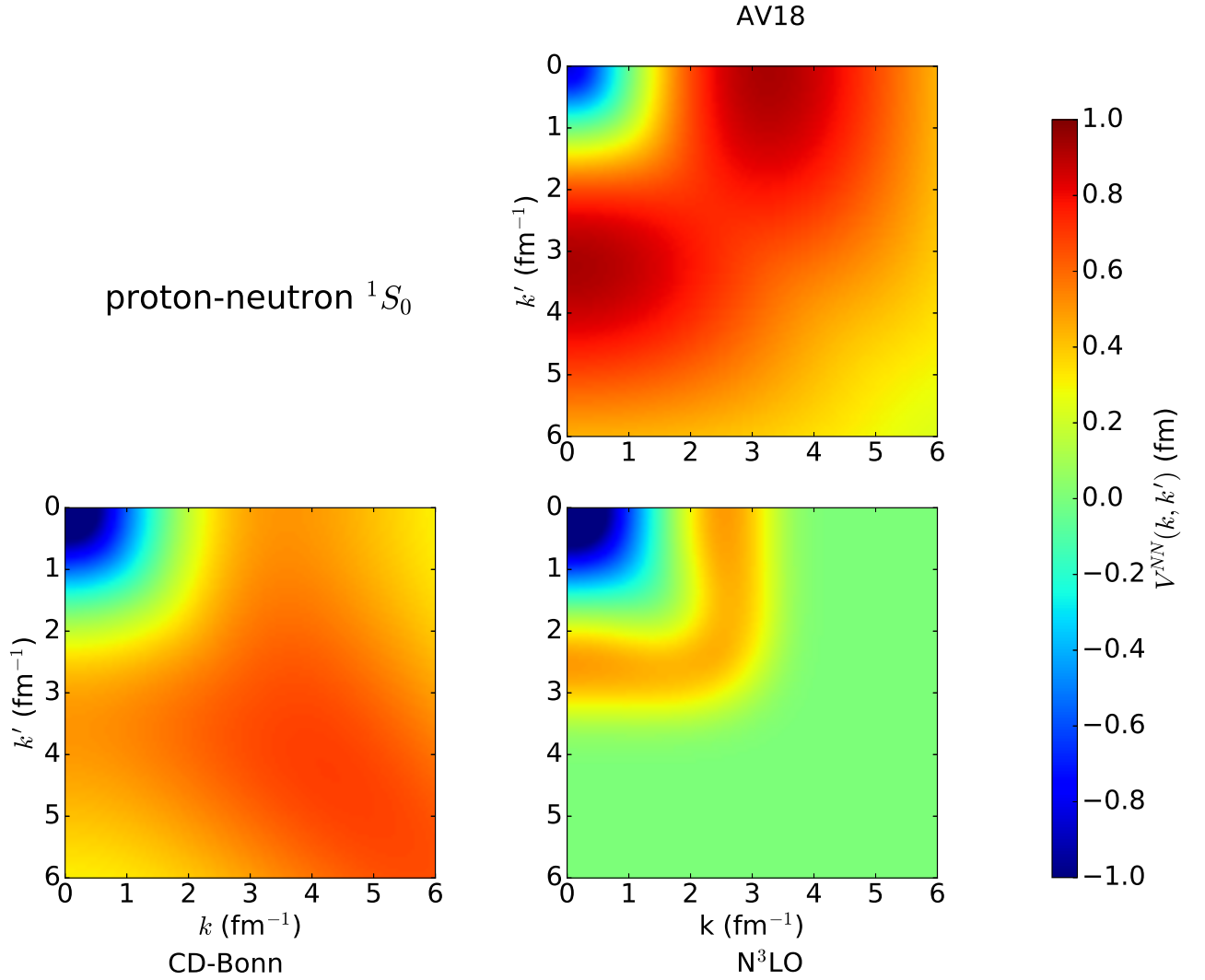
Figure 2.3: The *NN* interactions in the momentum representation of the *pn* $^1S_0$ channel for AV18, CD-Bonn, and N^{3}LO interactions.

strong repulsive coupling between the low- and high-momentum regions is observed for all the cases plotted in Fig. 2.3. This coupling relates the repulsive core of the *NN* interactions. Moreover, the *NN* interactions defined in the local form seem to have inevitably the repulsive core [16] In fact, in addition to the AV18 interaction, the repulsive core is observed in the local *NN* interaction by the Lattice QCD simulations [44] and by the chiral effective field theory [47]. By taking into account the non locality, however, we can avoid the repulsive core. According to Fig. 2.2 and 2.3, in fact, the N^{3}LO interaction is relatively soft compared with the other two interactions. Details about this issue is discussed in Sec. 2.2

Let us consider the convergence property of the calculations with the realistic *NN* interactions. As the simplest example, we calculate the ground-state energy of deuteron which is composed by proton

Figure 2.4: The deuteron ground-state energies as functions of N_{max} with the fixed $\hbar\omega$. We employ $\hbar\omega = 40$ MeV.

and neutron. To do that, we solve the Schrödinger equation,

$$H|\psi\rangle = E_{\mathrm{D}}|\psi\rangle, \tag{2.2}$$

with the deuteron ground-state energy E_{D} and wave function $|\psi\rangle$. Then, the Hamiltonian is

$$H = \frac{\mathbf{p}_{\mathrm{rel}}^2}{2\mu} + V^{NN}. \tag{2.3}$$

Here, $\mathbf{p}_{\mathrm{rel}}$ is relative momentum of proton and neutron, μ is reduced mass, and V^{NN} is NN interaction. Since the usual numerical calculations are performed in the space spanned by the harmonic-oscillator (HO) basis, we employ the HO basis representation here. Then, a parameter $\hbar\omega$ has to be introduced, which relates with the curvature of the HO potential. Note that calculated observables should not depend on $\hbar\omega$, if the numerical calculations are performed in the sufficiently large model space. We will revisit this point in the many-body (UMOA) calculations. Using the HO basis representation, the kinetic term can be expressed as

$$\left\langle nl \left| \frac{\mathbf{p}_{\mathrm{rel}}^2}{2\mu} \right| n'l' \right\rangle = \begin{cases} \frac{1}{2}\left(2n + l + \frac{3}{2}\right)\hbar\omega & \text{for} \quad n = n', \, l = l' \\ \frac{1}{2}\sqrt{n\left(n + l + \frac{1}{2}\right)}\hbar\omega & \text{for} \quad n + 1 = n', \, l = l' \\ 0 & \text{otherwise} \end{cases}. \tag{2.4}$$
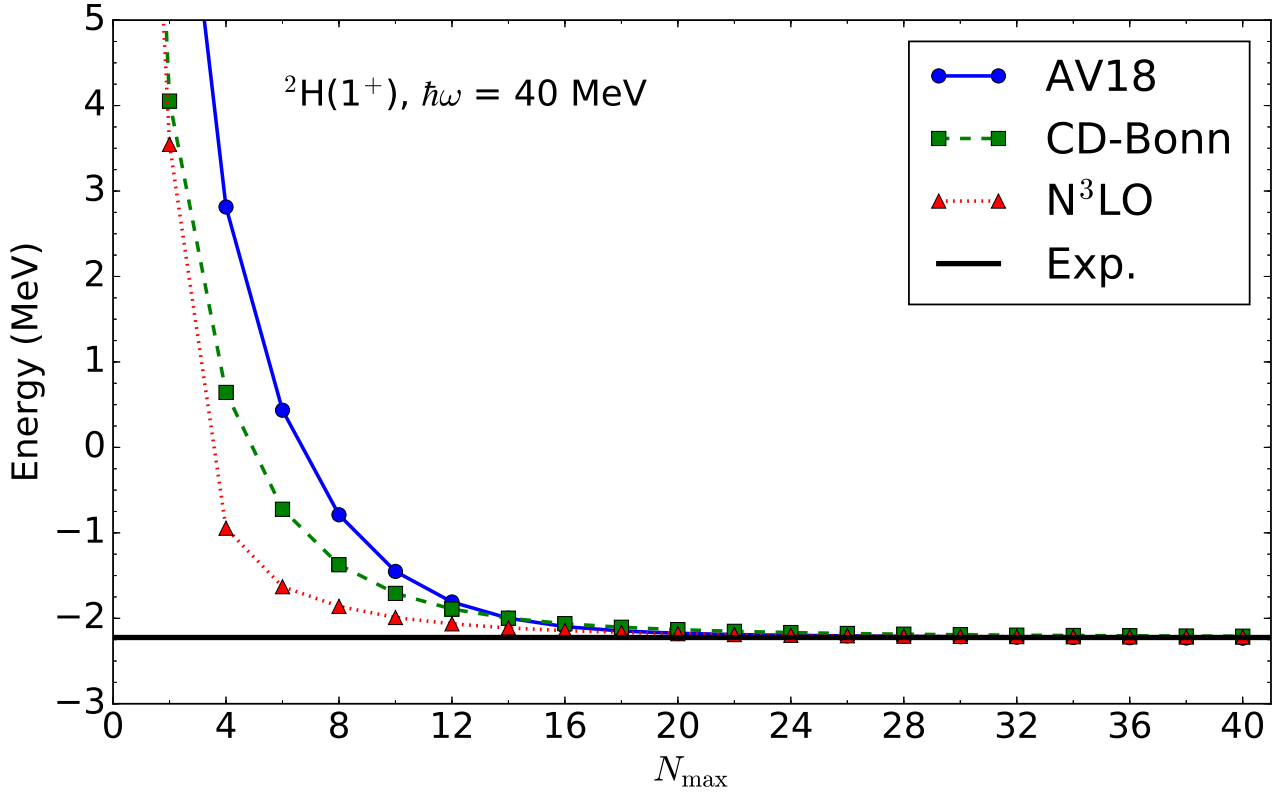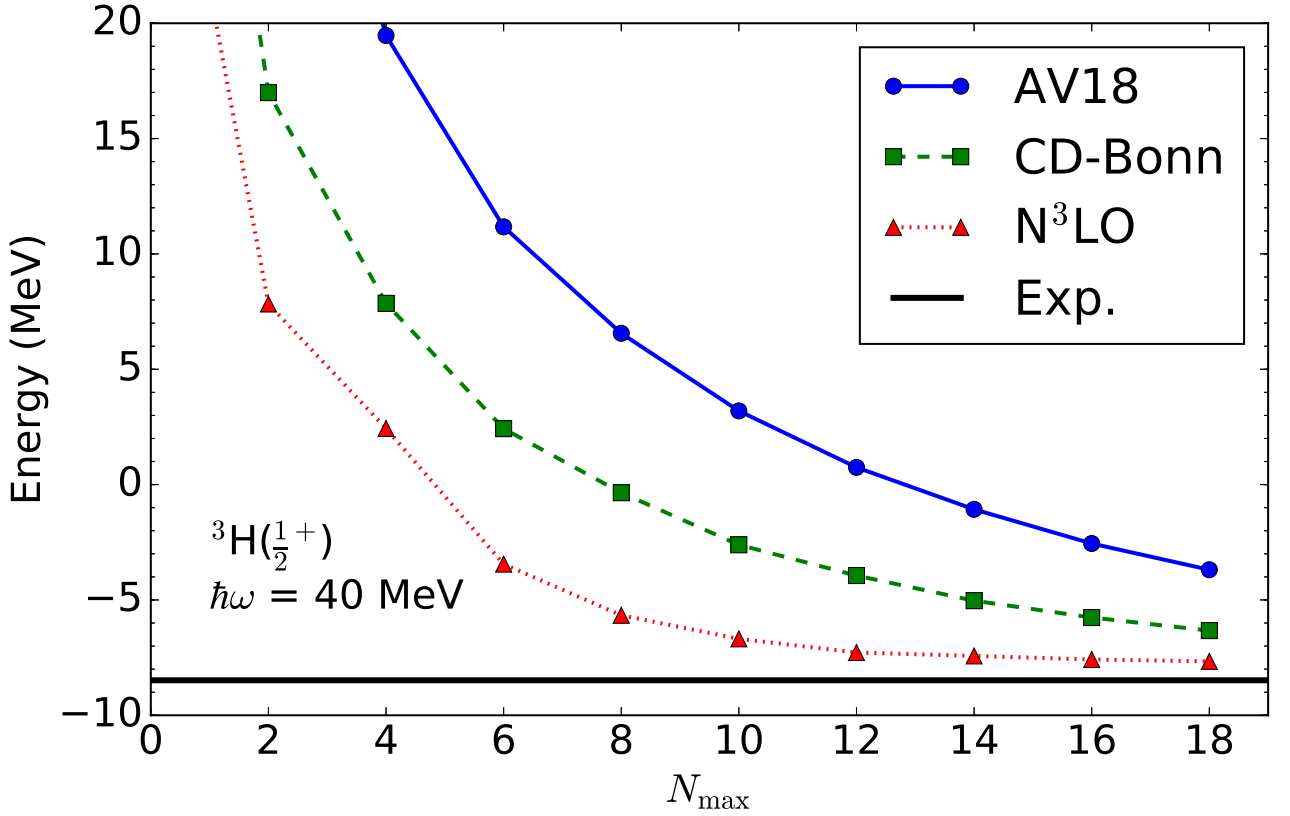
Figure 2.5: The triton (^{3}H) ground-state energies as functions of $N_{\max}$ with the fixed $\hbar\omega$. We employ $\hbar\omega = 40$ MeV.

Here, $\hbar\omega$ is the energy of HO basis employed in the calculations. The n and l denote the nodal and azimuthal quantum numbers, respectively. The derivation of the *NN* interaction in the HO basis representations is complicated a little and is shown in Appendix A. Applying Eq. (A.3) (Eq. (A.7)) for local (non-local) interaction, Eq. (2.2) can be the eigenvalue problem. We diagonalize the Hamiltonian for deuteron channel $J^\pi = 1^+$. In Fig. 2.4, the deuteron ground-state energies are shown as functions of $N_{\max}$ with the AV18, CD-Bonn, and N^{3}LO interactions. Here $N_{\max}$ is maximal principal quantum number included in the diagonalization and we use $\hbar\omega = 40$ MeV. The ground-state energies lower with increasing $N_{\max}$. The convergence of N^{3}LO interaction case is faster than that of AV18 and CD-Bonn interactions cases. This is consistent with the softness of the N^{3}LO interaction shown in Fig. 2.2 and 2.3. In the deuteron case, we can obtain the converged results in $N_{\max} > 24$ for all the interaction cases.

As a next step, we consider the ground state of the three-nucleon system ^{3}H. Although, we can diagonalize the Hamiltonian in the three-body Jacobi coordinate similar to the deuteron case, we here employ the product of the HO single-particle (sp) basis states. The combinations of the Jacobi coordinates rapidly increase, and we would not solve the six- or more than six-nucleons problems. On the other hand, the increase of the number the product of sp bases is relatively gentle compared to

that of Jacobi coordinate bases. Moreover, we know the basis transformation from relative and CM coordinates to product of the sp coordinates for the HO representations. This is reason why we use the product of the HO sp basis states. The Schrödinger equation is

$$H|\psi_k\rangle = E_k|\psi_k\rangle, \tag{2.5}$$

with

$$H = \frac{1}{3} \sum_{i<j=1}^{3} \frac{(\mathbf{p}_i - \mathbf{p}_j)^2}{2m} + \sum_{i<j=1}^{3} V_{ij}^{NN} \tag{2.6}$$

$$= \frac{2}{3} \sum_{i=1}^{3} \frac{\mathbf{p}_i^2}{2m} + \sum_{i<j=1}^{3} \left(V_{ij}^{NN} - \frac{\mathbf{p}_i \cdot \mathbf{p}_j}{3m} \right). \tag{2.7}$$

In our basis representation, the wave function $|\psi\rangle$ can be expanded into

$$|\psi_k\rangle = \sum_{abc} D_{k;abc}|abc\rangle. \tag{2.8}$$

Here, $D_{k;abc}$ is a diagonalization coefficient and $|abc\rangle$ is antisymmetrized three-nucleon state. The state $|a\rangle$ is short notation of $|n_a l_a j_a m_a t_a\rangle$. The n_a, l_a, j_a, m_a, and t_a are the HO nodal quantum number, orbital angular momentum, total angular momentum, third component of total angular momentum, and the label distinguishing the proton and neutron, respectively. Similar to Eq. (2.4), we have

$$\left\langle a \left| \frac{\mathbf{p}_1^2}{2m} \right| b \right\rangle = \begin{cases} \frac{1}{2} \left(2n_a + l_a + \frac{3}{2} \right) \hbar\omega \delta_{l_a l_b} \delta_{j_a j_b} \delta_{m_a m_b} \delta_{t_a t_b} & \text{for} \quad n_a = n_b \\ \frac{1}{2} \sqrt{n_a \left(n_a + l_a + \frac{1}{2} \right)} \hbar\omega \delta_{l_a l_b} \delta_{j_a j_b} \delta_{m_a m_b} \delta_{t_a t_b} & \text{for} \quad n_a + 1 = n_b \\ 0 & \text{otherwise} \end{cases} , \tag{2.9}$$

for the kinetic energy term. For the two-body term, we can use Eq. (A.14).

    Fig. 2.5 shows the calculated ground-state energy for ^{3}H with AV18, CD-Bonn, and N^{3}LO interactions as functions of N_{max}. In this calculation, we use $\hbar\omega = 40$ MeV and calculate up to $N_{max} = 18$. Beyond this N_{max}, the Talmi-Moshinsky transformation, Eq. (A.14), takes much time and we do not calculate. As shown in Fig. 2.5, the ground-state energies with various interactions lower with increasing N_{max}. For N^{3}LO interaction case, we can see the almost converged results and the energy at $N_{max} = 18$ is consistent with the exact solution -7.85 MeV, calculated by the no-core shell model with the Jacobi coordinate [48]. In contrast, the model space is not sufficiently large yet for AV18 and CD-Bonn interactions cases. The converged energies cannot be found for results with these interactions. We encounter the convergence problem even ^{3}H which is the second simplest case. It can be easily expected that obtaining the converged results is difficult in heavier nuclei calculations. To get over this problem, we can carry out two procedures. One is to transform the underlying interactions to tame the short-range repulsion, as discussed in Sec. 2.2. The other one is to use the other many-body calculation methods. In this section, we employ the computationally expensive exact diagonalization method. Taking the proper approximations, however, we can reduce the computational cost with keeping the required precision. We employ the unitary-model-operator approach (UMOA) introduced in Chap. 3.

2.2 Renormalization Technique

As mentioned in Sec. 2.1, it is almost impossible to apply the realistic *NN* interactions to the usual nuclear structure calculations because of the strong short-range correlations. To tame the strong short-range repulsion, the *G*-matrix was introduced by Brückner and his collaborators [14]. The *G*-matrix is constructed by summing up the particle-particle ladder diagrams and can be expected to capture the short-range physics. The *G*-matrix is widely employed in low-energy nuclear physics field. As shown in Ref. [16], however, the *G*-matrix is not defined to decouple the low- and high-momentum scales and does not ensure to improve the convergence of the numerical calculations. By adopting the concept of the effective interaction theories, we can construct the interactions designed for the model space we are interested in. Such an interaction is known as the Okubo-Lee-Suzuki (OLS) transformed interaction. Moreover, new prescriptions have been developed based on the renormalization group technique. Here, we briefly see the features of such softened *NN* interactions.

2.2.1 Okubo-Lee-Suzuki transformation

Here, we derive the OLS transformed interaction for the many-body systems from the realistic *NN* interactions. The OLS method is based on the energy-independent Hermitian effective-interaction theories. The form of the unitary transformation is given in Ref. [49]. The derivation with the mapping operator between the model space and its complement is established in Refs. [50, 51]. The fundamental ingredients employed in the effective-interaction theories are summarized in Appendix B. The concept of the OLS transformation is inherited to our many-body method, unitary-model-operator approach (UMOA), and the UMOA can also be called as in-medium OLS method.

Let us consider the Hamiltonian represented in the HO basis space:

$$H = \frac{1}{A} \sum_{i<j}^{A} \frac{(\mathbf{p}_i - \mathbf{p}_j)^2}{2m} + \sum_{i<j}^{A} V_{ij}^{NN}. \tag{2.10}$$

Note that we, here, consider only the *NN* interaction. To defined the projection operator, we separate the Hamiltonian into

$$H = \sum_{i<j}^{A} H_{ij,0} + \sum_{i<j}^{A} H_{ij,I}, \tag{2.11}$$

with

$$H_{ij,0} = \frac{1}{A} \left[\frac{(\mathbf{p}_i - \mathbf{p}_j)^2}{2m} + \frac{1}{2} m\Omega^2 (\mathbf{r}_i - \mathbf{r}_j)^2 \right], \tag{2.12}$$

$$H_{ij,I} = V_{ij}^{NN} - \frac{1}{2A} m\Omega^2 (\mathbf{r}_i - \mathbf{r}_j)^2. \tag{2.13}$$

Note that we add (subtract) the term $\sum m\Omega^2 (\mathbf{r}_i - \mathbf{r}_j)^2/2A$ to kinetic energy term (from interaction term), so that $H_{ij,0}$ is diagonal with respect to the relative HO basis states, i.e.,

$$H_{12,0}|nl\rangle = \left(2n + l + \frac{3}{2} \right) \hbar\Omega |nl\rangle. \tag{2.14}$$
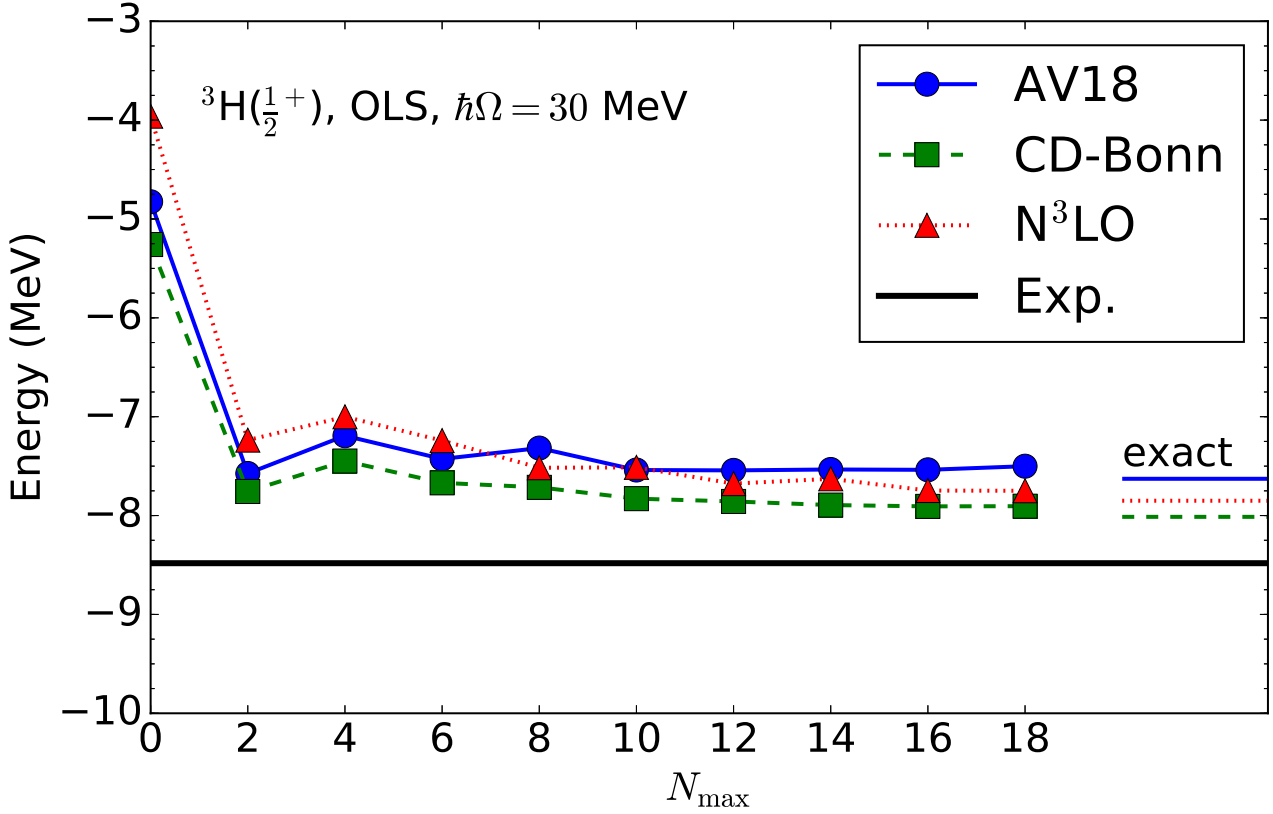
Figure 2.6: The triton ground-state energies calculated with the Okubo-Lee-Suzuki transformed interactions derived from AV18 (solid line), CD-Bonn (dashed line), and N^{3}LO (dotted line) interactions. The exact solutions are taken from Refs. [48, 52].

In this section, to avoid the confusion, we use Ω as the frequency of the HO potential and ω as the mapping operator defined in Appendix B. Now we can divide the whole two-body Hilbert space into the model space and its complement and introduce the projection operators,

$$P = \sum_{nl}^{2n+l \leq N_{\max}} |nl\rangle\langle nl|, \quad Q = \sum_{nl}^{2n+l > N_{\max}} |nl\rangle\langle nl|. \tag{2.15}$$

Here, P and Q are projection operators projecting into the model space and outside of the model space, respectively. The summation in Eq. (2.15) for P (Q) runs over n and l satisfying $2n + l \leq N_{\max}$ ($2n + l > N_{\max}$). The boundary $N_{\max}$ defines the model space.

To derive the effective NN interaction, as the next step, we solve the Schrödinger equation,

$$(H_{12,0} + H_{12,I})|\psi_k\rangle = E_k|\psi_k\rangle, \tag{2.16}$$

and obtain the mapping operator ω by using Eq. (B.17). Once ω is determined, we can derive the unitary transformation operator $e^{S_{12}}$ by Eq. (B.40). The transformed Hamiltonian $\widetilde{H}_{12}$ is

$$\widetilde{H}_{12} = e^{-S_{12}} H_{12} e^{S_{12}}. \tag{2.17}$$

Then, the effective interaction can be given by

$$\widetilde{V}^{NN}_{12,\text{eff}} = P\left(\widetilde{H}_{12} - H_{12,0}\right)P. \tag{2.18}$$

Obviously, the transformation Eq. (2.17) induces the many-body interactions. The induced many-body interactions are neglected here. However, it can be expected that effects of such induced *NN* interaction are small when we take sufficiently large model space, because of

$$\widetilde{V}_{12,\text{eff}} \longrightarrow V^{NN}_{12} - \frac{1}{2A}m\Omega^2(\mathbf{r}_1 - \mathbf{r}_2)^2, \quad (N_{\text{max}} \to \infty), \tag{2.19}$$

$$(\text{induced many-body interaction}) \longrightarrow 0, \quad (N_{\text{max}} \to \infty). \tag{2.20}$$

The effect of the induced many-body interaction are investigated in the no-core shell model (NCSM) [53]. Using the derived effective *NN* interaction, the Hamiltonian designed for our model space is

$$H_{\text{OLS}} = \frac{1}{A}\sum_{i<j}\left[\frac{(\mathbf{p}_i - \mathbf{p}_j)^2}{2m} + \frac{1}{2}m\Omega^2(\mathbf{r}_i - \mathbf{r}_j)^2\right] + \sum_{i<j}^{A}\widetilde{V}^{NN}_{ij,\text{eff}}, \tag{2.21}$$

$$= \left(1 - \frac{1}{A}\right)\sum_{i=1}^{A}\left(\frac{\mathbf{p}_i^2}{2m} + \frac{1}{2}m\Omega^2\mathbf{r}_i^2\right) + \sum_{i<j}^{A}\left(\widetilde{V}^{NN}_{ij,\text{eff}} - \frac{\mathbf{p}_i \cdot \mathbf{p}_j}{Am} - \frac{m\Omega^2\mathbf{r}_i \cdot \mathbf{r}_j}{A}\right). \tag{2.22}$$

Finally, we demonstrate the calculation results with the OLS transformed Hamiltonian. The original *NN* interactions are AV18, CD-Bonn, and chiral N³LO interactions. Same as the calculation done in Sec. 2.1, we employ the exact diagonalization method with the Slater determinant basis states. Fig. 2.6 shows the ground-state energy of triton as functions of N_{max} at fixed $\hbar\Omega = 30$ MeV. Comparing with Fig. 2.5, the convergence properties are accelerated by OLS transformation. The calculated results at $N_{\text{max}} = 18$ are reasonably close to exact solutions and will converge to those if we extend our model space. Since we truncate the induced three-body interaction, however, the variational principle is no longer preserved. For this reason, the ground-state energies do not behave monotonically and are seen oscillating as functions of N_{max}. This feature can be problem, if we calculate heavier nuclei. As the mass number increases, calculation demands the computational cost. Due to this non-monotonic behavior, it is difficult to estimate the proper results from those with the small N_{max}. To avoid this problem, one can use the softened interactions based on the renormalization group technique, which are introduced in Sec. 2.2.2 and Sec. 2.2.3.

2.2.2 Low-Momentum *NN* Interaction ($V_{\text{low k}}$)

So far, we have serious issue about nuclear interactions for applications. As discussed in Sec. 2.1, the bare *NN* interactions are generally too hard to treat in usual nuclear structure calculations. Let us remind the origin of this hardness. The hardness comes from the coupling between the low- and high-momentum region (see Fig. 2.3). Here, low and high momenta can typically be divided at 2 fm⁻¹. We simply consider the suppression of the coupling between low- and high-momentum regions. In this context, the concept is completely same as the OLS transformation except for the momentum
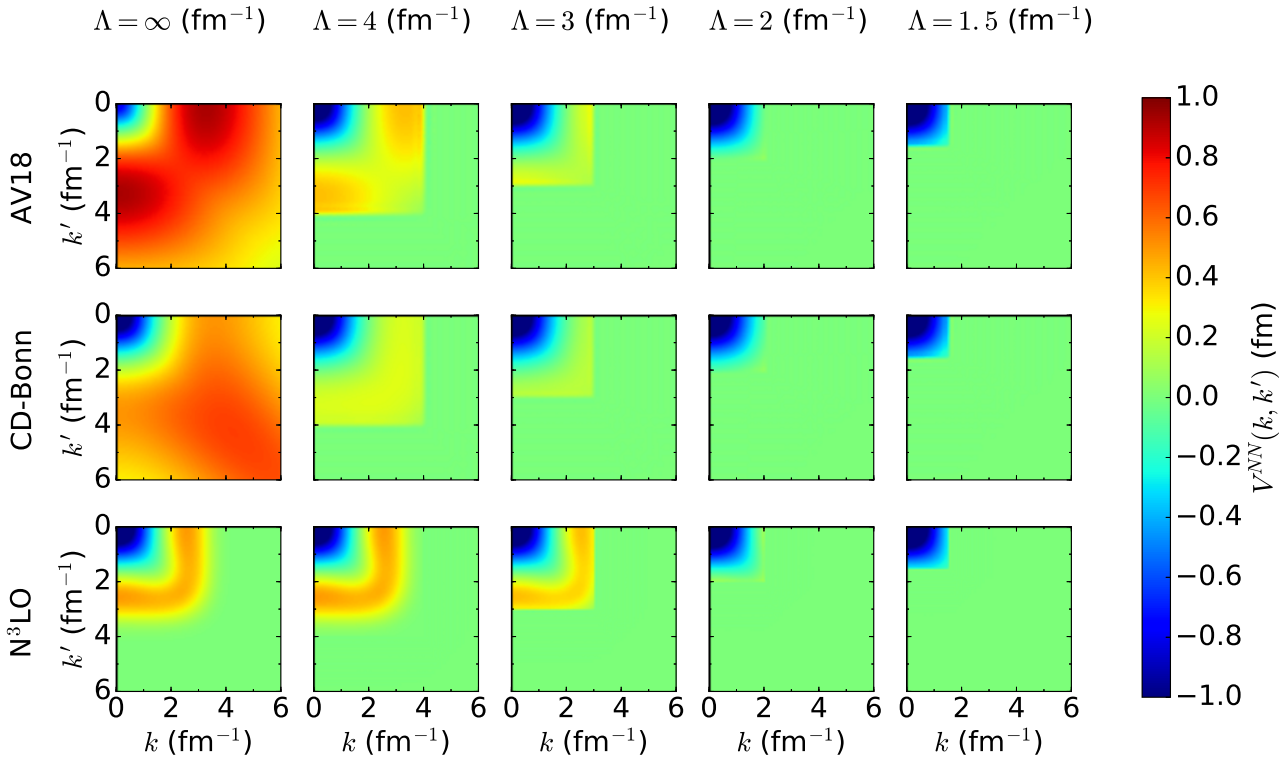
Figure 2.7: The $V_{\text{low k}}$ interactions for pn $^1S_0$ channel derived from AV18 (top), CD-Bonn (middle), and N^{3}LO (bottom) interactions as functions of relative momentum k and k'. Interactions shown here are evolved from $\Lambda = \infty$ fm^{-1} (left) to $\Lambda = 1.5$ fm^{-1} (right).

representation. Obviously, we introduce the decoupling scale Λ. Such an interaction is known as the low-momentum NN or $V_{\text{low k}}$ interaction.

The derivation of the $V_{\text{low k}}$ interaction is not unique. The $V_{\text{low k}}$ interaction was firstly formulated by Bogner et. al [54]. They define the $V_{\text{low k}}$ interaction so that the T matrix is invariant with respect to the change of the resolution scale Λ. Another derivation was given by Fujii et. al. [55]. In this thesis, we use the $V_{\text{low k}}$ interaction introduced by Fujii.

Let us consider the momentum-space Hamiltonian for NN system, i.e.,

$$H_{12}(\hat{\mathbf{k}}, \hat{\mathbf{k}}') = \frac{\hat{\mathbf{k}}^2}{2}\delta(\hat{\mathbf{k}} - \hat{\mathbf{k}}') + V^{NN}(\hat{\mathbf{k}}, \hat{\mathbf{k}}'). \tag{2.23}$$

Here, $\hat{\mathbf{k}}$ and $\hat{\mathbf{k}}'$ are relative momentum operators of NN system for outgoing and incoming states, respectively. Note that we employ the scattering unit, $\hbar = 1$, $c = 1$, and $\mu = 1$. We divide the NN Hilbert space into low-momentum P_Λ space and high-momentum Q_Λ space. The projection operator for each space can be defined as

$$P_\Lambda = \int_{|\mathbf{k}| \leq \Lambda} d^3\mathbf{k}|\mathbf{k}\rangle\langle\mathbf{k}|, \tag{2.24}$$

$$Q_\Lambda = \int_{|\mathbf{k}| > \Lambda} d^3\mathbf{k}|\mathbf{k}\rangle\langle\mathbf{k}|, \tag{2.25}$$
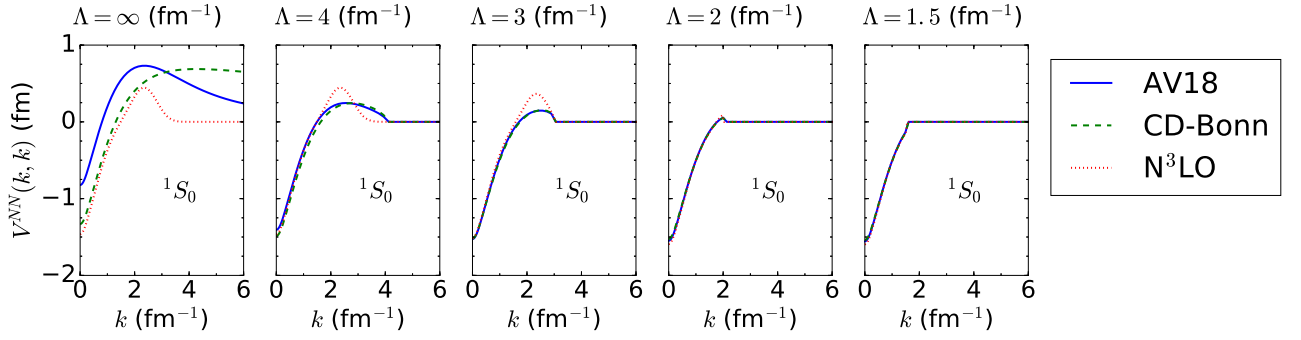
Figure 2.8: The diagonal component of $V_{\text{low k}}$ interactions for pn $^1S_0$ channel derived from AV18 (solid line), CD-Bonn (dashed line), and N^{3}LO (dotted line) interactions and evolved from $\Lambda = \infty$ fm^{-1} (left) to $\Lambda = 1.5$ fm^{-1} (right).
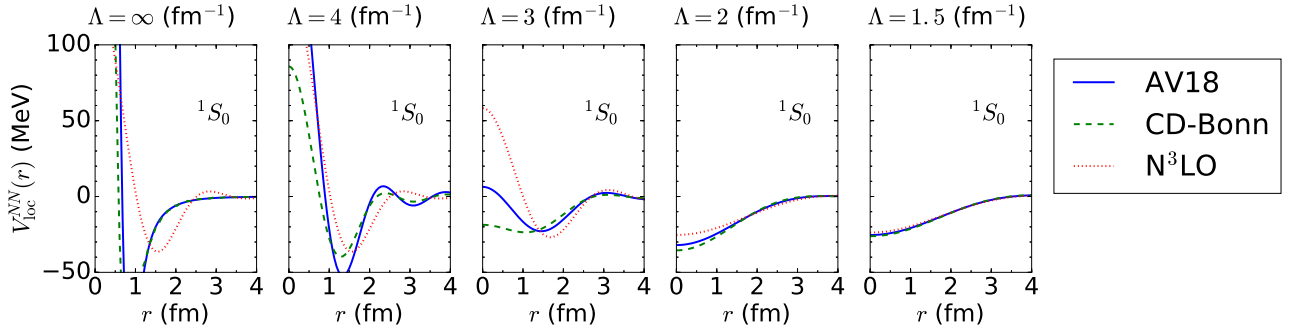
Figure 2.9: The $V_{\text{low k}}$ interactions after local projection [46] for pn $^1S_0$ channel derived from AV18 (solid line), CD-Bonn (dashed line), and N^{3}LO (dotted line) interactions and evolved from $\Lambda = \infty$ fm^{-1} (left) to $\Lambda = 1.5$ fm^{-1} (right).

with momentum eigenstate $|\mathbf{k}\rangle$. The Schrödinger equation for the Hamiltonian is

$$H_{12}(\hat{\mathbf{k}}, \hat{\mathbf{k}}')|\psi_n\rangle = E_n|\psi_n\rangle, \tag{2.26}$$

with the nth eigen energy E_n and eigenstate $|\psi_n\rangle$. Eq. (2.26) can be rewritten in an integral form as [55]

$$\int_{|k|<\infty} d^3\mathbf{k}\langle\mathbf{k}'|\frac{1}{2}\hat{\mathbf{k}}^2\delta(\hat{\mathbf{k}} - \hat{\mathbf{k}}') + V^{NN}(\hat{\mathbf{k}}, \hat{\mathbf{k}}')|\mathbf{k}\rangle\langle\mathbf{k}|\psi_n\rangle = E_n\langle\mathbf{k}'|\psi_n\rangle. \tag{2.27}$$

Eq. (2.27) is eigenvalue equation with the momentum representation. Solving Eq. (2.27), we obtain $\omega(\hat{\mathbf{q}}, \hat{\mathbf{p}})$ with Eq. (B.17). Here, $\hat{\mathbf{q}}$ and $\hat{\mathbf{p}}$ are momentum operators belong to Q and P spaces, respectively. The unitary transformation operator $e^{s_{12}(\hat{\mathbf{k}},\hat{\mathbf{k}}')}$ can be calculated with Eq. (B.40). The two-body transformed Hamiltonian $\widetilde{H}_{12}(\hat{\mathbf{k}}, \hat{\mathbf{k}}')$ is

$$\widetilde{H}_{12}(\hat{\mathbf{k}}_1, \hat{\mathbf{k}}_2) = \int d^3\mathbf{k}_3\,d^3\mathbf{k}_4\,e^{-s_{12}(\hat{\mathbf{k}}_1,\hat{\mathbf{k}}_3)}\,|\mathbf{k}_3\rangle\langle\mathbf{k}_3|H(\hat{\mathbf{k}}_3, \hat{\mathbf{k}}_4)|\mathbf{k}_4\rangle\langle\mathbf{k}_4|\,e^{s_{12}(\hat{\mathbf{k}}_4,\hat{\mathbf{k}}_2)}. \tag{2.28}$$
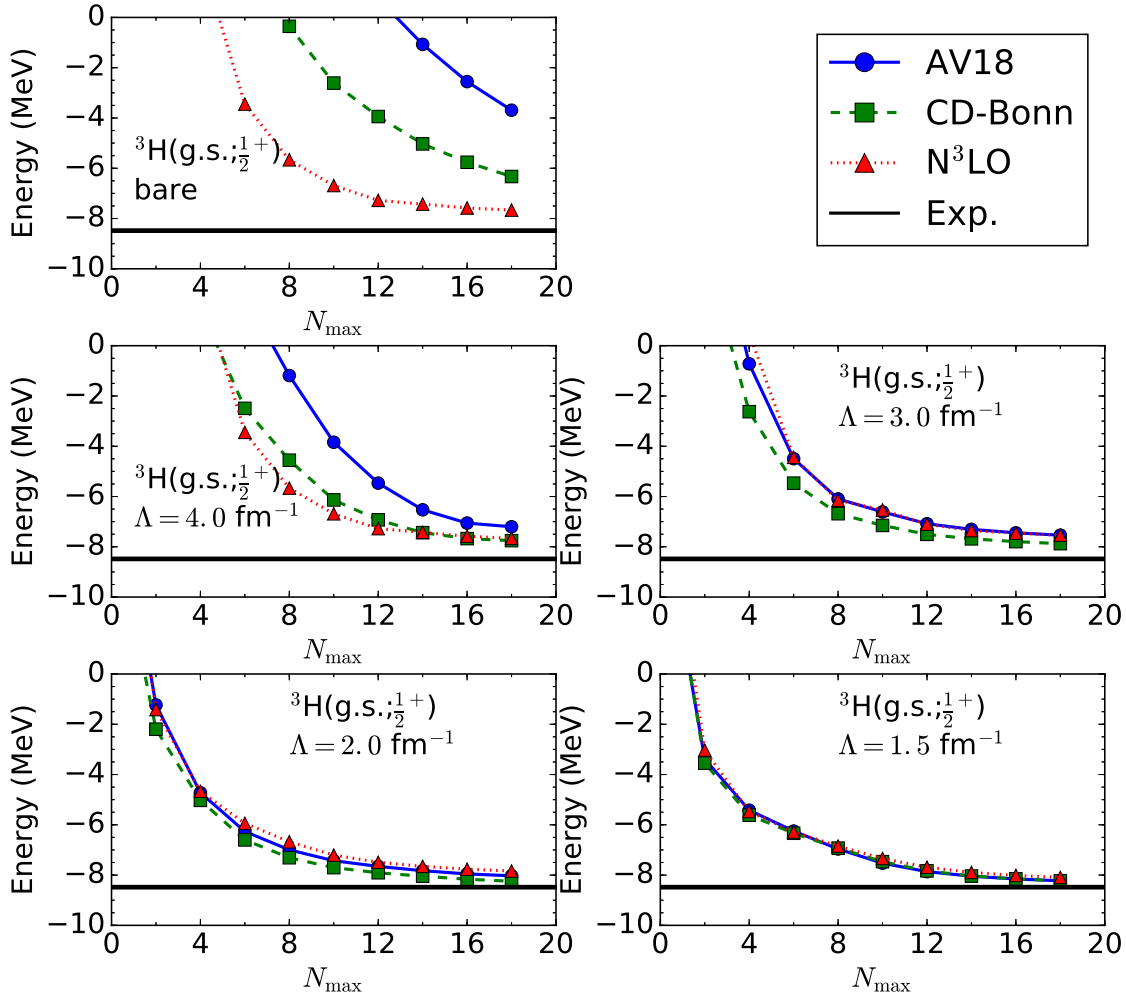
Figure 2.10: The ground-state energies for triton (^{3}H).

The definition of the $V_{\text{low k}}$ in this thesis is

$$V_{\text{low k}}(\hat{\mathbf{k}}, \hat{\mathbf{k}}') = P_\Lambda \left[\widetilde{H}_{12}(\hat{\mathbf{k}}, \hat{\mathbf{k}}') - \frac{1}{2}\mathbf{k}^2 \delta(\mathbf{k} - \mathbf{k}') \right] P_\Lambda. \tag{2.29}$$

Also, similar formulation would be possible for the many-body system and one can obtain the many-body induced interactions. Note that the Gauss-Legendre quadrature is employed, in the actual numerical calculation.

Now, let us see the features of $V_{\text{low k}}$ interaction. Fig. 2.7 shows the evolutions of $V_{\text{low k}}$ interactions represented in the momentum space for proton-neutron $^1S_0$ channel. As demonstrated in Fig. 2.7, the interaction limited to small square whose size is Λ. Moreover, one can observe that the interaction-model dependence looks to be collapsed as Λ decreases. To make sure numerically this, we plot the diagonal components of $V_{\text{low k}}$ interaction for proton-neutron $^1S_0$ in Fig. 2.8. We can see that the quantitative collapse occurs around $\Lambda = 2$ fm^{-1}. This suggests us the universality of $V_{\text{low k}}$ interactions. Note that this universality is observed for all partial-wave channels.
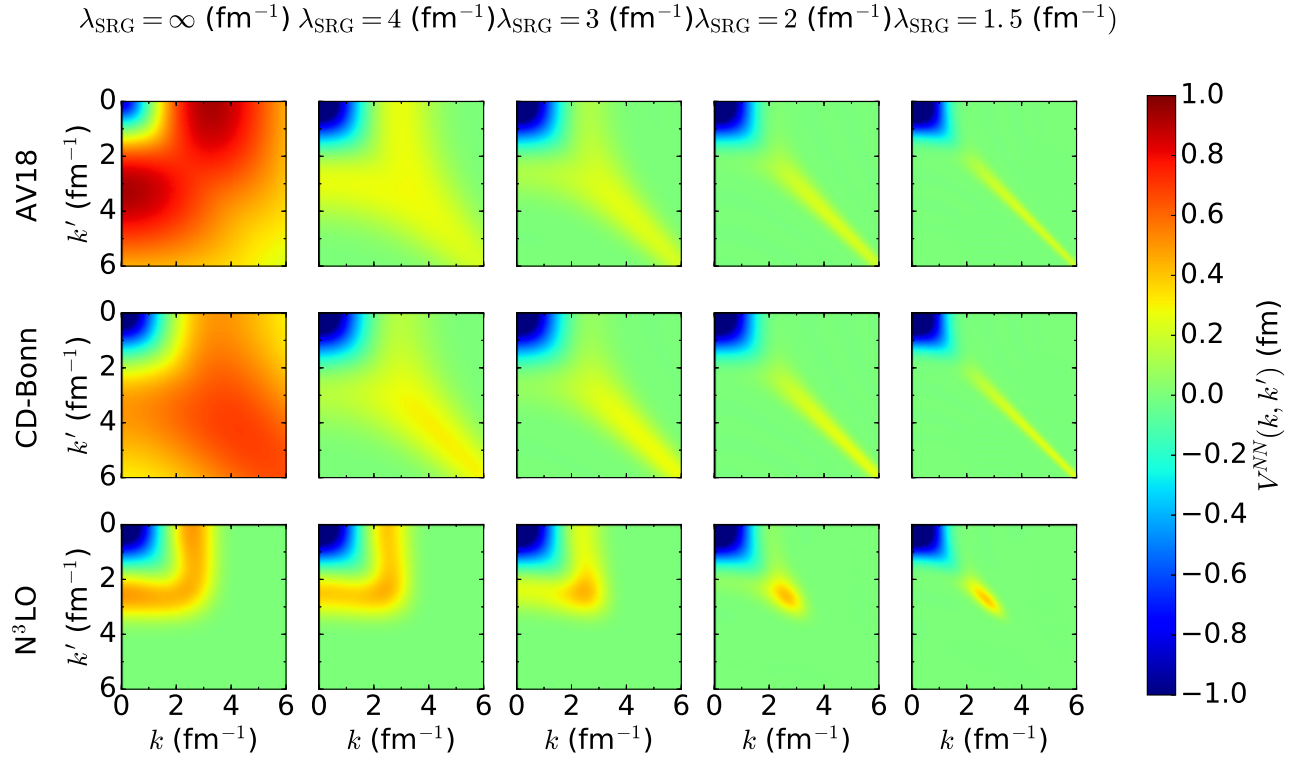
Figure 2.11: The SRG transformed *NN* interactions for *pn* $^1S_0$ channel derived from AV18 (top), CD-Bonn (middle), and N^{3}LO (bottom) interactions as functions of relative momentum k and k'. Interactions shown here are evolved from $\lambda_{\mathrm{SRG}} = \infty$ fm^{-1} (left) to $\lambda_{\mathrm{SRG}} = 1.5$ fm^{-1} (right).

Next, we check the removal of the repulsive core. Fig. 2.9 shows the evolution of $V_{\mathrm{low\ k}}$ interactions after the local projection [46] for proton-neutron $^1S_0$ channel. As found in this figure, the suppression of short-range singularity are observed with decreasing Λ. In the figures with $\Lambda \leq 2.0$ fm^{-1}, the repulsive part of the interaction is completely removed. One may think the breaking of the Pauli exclusion principle, due to the melt down of the core part of the *NN* interaction. However, let us remind that the interaction in shorter than around $1/\Lambda$ is no longer valid. Same as the momentum representation, the universality of $V_{\mathrm{low\ k}}$ interactions is confirmed in the coordinate representation.

Finally, we see the speed up of the convergence with calculations of the ground-state energy for the triton in Fig. 2.10. Especially, for $\Lambda \lesssim 3$ fm^{-1} we can find the converged results. As expected from the collapse of the interaction-model dependence, for $\Lambda \lesssim 3$ fm^{-1}, the converged results are practically independent of the initial interaction. While, the converged results depend on Λ due to the effect of the truncated induced three-nucleon (3*N*) interaction. The derivation of $V_{\mathrm{low\ k}}$ interaction is formulated in the *NN* system, and so far, the contributions of the induced 3*N* interactions are investigated with the similarity renormalization group (SRG) [56, 57].
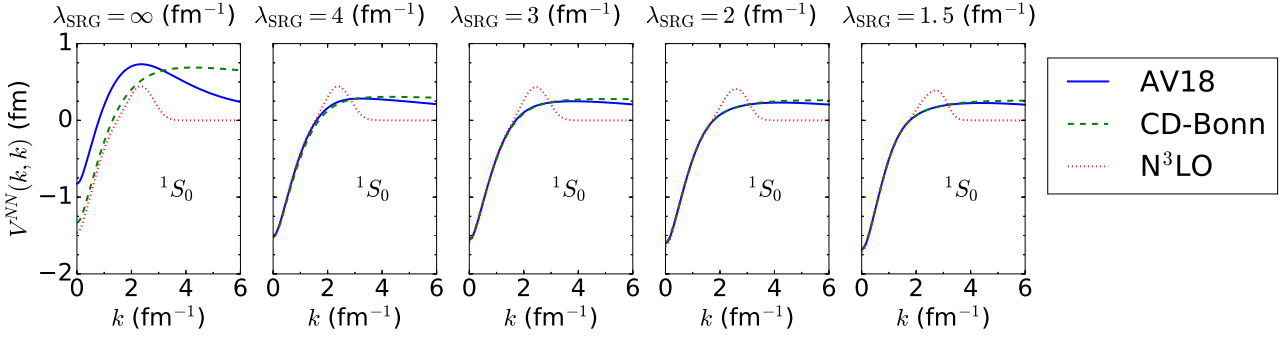
Figure 2.12: The diagonal component of the SRG transformed *NN* interactions for *pn* $^1S_0$ channel derived from AV18 (solid line), CD-Bonn (dashed line), and N^{3}LO (dotted line) interactions and evolved from $\lambda_{\mathrm{SRG}} = \infty$ fm^{-1} (left) to $\lambda_{\mathrm{SRG}} = 1.5$ fm^{-1} (right).
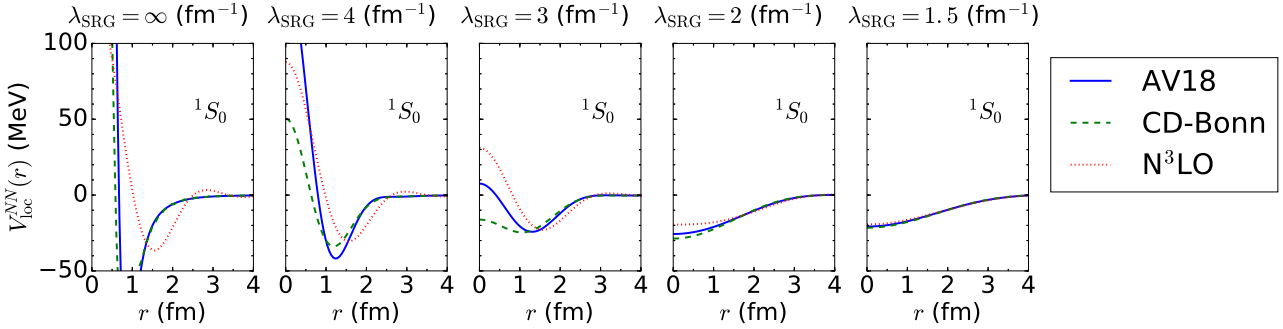
Figure 2.13: The SRG transformed *NN* interactions after local projection [46] for *pn* $^1S_0$ channel derived from AV18 (solid line), CD-Bonn (dashed line), and N^{3}LO (dotted line) interactions and evolved from $\lambda_{\mathrm{SRG}} = \infty$ fm^{-1} (left) to $\lambda_{\mathrm{SRG}} = 1.5$ fm^{-1} (right).

2.2.3 Similarity Renormalization Group

As the another way to decouple the low- and high-momentum regions, the SRG method is known [58]. In the $V_{\mathrm{low\ k}}(\mathbf{k}, \mathbf{k}')$ interaction, our goal is to construct the interaction renormalized into small square satisfying $|\mathbf{k}|, |\mathbf{k}'| \leq \Lambda$. On the other hand, we here aim the transformed Hamiltonian having the band diagonal form with the SRG transformation.

We firstly consider the unitary transformation of the initial Hamiltonian,

$$H(\alpha) = U^\dagger(\alpha)H(0)U(\alpha), \tag{2.30}$$

with the operator $U(\alpha)$. Here, α is called as the flow parameter which relates with the energy scale of $H(\alpha)$. In the SRG approach, we obtain $H(\alpha)$ by continuous transformation defined at each value of α. To do this, we take the derivative of Eq. (2.30),

$$\frac{H(\alpha)}{d\alpha} = \frac{dU^\dagger(\alpha)}{d\alpha}U(\alpha)H(\alpha) + H(\alpha)U^\dagger(\alpha)\frac{dU(\alpha)}{d\alpha}. \tag{2.31}$$
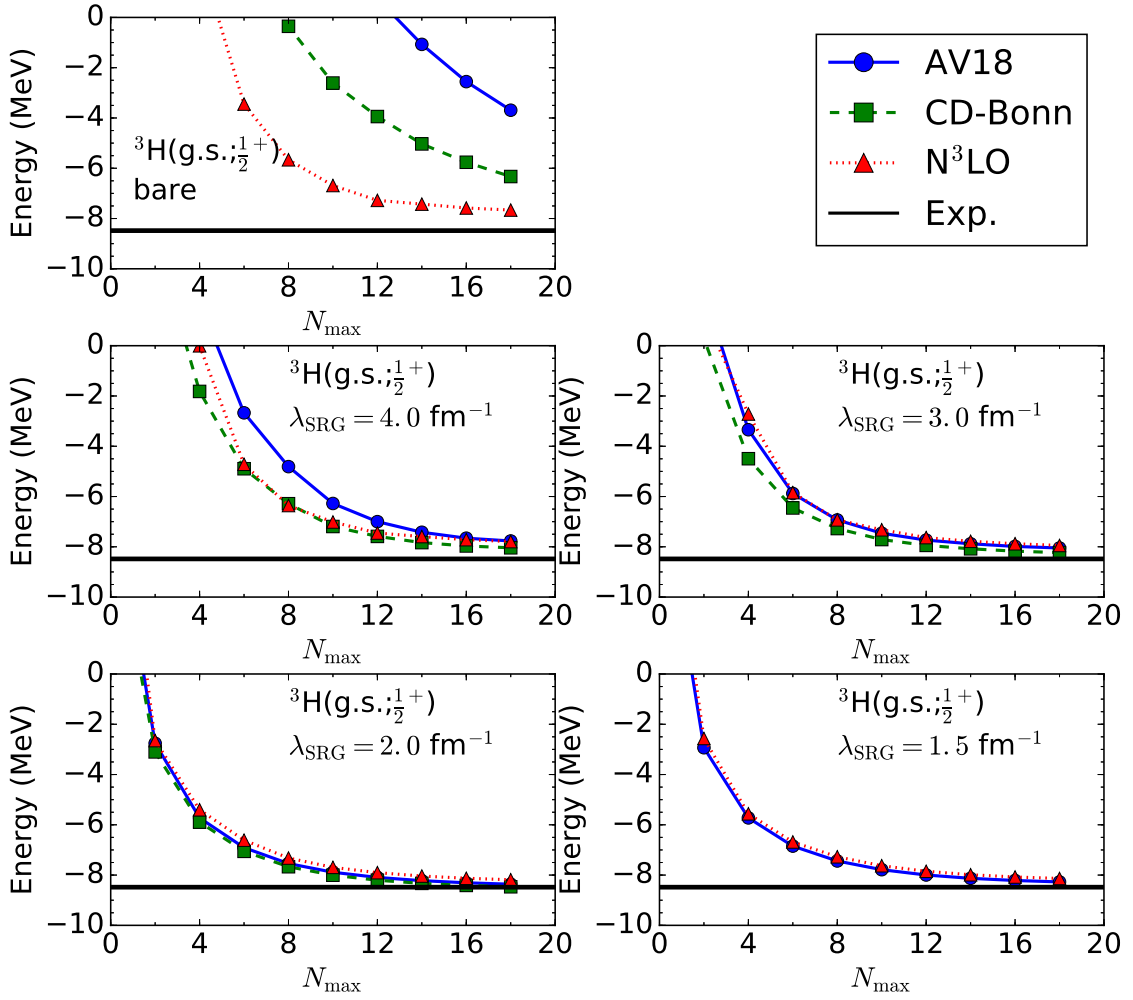
Figure 2.14: The ground-state energies for triton (^{3}H).

By using the identity,

$$0 = \frac{d\left(U^\dagger(\alpha)U(\alpha)\right)}{d\alpha} = \frac{dU^\dagger(\alpha)}{d\alpha}U(\alpha) + U^\dagger(\alpha)\frac{dU(\alpha)}{d\alpha}, \quad (2.32)$$

the operator $\eta(\alpha)$ is defined as

$$\eta(\alpha) = \frac{dU^\dagger(\alpha)}{d\alpha}U(\alpha). \quad (2.33)$$

Obviously, $\eta(\alpha)$ has to satisfy the anti-Hermitian condition $\eta^\dagger(\alpha) = -\eta(\alpha)$. The standard choice of $\eta(\alpha)$ is the commutator of arbitrary operator $G(\alpha)$ with the Hamiltonian $H(\alpha)$,

$$\eta(\alpha) = [G(\alpha), H(\alpha)]. \quad (2.34)$$

Here, $G(\alpha)$ is called as the generator of the SRG transformation. The choice of $G(\alpha)$ widely used is $G(\alpha) = T$ with the kinetic energy term,

$$T = \frac{1}{2}\mathbf{k}^2. \quad (2.35)$$

Note that one can take the other choices as discussed in Ref [59]. Then, our flow equation Eq. (2.31) becomes

$$\frac{dH(\alpha)}{d\alpha} = [[T, H(\alpha)], H(\alpha)].$$ (2.36)

Writing down this equation explicitly, we have

$$\frac{dV(\mathbf{k}, \mathbf{k}; \alpha)}{d\alpha} = -\frac{1}{4}(k^2 - \mathbf{k'}^2)^2 V(\mathbf{k}, \mathbf{k'}; \alpha) + \frac{1}{2} \int d^3\mathbf{q} V(\mathbf{k}, \mathbf{q}; \alpha)(k^2 - 2\mathbf{q}^2 + \mathbf{k'}^2) V(\mathbf{q}, \mathbf{k'}; \alpha).$$ (2.37)

The definition of the interaction is $V(\mathbf{k}, \mathbf{k'}; \alpha) = H(\mathbf{k}, \mathbf{k'}; \alpha) - T$. In the actual calculations, we solve Eq. (2.37) with the Gauss-Legendre quadrature. For the matrix element far from the diagonal which means $|k^2 - \mathbf{k'}^2| >> V(\alpha)$, the second term in the right hand side in Eq. (2.37) is much smaller than the first term and, the matrix element is

$$V(\mathbf{k}, \mathbf{k'} : \alpha) \simeq V(\mathbf{k}, \mathbf{k'} : \alpha = 0)e^{\alpha(k^2 - \mathbf{k'}^2)^2/4}.$$ (2.38)

As found in this equation, the off diagonal matrix element, far from the diagonal, is exponentially suppressed with increasing α. Since the exponent has to be dimensionless, α has unit of fm^4. It is useful to define the alternative flow parameter $\lambda_{\text{SRG}} = \alpha^{-1/4}$. Note that λ_{SRG} has unit of fm^{-1} which is same as the momentum.

Now, let us see the features of SRG transformed interaction. Figs. 2.11 show evolutions of SRG transformed interactions represented in the momentum space for proton-neutron $^1S_0$ channel. As demonstrated in Fig. 2.11, the coupling is decoupled at the value of λ_{SRG}. Moreover, one can observe that the interaction-model dependence looks to be collapsed as λ_{SRG} decreases. Same as in the case of $V_{\text{low k}}$ interaction, we plot the diagonal components of the SRG transformed *NN* interaction for proton-neutron $^1S_0$ in Fig. 2.12 to check the collapse of the model-dependence at $k \leq \lambda_{\text{SRG}}$. Similarly to the $V_{\text{low k}}$ interaction, the collapse of the model-dependence occurs around $\lambda_{\text{SRG}} = 2$ fm^{-1} and universality of the SRG transformed *NN* interaction is appeared.

Similarly to the case of $V_{\text{low k}}$ interactions, we can confirm the suppression of the repulsive core in the SRG transformed *NN* interactions. Fig. 2.9 shows the evolution of SRG transformed *NN* interactions after the local projection [46] for proton-neutron $^1S_0$ channel. As found in this figure, the suppression of short-range singularity are observed with decreasing Λ. In the figures with $\lambda_{\text{SRG}} \leq 2.0$ fm^{-1}, the repulsive part of the interaction is completely vanished.

One can observe the acceleration of the convergence from the triton ground-state energies shown in Fig. 2.14. Note that the SRG evolution at $\lambda_{\text{SRG}} = 1.5$ fm^{-1} of CD-Bonn interaction is numerically unstable and omitted in Fig. 2.14. Same as the $V_{\text{low k}}$ interactions cases, it is observed that the ground-state energies do not depend on the choice of the initial-interactions and depend on λ_{SRG}. This λ_{SRG}-dependence can be reduced by including the induced three-nucleon interaction [56, 57].

One of the advantages in use, instead of the $V_{\text{low k}}$ procedure, of the SRG transformation is simplicity of the extension to the *A*-body system. Although, we use only the *NN* interactions in the present study, the three-body SRG transformation is noted [16]. Let $H(\alpha)$ be the three-body Hamiltonian evolved to α,

$$H(\alpha) = T_{\text{rel}} + V_{12}(\alpha) + V_{23}(\alpha) + V_{31}(\alpha) + V_{123}(\alpha) = T_{\text{rel}} + V(\alpha).$$ (2.39)

Note that the three-body interaction $V_{123}(\alpha)$ appears even if the initial Hamiltonian is associated with only the *NN* interaction. The relative kinetic energy term can be decomposed into

$$T_{\text{rel}} = T_{12} + T_3 = T_{23} + T_1 = T_{31} + T_2, \tag{2.40}$$

and so T_i can commute with the two-body interaction V_{jk}. Since T_{rel} is independent of α, the three-body SRG flow equation is

$$\frac{dH(\alpha)}{d\alpha} = \frac{dV_{12}(\alpha)}{d\alpha} + \frac{dV_{23}(\alpha)}{d\alpha} + \frac{dV_{31}(\alpha)}{d\alpha} + \frac{dV_{123}(\alpha)}{d\alpha} = [[T_{\text{rel}}, V(\alpha)], H(\alpha)]. \tag{2.41}$$

Using the two-body SRG flow equations,

$$\frac{dV_{ij}(\alpha)}{d\alpha} = [[T_{ij}, V_{ij}(\alpha)], (T_{ij} + V_{ij}(\alpha))], \tag{2.42}$$

we can extract the flow equation for the three-body interaction,

$$\frac{dV_{123}(\alpha)}{d\alpha} = \sum_{(ijk)}^{3} \{[[T_{ij}, V_{ij}(\alpha)], (T_k + V_{ki} + V_{jk} + V_{ijk})]\} + [[T_{\text{rel}}, V_{123}], H(\alpha)]. \tag{2.43}$$

Here, $\sum_{(ijk)}^{3}$ acts as $\sum_{(ijk)}^{3} f(ijk) = f(123) + f(231) + f(312)$.

Chapter 3

Unitary-Model-Operator Approach

As mentioned in Chap. 2, the applications of the exact diagonalization are almost impossible for heavier system beyond the mass number (A) around 12. Then, it is unavoidable to use the some approximations. To consider the acceptable approximations, we should recall the two fundamental nuclear properties. First, the mean free path of nucleon in nucleus is comparable the size of nucleus. Second, the energy scale of nucleons in nucleus is several MeV. These imply that the nucleon-nucleon scattering rarely happens in the nucleus and the nucleons near the Fermi surface play the important role. One might think of that the Hartree-Fock (HF) method can be good approximation to understand such systems. However, the HF calculations with the realistic NN interactions fail to reproduce even the ground-state properties of stable nuclei, see Table 1.1, because the realistic NN interactions induce the many-body correlations which cannot be included in the HF method. We should take into account the many-body correlations to understand the nuclear structure with the realistic NN interactions. Therefore, we consider the particle-hole excitations on top of the reference state.

In this chapter, we discuss the theoretical structure of the UMOA. The UMOA is firstly introduced based on the cluster expansion by Providência and Shakin to investigate the effects of the short-range correlation to the nuclear wave function [35, 36]. Then, the correlation operator and short-range correlation were empirically determined and discussed. The self-consistent determination of the correlation operator was established in Refs. [37, 60]. In the UMOA, we perform the Okubo-Lee-Suzuki transformation for many-body Hamiltonian to decouple the $np n$h excitations. In Sec. 3.1, the general transformed Hamiltonian in the UMOA is discussed to clarify frameworks employed in earlier and this works. In Sec. 3.2, we discuss the decoupling equation determining the transformation employed in the UMOA. In Sec. 3.3, how to calculate the observables in the UMOA are mentioned. The calculation method for excited states and neighbors of shell closures are discussed in Sec. 3.4. Finally, the actual calculation procedure is given in Sec. 3.5

3.1   Similarity Transformation

Let us start from the many-body Schrödinger equation,

$$H|\Psi\rangle = E|\Psi\rangle, \tag{3.1}$$

with the energy E and wave function $|\Psi\rangle$. At this stage, we consider only the ground state. The excited state can be described by the particle-hole excitations from the ground-state and how to calculate is discussed in Sec. 3.4. The H is a general intrinsic Hamiltonian,

$$H = \sum_i^A \frac{\mathbf{p}_i^2}{2m} - T_{\text{c.m.}} + \sum_{i<j}^A V_{ij} + \sum_{i<j<k}^A V_{ijk} + \cdots, \tag{3.2}$$

with the mass number A, the momentum of the ith nucleon $\mathbf{p}_i$, the nucleon mass m, the NN interaction V_{ij}, the three-nucleon interaction V_{ijk}, and so on. Here, T_{CM} denotes the center-of-mass (CM) kinetic energy and can be decomposed into

$$T_{\text{CM}} = \frac{\mathbf{P}_{\text{CM}}}{2mA} = \sum_i^A \frac{\mathbf{p}_i^2}{2Am} + \sum_{i<j}^A \frac{\mathbf{p}_i \cdot \mathbf{p}_j}{Am}. \tag{3.3}$$

Then, H can be rewritten as

$$H = \sum_i^A t_i + \sum_{i<j}^A v_{ij} + \sum_{i<j<k}^A v_{ijk} + \cdots, \tag{3.4}$$

with $t_i = \frac{A-1}{A}\frac{\mathbf{p}_i^2}{2m}$, $v_{ij} = V_{ij} - \mathbf{p}_i \cdot \mathbf{p}_j/Am$, $v_{ijk} = V_{ijk}$, etc.

   To decouple the 0p0h state with npnh states, the similarity transformation of the original Hamiltonian is considered,

$$\widetilde{H} = U^\dagger(H + W)U - U^\dagger W U, \tag{3.5}$$

with the unitary operator U. Here, W is introduced as the auxiliary potential to consider the medium effect and is

$$W = \sum_{i=1}^A W^{(i)}. \tag{3.6}$$

The superscript (i) means the number of interacting particles. The one-, two- and n-body auxiliary potentials are, for example,

$$W^{(1)} = \sum_{i=1}^A w_i, \tag{3.7}$$

$$W^{(2)} = \sum_{i<j}^A w_{ij}, \tag{3.8}$$

$$W^{(n)} = \sum_{i_1<i_2<\cdots<i_n}^A w_{i_1 i_2 \cdots i_n}. \tag{3.9}$$

Here, $w_{i_1 \cdots i_n}$ is the n-body auxiliary potential acting on the particles labeled i_1 to i_n. At this stage, auxiliary potentials are completely arbitrary. In the actual calculations, we determine W self-consistently with the transformed interactions appeared in Eqs. (3.26) and (3.27). Details are discussed in the end

of this section. With this transformation (3.5), the original Schrödinger equation, Eq. (3.1), is also transformed to

$$\widetilde{H}|\Phi\rangle = E|\Phi\rangle, \tag{3.10}$$

where,

$$|\Phi\rangle = U^{\dagger}|\Psi\rangle. \tag{3.11}$$

Here, $|\Phi\rangle$ is introduced as the reference state. Since $|\Phi\rangle$ is, in principle, arbitrary, we can take the simplest form as $|\Phi\rangle$. In this thesis, we take $|\Phi\rangle$ as a single Slater determinant such as the particle-hole vacuum and Hartree-Fock (HF) states. The definition of the operator U is not unique, and leads the different calculation method such as the coupled-cluster method. Here, we define that U is the products of the exponential operators [61],

$$U = e^{S^{(1)}} e^{S^{(2)}} \cdots e^{S^{(n)}}. \tag{3.12}$$

The exponents $S^{(1)}$, $S^{(2)}$, ..., $S^{(n)}$ are the one-, two-, ..., and n-body correlation operators, and are defined as

$$S^{(1)} = \sum_{i}^{A} s_i, \tag{3.13}$$

$$S^{(2)} = \sum_{i<j}^{A} s_{ij}, \tag{3.14}$$

$$S^{(n)} = \sum_{i_1<\cdots<i_n}^{A} s_{i_1\cdots i_n}, \tag{3.15}$$

respectively. Here, $s_{i_1\cdots i_n}$ is correlation operator acting on n particles labeled by $i_1, \cdots, i_n$. The correlation operators are anti-Hermitian and have to satisfy

$$S^{(n)\dagger} = -S^{(n)}, \tag{3.16}$$

because U is unitary.

We note the property of the correlation operators. The condition Eq. (3.16) corresponds to that the correlation operators can be decomposed into

$$S^{(n)} = T^{(n)} - T^{(n)\dagger}. \tag{3.17}$$

Here, $T^{(n)}$ is n-particle-n-hole excitation operator constructed by n-particle and n-hole creation operators. Also, $T^{(n)\dagger}$ is n-particle-n-hole de-excitation operator and includes only annihilation operators. The $T^{(n)\dagger}$ relate with the cluster operator appeared in the CCM. The formulation of the coupled-cluster theory is briefly given in Appendix C. Since $T^{(n)}$ is only composed by creation operators and is Fermion operator, every $T^{(n)}$ is commutable each other,

$$\left[T^{(m)}, T^{(n)}\right] = 0. \tag{3.18}$$
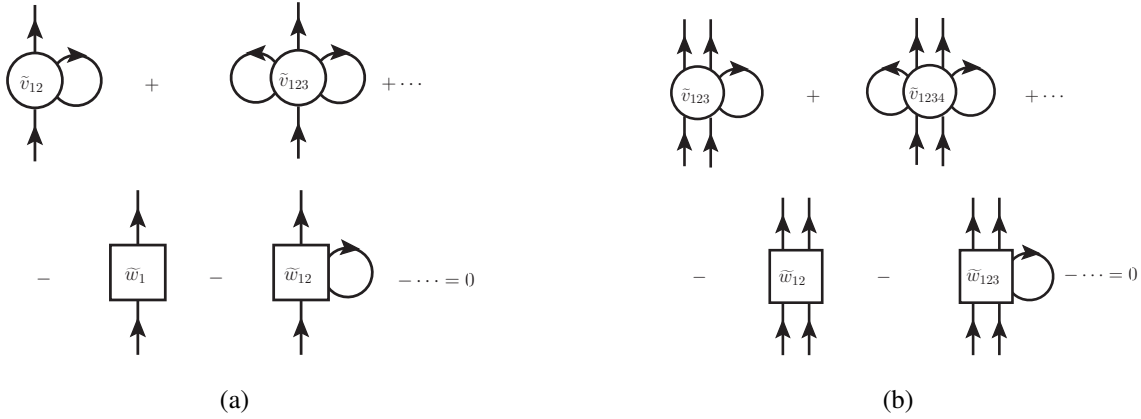
Figure 3.1: Cancellations of bubble-diagram contributions for one-body (a) and two-body (b) parts.

Obviously, we have

$$\left[T^{(m)\dagger}, T^{(n)\dagger}\right] = 0. \tag{3.19}$$

In contrast, $S^{(n)}$ is generally not commutable because both of creation and annihilation operators are included in $S^{(n)}$. The commutation relations for $S^{(n)}$ are

$$\left[S^{(m)}, S^{(n)}\right] = 0 \quad \text{for } m = n = 1,$$

$$\left[S^{(m)}, S^{(n)}\right] \neq 0 \quad \text{otherwise.} \tag{3.20}$$

Generally, the transformed Hamiltonian $\widetilde{H}$ can be expanded by the Baker-Campbell-Hausdorff (BCH) formula as found in the CCM [24]. The BCH expansion terminates with the finite order in the CCM becaus of Eq. (3.19). This is one of the advantages of using the CCM. In contrast, the BCH expansion does not terminate with the finite order in the UMOA, due to Eq. (3.20). Instead of using the BCH formula, the UMOA employs the cluster expansion introduced by Providência and Shakin [35]. We decompose $\widetilde{H}$ into

$$\widetilde{H} = \widetilde{H}^{(1)} + \widetilde{H}^{(2)} + \widetilde{H}^{(3)} + \cdots, \tag{3.21}$$

according to the number of interacting particles. Note that the three- and higher-body terms can be induced by the transformation, even if the initial Hamiltonian includes up to the two-body interaction. Here, we show the explicit expressions of the one-, two-, and n-body cluster terms as examples:

$$\widetilde{H}^{(1)} = \sum_i^A \widetilde{h}_i, \tag{3.22}$$

$$\widetilde{H}^{(2)} = \sum_{i<j}^A \widetilde{v}_{ij} - \sum_i^A \widetilde{w}_i, \tag{3.23}$$

$$\widetilde{H}^{(n)} = \sum_{i_1<\cdots<i_n}^A \widetilde{v}_{i_1\cdots i_n} - \sum_{i_1<\cdots<i_{n-1}}^A \widetilde{w}_{i_1\cdots i_{n-1}}, \quad \text{for} \quad 3 \leq n \leq A, \tag{3.24}$$

with

$$\widetilde{h}_1 = e^{-s_1} h_1 e^{s_1} = e^{-s_1}(t_1 + w_1)e^{s_1}, \tag{3.25}$$

$$\widetilde{v}_{12} = e^{-s_{12}} e^{-(s_1+s_2)}(h_1 + h_2 + v_{12} + w_{12})e^{s_1+s_2}e^{s_{12}} - (\widetilde{h}_1 + \widetilde{h}_2), \tag{3.26}$$

$$\widetilde{v}_{12\cdots n} = e^{-s_{1\cdots n}} \cdots e^{-(\sum_{i<j} s_{ij})} e^{-(\sum_i s_i)} \left(\sum_i h_i + \sum_{k=2}^{n} \sum_{i_1 < \cdots < i_k} v_{i_1 \cdots i_k} + \sum_{k=2}^{n} \sum_{i_1 < \cdots < i_k} w_{i_1 \cdots i_k} \right) e^{\sum_i s_i} e^{\sum_{i<j} s_{ij}} \cdots e^{s_{1\cdots n}}$$
$$- \left(\sum_i \widetilde{h}_i + \sum_{k=2}^{n-1} \sum_{i_1 < \cdots < i_k} \widetilde{v}_{i_1 \cdots i_k} \right), \quad \text{for} \quad 3 \le n \le A. \tag{3.27}$$

Also, the transformed auxiliary potentials $\widetilde{w}_1$ and $\widetilde{w}_{12}$ in Eqs. (3.22) and (3.23) are

$$\widetilde{w}_1 = e^{-s_1} w_1 e^{s_1}, \tag{3.28}$$

$$\widetilde{w}_{12} = e^{-s_{12}} e^{-(s_1+s_2)}(w_1 + w_2 + w_{12})e^{s_1+s_2}e^{s_{12}} - (\widetilde{w}_1 + \widetilde{w}_2). \tag{3.29}$$

More generally, we have the *n*-body transformed auxiliary potential,

$$\widetilde{w}_{12\cdots n} = e^{-s_{12\cdots n}} \cdots e^{-(\sum_{i<j} s_{ij})} e^{-(\sum_i s_i)} \left(\sum_{k=1}^{n} \sum_{i_1 < i_2 < \cdots < i_k} w_{i_1 i_2 \cdots i_k} \right) e^{\sum_i s_i} e^{\sum_{i<j} s_{ij}} \cdots e^{s_{12\cdots n}} - \left(\sum_{k=1}^{n-1} \sum_{i_1 < i_2 < \cdots < i_k} \widetilde{w}_{i_1 i_2 \cdots i_k} \right). \tag{3.30}$$

To determine the transformed auxiliary potentials, we recall the one-body potential employed in the HF method. The one-body potential cancels with the bubble-diagram contributions of the two-body interaction in the HF calculations. This condition can be applied to the present case. Since the transformed Hamiltonian contains many-body transformed interactions and auxiliary potentials, the bubble-diagram contributions come from $\widetilde{v}_{12}$, $\widetilde{v}_{123}$, $\cdots$ and $\widetilde{w}_1$, $\widetilde{w}_{12}$, $\cdots$. The conditions of the cancellations for one- and two-body are shown in Fig. 3.1. The analytical expressions corresponding to Fig. 3.1 are

$$\sum_{\lambda \le \rho_F} \langle \alpha\lambda | \widetilde{v}_{12} | \beta\lambda \rangle + \frac{1}{2!} \sum_{\lambda\mu \le \rho_F} \langle \alpha\lambda\mu | \widetilde{v}_{123} | \beta\lambda\mu \rangle + \cdots - \langle \alpha | \widetilde{w}_1 | \beta \rangle - \sum_{\lambda \le \rho_F} \langle \alpha\lambda | \widetilde{w}_{12} | \beta\lambda \rangle - \cdots = 0, \tag{3.31}$$

for the one-body term and

$$\sum_{\lambda \le \rho_F} \langle \alpha\beta\lambda | \widetilde{v}_{123} | \gamma\delta\lambda \rangle + \frac{1}{2!} \sum_{\lambda\mu \le \rho_F} \langle \alpha\beta\lambda\mu | \widetilde{v}_{1234} | \gamma\delta\lambda\mu \rangle + \cdots - \langle \alpha\beta | \widetilde{w}_{12} | \gamma\delta \rangle - \sum_{\lambda \le \rho_F} \langle \alpha\beta\lambda | \widetilde{w}_{123} | \gamma\delta\lambda \rangle - \cdots = 0, \tag{3.32}$$

for the two-body term. Here, ρ_F denotes the Fermi level and $|\alpha_1 \cdots \alpha_n\rangle$ is antisymmetrized and normalized *n*-body state. The conditions of the cancellations for three- and higher-body terms are given in the same way. Thus, the matrix element of the transformed auxiliary potential is [61, 62]

$$\langle \alpha | \widetilde{w}_1 | \beta \rangle = \sum_{\lambda_1 \le \rho_F} \langle \alpha\lambda_1 | \widetilde{v}_{12} | \beta\lambda_1 \rangle - \frac{1}{2!} \sum_{\lambda_1 \lambda_2 \le \rho_F} \langle \alpha\lambda_1\lambda_2 | \widetilde{v}_{123} | \beta\lambda_1\lambda_2 \rangle + \cdots, \tag{3.33}$$

for the one-body field,

$$\langle \alpha\beta | \widetilde{w}_{12} | \gamma\delta \rangle = \sum_{\lambda_1 \le \rho_F} \langle \alpha\beta\lambda_1 | \widetilde{v}_{123} | \gamma\delta\lambda_1 \rangle - \frac{1}{2!} \sum_{\lambda_1 \lambda_2 \le \rho_F} \langle \alpha\beta\lambda_1\lambda_2 | \widetilde{v}_{1234} | \gamma\delta\lambda_1\lambda_2 \rangle + \cdots. \tag{3.34}$$

for the two-body field. In the same way, we can derive the matrix element of the general n-body transformed auxiliary potential,

$$\langle \alpha_1 \cdots \alpha_n | \widetilde{w}_{12\cdots n} | \beta_1 \cdots \beta_n \rangle = \sum_{m \geq 1} \frac{(-1)^{m+1}}{m!} \sum_{\lambda_1 \cdots \lambda_m \leq \rho_F} \langle \alpha_1 \cdots \alpha_n \lambda_1 \cdots \lambda_m | \widetilde{v}_{12\cdots n+m} | \beta_1 \cdots \beta_n \lambda_1 \cdots \lambda_m \rangle. \quad (3.35)$$

Note that we have the transformed auxiliary potentials up to $A - 1$-body terms and A-body term is not appeared. By solving Eqs. (3.28) and (3.29) inversely, the auxiliary potentials w_1 and w_{12} are given in terms of the transformed auxiliary potentials $\widetilde{w}_1$ and $\widetilde{w}_{12}$ [61, 62],

$$w_1 = e^{s_1} \widetilde{w}_1 e^{-s_1}, \quad (3.36)$$

$$w_{12} = e^{s_1+s_2} e^{s_{12}} (\widetilde{w}_1 + \widetilde{w}_2 + \widetilde{w}_{12}) e^{-s_{12}} e^{-(s_1+s_2)} - (w_1 + w_2). \quad (3.37)$$

Also, we have

$$w_{12\cdots n} = e^{\sum_i s_i} e^{\sum_{i<j} s_{ij}} \cdots e^{s_{12\cdots n}} \left(\sum_{k=1}^{n} \sum_{i_1 < i_2 < \cdots < i_k}^{n} \widetilde{w}_{i_1 i_2 \cdots i_k} \right) e^{-s_{12\cdots n}} \cdots e^{-(\sum_{i<j} s_{ij})} e^{-(\sum_i s_i)} - \left(\sum_{k=1}^{n-1} \sum_{i_1 < i_2 < \cdots < i_k}^{n} w_{i_1 i_2 \cdots i_k} \right), \quad (3.38)$$

for the general n-body auxiliary potential.

Before considering the physical meaning of this choice of the auxiliary potentials, we rewrite the operators in the second-quantization form. Let $c_a^\dagger$ and c_a be the creation and annihilation operators of the HO quantum state a. Here, a is the set of n_a, l_a, j_a, m_a, and t_a. The n_a, l_a, j_a, m_a, and t_a are the HO nodal quantum number, orbital angular momentum, total angular momentum, third component of total angular momentum, and the label distinguishing the proton and neutron, respectively. In terms of creation and annihilation operators, the one-, two- and n-body operators can be rewritten as

$$O^{(1)} = \sum_i o_i = \sum_{a_1 a_2} \langle a_1 | o | a_2 \rangle c_{a_1}^\dagger c_{a_2}, \quad (3.39)$$

$$O^{(2)} = \sum_{i<j} o_{ij} = \left(\frac{1}{2!} \right)^2 \sum_{a_1 a_2 a_3 a_4} \langle a_1 a_2 | o | a_3 a_4 \rangle c_{a_1}^\dagger c_{a_2}^\dagger c_{a_4} c_{a_3}, \quad (3.40)$$

$$O^{(n)} = \sum_{i_1 < \cdots < i_n} o_{i_1 \cdots i_n} = \left(\frac{1}{n!} \right)^2 \sum_{a_1 \ldots a_{2n}} \langle a_1 \cdots a_n | o | a_{n+1} \cdots a_{2n} \rangle c_{a_1}^\dagger \cdots c_{a_n}^\dagger c_{a_{2n}} \cdots c_{a_{n+1}}, \quad (3.41)$$

respectively. By using Eqs. (3.39), (3.40), and (3.41), the transformed Hamiltonian can be rewritten as

$$\widetilde{H} = \sum_{a_1 a_2} \langle a_1 | \widetilde{h}_1 | a_2 \rangle c_{a_1}^\dagger c_{a_2} + \left(\frac{1}{2!} \right)^2 \sum_{a_1 a_2 a_3 a_4} \langle a_1 a_2 | \widetilde{v}_{12} | a_3 a_4 \rangle c_{a_1}^\dagger c_{a_2}^\dagger c_{a_4} c_{a_3}$$

$$+ \left(\frac{1}{3!} \right)^2 \sum_{a_1 a_2 a_3 a_4 a_5 a_6} \langle a_1 a_2 a_3 | \widetilde{v}_{123} | a_4 a_5 a_6 \rangle c_{a_1}^\dagger c_{a_2}^\dagger c_{a_3}^\dagger c_{a_6} c_{a_5} c_{a_4} + \cdots$$

$$- \sum_{a_1 a_2} \langle a_1 | \widetilde{w}_1 | a_2 \rangle c_{a_1}^\dagger c_{a_2} + \left(\frac{1}{2!} \right)^2 \sum_{a_1 a_2 a_3 a_4} \langle a_1 a_2 | \widetilde{w}_{12} | a_3 a_4 \rangle c_{a_1}^\dagger c_{a_2}^\dagger c_{a_4} c_{a_3} - \cdots . \quad (3.42)$$

As discussed in the first paragraph of this chapter, we should consider the particle-hole excitations on top of the reference state. Since the transformed Hamiltonian Eq. (3.42) is written with respect to the nucleon vacuum state $|0\rangle$, we take the normal ordering of Eq. (3.42) with respect to the uncorrelated reference state $|\Phi\rangle$. Then, the transformed Hamiltonian is

$$\widetilde{H} = E_0 + \sum_{a_1 a_2} \langle a_1 | \widetilde{h}_1 | a_2 \rangle \colon c_{a_1}^\dagger c_{a_2} \colon + \left(\frac{1}{2!}\right)^2 \sum_{a_1 a_2 a_3 a_4} \langle a_1 a_2 | \widetilde{v}_{12} | a_3 a_4 \rangle \colon c_{a_1}^\dagger c_{a_2}^\dagger c_{a_4} c_{a_3} \colon$$
$$+ \left(\frac{1}{3!}\right)^2 \sum_{a_1 a_2 a_3 a_4 a_5 a_6} \langle a_1 a_2 a_3 | \widetilde{v}_{123} | a_4 a_5 a_6 \rangle \colon c_{a_1}^\dagger c_{a_2}^\dagger c_{a_3}^\dagger c_{a_6} c_{a_5} c_{a_4} \colon + \cdots, \qquad (3.43)$$

or compactly,

$$\widetilde{H} = E_0 + \sum_{a_1 a_2} \langle a_1 | \widetilde{h}_1 | a_2 \rangle \colon c_{a_1}^\dagger c_{a_2} \colon$$
$$+ \sum_{n \geq 2}^{A} \left(\frac{1}{n!}\right)^2 \sum_{a_1 \cdots a_{2n}} \langle a_1 \cdots a_n | \widetilde{v}_{1 \cdots n} | a_{n+1} \cdots a_{2n} \rangle \colon c_{a_1}^\dagger \cdots c_{a_n}^\dagger c_{a_{2n}} \cdots c_{a_{n+1}} \colon . \qquad (3.44)$$

Here, $\colon c_{a_1}^\dagger \cdots c_{a_n}^\dagger c_{a_{2n}} \cdots c_{a_{n+1}} \colon$ means that the n-creation and n-annihilation operators are normal ordered with respect to $|\Phi\rangle$ and satisfies

$$\colon c_{a_1}^\dagger \cdots c_{a_n}^\dagger c_{a_{2n}} \cdots c_{a_{n+1}} \colon |\Phi\rangle = 0. \qquad (3.45)$$

The E_0 is energy of reference state because of $\langle \Phi | \widetilde{H} | \Phi \rangle = E_0$, and is

$$E_0 = \sum_{a_1 \leq \rho_F} \langle a_1 | \widetilde{h}_1 | a_1 \rangle + \sum_{n \geq 2}^{A} \frac{(-1)^{n+1}}{n!} \sum_{a_1 \cdots a_n \leq \rho_F} \langle a_1 \cdots a_n | \widetilde{v}_{1 \cdots n} | a_1 \cdots a_n \rangle. \qquad (3.46)$$

For example, we show the energy up to the three-body cluster term:

$$E_0 \simeq \sum_{a_1 \leq \rho_F} \langle a_1 | \widetilde{h}_1 | a_1 \rangle - \frac{1}{2!} \sum_{a_1 a_2 \leq \rho_F} \langle a_1 a_2 | \widetilde{v}_{12} | a_1 a_2 \rangle + \frac{1}{3!} \sum_{a_1 a_2 a_3 \leq \rho_F} \langle a_1 a_2 a_3 | \widetilde{v}_{123} | a_1 a_2 a_3 \rangle. \qquad (3.47)$$

As clarified in Eq. (3.44), the transformed auxiliary potentials formally vanishes and the n-body part is described by only the n-body transformed interaction. The choice of the transformed auxiliary potentials in Eqs. (3.33), (3.34), and (3.35) leads the simple transformed Hamiltonian. According to Eqs (3.27), (3.35), and (3.38), $\widetilde{w}_1, \widetilde{w}_{12}, \cdots \widetilde{w}_{12 \cdots A-1}$ and $\widetilde{v}_1, \widetilde{v}_{12}, \cdots \widetilde{v}_{12 \cdots A}$ depend on each other. Therefore, we solve those iteratively in the actual calculations.

3.2 Decoupling Equation

The essential point in the UMOA is to determine the correlation operators. The correlation operators are determined so that the transformed Hamiltonian does not induce the particle-hole excitations. This

concept is very similar to the Okubo-Lee-Suzuki (OLS) transformation introduced in Sec. 2.2.1. The equations shown here overlap with those shown in Appendix B.

Since we have one-, two-, and many-body correlation operators in the UMOA, at first, we should mention how the correlation operators can be determined. Owing to the definition of the unitary operator U in Eq. (3.12), $\exp S^{(n)}$ appears only in the n- and higher-body cluster terms and does not affect the cluster terms lower than the n-body. For example, more than two-body correlation operators do not show up in Eq. (3.22) and (3.25). In other words, the determination of the n-body correlation operator does not depend on the determinations of the correlation operators lower than n-body and we solve correlation operators in the order from one-body to A-body.

Now, we focus on the determination of the n-body correlation operator $S^{(n)}$. The correlation operator $S^{(n)}$ is determined so that $\widetilde{H}^{(n)}$, appeared in Eq. (3.24), has no matrix elements between the 0p0h and npnh states. For this purpose, we define the projection operators $P^{(n)}$ and $Q^{(n)}$ projecting onto the space of n particles occupying the orbits below and above the Fermi level, respectively. Then, the decoupling condition can be written as

$$Q^{(n)}\widetilde{H}^{(n)}P^{(n)} = P^{(n)}\widetilde{H}^{(n)}Q^{(n)} = 0, \tag{3.48}$$

with $P^{(n)}$ and $Q^{(n)}$. Since $P^{(n)}$ and $Q^{(n)}$ have no common states, we have

$$Q^{(n)}\left(\sum_{i_n < \cdots < i_{n-1}}^{A} \widetilde{w}_{i_1 \cdots i_{n-1}} \right) P^{(n)} = 0, \tag{3.49}$$

$$Q^{(n)}\left(\sum_{i}^{n} \widetilde{h}_i + \sum_{k=2}^{n-1} \sum_{i_1 < \cdots < i_k}^{n} \widetilde{v}_{i_1 \cdots i_k} \right) P^{(n)} = 0, \tag{3.50}$$

in Eqs. (3.24) and (3.27). The decoupling condition, Eq. (3.48), can be rewritten as

$$Q^{(n)}e^{-S^{(n)}}\widetilde{H}'^{(n)}e^{S^{(n)}}P^{(n)} = P^{(n)}e^{-S^{(n)}}\widetilde{H}'^{(n)}e^{S^{(n)}}Q^{(n)} = 0, \tag{3.51}$$

with

$$\widetilde{H}'^{(n)} = e^{-(\sum_{i_1 < \cdots < i_{n-1}} s_{i_1 \cdots i_{n-1}})} \cdots e^{-(\sum_i s_i)} \left(\sum_i^n h_i + \sum_{k=2}^n \sum_{i_1 < \cdots < i_k}^n v_{i_1 \cdots i_k} + \sum_{k=2}^n \sum_{i_1 < \cdots < i_k}^n w_{i_1 \cdots i_k} \right) e^{\sum_i s_i} \cdots e^{\sum_{i_1 < \cdots < i_{n-1}} s_{i_1 \cdots i_{n-1}}}. \tag{3.52}$$

As discussed in Appendix B, one of the solutions of Eq. (3.51) is given by

$$S^{(n)} = \operatorname{arctanh}(\omega^{(n)} - \omega^{(n)\dagger}), \tag{3.53}$$

with

$$\omega^{(n)} = \sum_{k=1}^{d} Q^{(n)}|\psi_k^{(n)}\rangle\langle\widetilde{\phi}_k^{(n)}|P^{(n)}. \tag{3.54}$$

Here, d is the dimension of the $P^{(n)}$ space. The state $\langle\widetilde{\phi}_k^{(n)}|$ is bi-orthogonal state and is defined to satisfy

$$\langle\widetilde{\phi}_k^{(n)}|\phi_l^{(n)}\rangle = \delta_{kl}, \quad |\phi_k^{(n)}\rangle = P^{(n)}|\psi_k^{(n)}\rangle. \tag{3.55}$$
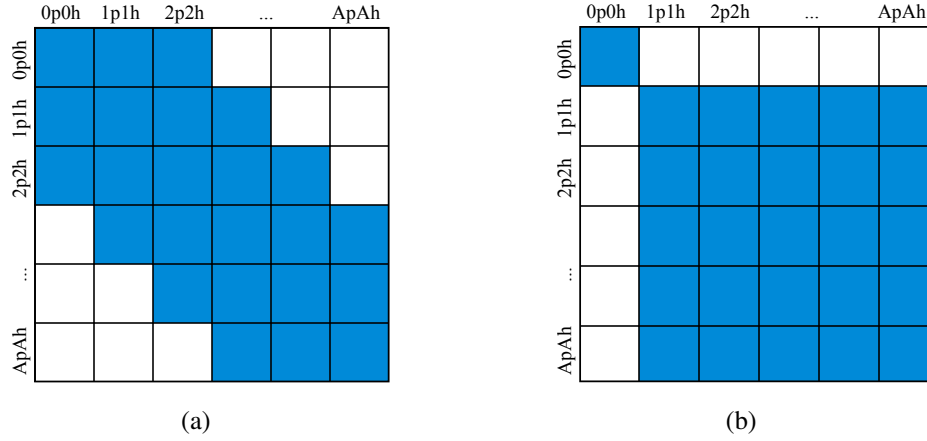
Figure 3.2: Schematic representations of original and transformed Hamiltonians. The left (right) panel shows the original (transformed) Hamiltonian. The shaded regions mean that the matrices have finite values.

Here, $|\psi_k^{(n)}\rangle$ is an eigenvector of the n-body Schrödinger equation in the $P^{(n)} + Q^{(n)}$ space,

$$(P^{(n)} + Q^{(n)})\widetilde{H}'^{(n)}(P^{(n)} + Q^{(n)})|\psi_k^{(n)}\rangle = E_k|\psi_k^{(n)}\rangle, \tag{3.56}$$

where E_k is a kth eigenvalue. Moreover, $\exp S^{(n)}$ can be expressed in terms of $\omega^{(n)}$ [27],

$$e^{S^{(n)}} = (1 + \omega^{(n)} - \omega^{(n)\dagger})(1 + \omega^{(n)\dagger}\omega^{(n)} + \omega^{(n)}\omega^{(n)\dagger})^{-1/2}. \tag{3.57}$$

The explicit expression of $e^{S^{(n)}}$ is given by Eqs. (B.52)- (B.55). Note that the solution of $\omega^{(n)}$ depends on the choice of a set of d eigenstates. In the present work, we choose d eigenstates with the largest overlap with the reference state. This choice is reasonable as long as we consider only the ground state.

3.3 Ground-State Energy and Observables

Here, we discuss the way to calculate the ground-state energy and expectation values of operators. Let us suppose that the correlation operators are determined. After solving the decoupling equations, we can construct $\widetilde{H}$, as discussed in Sec. 3.1. Figs. 3.2(a) and 3.2(b) show the schematic representations of original and transformed Hamiltonians. In Fig. 3.2(a), we assume that the original Hamiltonian constructed up to the two-body interaction. Note that the transformed Hamiltonian generally have the induced many-body interactions which are illustrated by the coupling, for example, between 1p1h and *ApAh* parts. As shown in Fig. 3.2(b), $\widetilde{H}$ must not induce 1p1h, 2p2h, $\cdots$, *ApAh* excitations. Therefore, the ground-state energy is equal to the energy by the reference state:

$$E_{\text{g.s.}} = \langle\Psi|H|\Psi\rangle = (\langle\Psi|U)U^\dagger H U(U^\dagger|\Psi\rangle) = \langle\Phi|\widetilde{H}|\Phi\rangle = E_0. \tag{3.58}$$

Here, E_0 is already given in Eq. (3.46).

Next, we mention how to obtain the expectation values in the UMOA. One of the advantages in the UMOA is that we can use the transformed operators to obtain the observables. In principle, one can use the transformed operator to obtain the observables in the CCM. Due to the non-Hermiticity in the CCM, however, one has to solve the coupled-cluster equation for the both of left and right eigenvector to obtain the transformation operator. In another way, one can apply the Hellmann-Feynman theorem to obtain the other observables, as found in the most of the recent works in the CCM (see e.g. [24]). In the UMOA, the calculation of observables is same as the energy case and is rather simple. Let O be an arbitrary operator which we want to calculate the expectation value.

$$O = \sum_{n=1}^{A} O^{(n)} = \sum_{n=1}^{A} \sum_{i_1 < \cdots < i_n}^{A} o_{i_1 \cdots i_n}. \tag{3.59}$$

Here, $o_{i_1 \cdots i_n}$ is n-body operator acting on particles labeled from i_1 to i_n. What we want to calculate here is

$$\langle \Psi | O | \Psi \rangle = \langle \Phi | \widetilde{O} | \Phi \rangle, \tag{3.60}$$

with

$$\widetilde{O} = U^\dagger O U. \tag{3.61}$$

In the same way as the Hamiltonian, we apply the cluster expansion to $\widetilde{O}$,

$$\widetilde{O} = \sum_{n=1}^{A} \widetilde{O}^{(n)} = \sum_{n=1}^{A} \sum_{i_1 < \cdots < i_n} \widetilde{o}_{i_1 \cdots i_n}. \tag{3.62}$$

Here, we show the explicit expression of one-, two-, and n-body transformed operators:

$$\widetilde{o}_1 = e^{-s_1} o_1 e^{s_1}, \tag{3.63}$$

$$\widetilde{o}_{12} = e^{-s_{12}} e^{-(s_1+s_2)} (o_1 + o_2 + o_{12}) - (\widetilde{o}_1 + \widetilde{o}_2), \tag{3.64}$$

$$\widetilde{o}_{1 \cdots n} = e^{-s_{1 \cdots n}} \cdots e^{-\sum_{i=1}^{n} s_i} \left(\sum_{k=1}^{n} \sum_{i_1 < \cdots < i_k} o_{i_1 \cdots i_k} \right) e^{\sum_{i=1}^{n} s_i} \cdots e^{s_{1 \cdots n}} - \left(\sum_{k=1}^{n-1} \sum_{i_1 < \cdots < i_k} \widetilde{o}_{i_1 \cdots i_k} \right). \tag{3.65}$$

By using the second quantization and taking the normal ordering with respect to $|\Phi\rangle$, the expectation value is

$$\langle \Phi | \widetilde{O} | \Phi \rangle = \sum_{n=1}^{A} \sum_{a_1 \cdots a_n \leq \rho_F} \frac{1}{n!} \langle a_1 \cdots a_n | \widetilde{o}_{1 \cdots n} | a_1 \cdots a_n \rangle. \tag{3.66}$$

The explicit expressions for various bare operators are given in Appendix E.1.

3.4   Equation of Motion Technique

So far, we discuss the ground-state of closed shell system with the mass number A. To extend the applicable region of the UMOA, we consult the equation of motion technique adopted in the CCM [24].

First, let us consider the excited states of A-body closed shell nuclei. As found in Sec. 3.3, the ground state for $\widetilde{H}$ is uncorrelated reference state $|\Phi^A\rangle$ of A-body system. Here, we add the superscript A meaning the mass number. Since, the excited states of $\widetilde{H}$ are orthogonal to the ground-state, in principle, those can be exhausted by the linear combinations of 1p1h, 2p2h, $\cdots$, ApAh excitations. Therefore, the excited state of A-body system labeled by k can be written as

$$|\Phi_k^A\rangle = \left[\sum_{a>\rho_F}\sum_{i\leq\rho_F} r_i^a c_a^\dagger c_i + \left(\frac{1}{2!}\right)^2 \sum_{ab>\rho_F}\sum_{ij\leq\rho_F} r_{ij}^{ab} c_a^\dagger c_b^\dagger c_j c_i + \cdots\right]|\Phi^A\rangle, \tag{3.67}$$

or

$$|\Phi_k^A\rangle = \sum_{n=1}^{A}\left(\frac{1}{n!}\right)^2 \sum_{a_1\cdots a_n>\rho_F}\sum_{i_1\cdots i_n\leq\rho_F} r_{i_1\cdots i_n}^{a_1\cdots a_n} c_{a_1}^\dagger \cdots c_{a_n}^\dagger c_{i_n}\cdots c_{i_1}|\Phi^A\rangle, \tag{3.68}$$

with the coefficients $r_{i_1\cdots i_n}^{a_1\cdots a_n}$ satisfying

$$\sum_{n=1}^{A}\left(\frac{1}{n!}\right)^4 \sum_{a_1\cdots a_n>\rho_F}\sum_{i_1\cdots i_n\leq\rho_F} \left(r_{i_1\cdots i_n}^{a_1\cdots a_n}\right)^2 = 1. \tag{3.69}$$

Note that we omit the k-dependence of $r_{i_1\cdots i_n}^{a_1\cdots a_n}$ for the simplicity. Since $|\Phi^A\rangle$ is factorized in Eq. (3.67), we can write Eq. (3.67) as

$$|\Phi_k^A\rangle = R_k^A|\Phi^A\rangle, \tag{3.70}$$

with the generator of excited state R_k^A:

$$R_k^A = \sum_{n=1}^{A}\left(\frac{1}{n!}\right)^2 \sum_{a_1\cdots a_n>\rho_F}\sum_{i_1\cdots i_n\leq\rho_F} r_{i_1\cdots i_n}^{a_1\cdots a_n} c_{a_1}^\dagger \cdots c_{a_n}^\dagger c_{i_n}\cdots c_{i_1}. \tag{3.71}$$

The Schrödinger equation for the excited state is

$$\widetilde{H}R_k^A|\Phi^A\rangle = E_k R_k^A|\Phi^A\rangle. \tag{3.72}$$

Here, E_k is the energy of the kth excited state. By solving Eq. (3.72), the coefficient $r_{i_1\cdots i_n}^{a_1\cdots a_n}$ is determined. Eq. (3.72) is eigenvalue problem of matrix $\widetilde{H}$ in the 1p1h, 2p2h, $\cdots$, ApAh spaces (larger shaded square in Fig. 3.2(b)). In the actual calculations, we have to truncate more than 2p2h excitations due to the dimension of the matrix. The explicit expressions for the matrix elements are given in Appendix D.2.

Similarly to the excited state, we can apply this approach to the system with the mass number $A \pm 1$. The generator for the $A + 1$ ($A - 1$) system is constructed to take into account the all possible excitations adding (removing) one-particle to (from) the reference state. Then, the generators of such states are

$$R_k^{A+1} = \sum_{a} r^a c_a^\dagger + \sum_{n=2}^{A}\frac{1}{n!(n-1)!} \sum_{a_1\cdots a_n>\rho_F}\sum_{i_1\cdots i_{n-1}\leq\rho_F} r_{i_1\cdots i_{n-1}}^{a_1\cdots a_n} c_{a_1}^\dagger \cdots c_{a_n}^\dagger c_{i_{n-1}}\cdots c_{i_1}, \tag{3.73}$$

$$R_k^{A-1} = \sum_{i} r_i c_i + \sum_{n=2}^{A}\frac{1}{n!(n-1)!} \sum_{a_1\cdots a_{n-1}>\rho_F}\sum_{i_1\cdots i_n\leq\rho_F} r_{i_1\cdots i_{n-1}}^{a_1\cdots a_n} c_{a_1}^\dagger \cdots c_{a_{n-1}}^\dagger c_{i_n}\cdots c_{i_1}. \tag{3.74}$$

Also, the Schrödinger equations are

$$\widetilde{H}(A+1)R_k^{A+1}|\Phi^A\rangle = E_k R_k^{A+1}|\Phi^A\rangle, \tag{3.75}$$

$$\widetilde{H}(A-1)R_k^{A-1}|\Phi^A\rangle = E_k R_k^{A-1}|\Phi^A\rangle. \tag{3.76}$$

Note that we should remind the A-dependence of $\widetilde{H}$ coming from the CM kinetic energy term, see Eq. (3.2). Unfortunately, the energy of the CM motions is comparable to that of the intrinsic motions in nuclear system. Since $\widetilde{H}(A \pm 1)$ is different from $\widetilde{H}(A)$, we have to recalculate $\widetilde{H}(A \pm 1)$ for the $(A \pm 1)$-body system. Due to the dimension of the Hamiltonian matrix, we diagonalize $\widetilde{H}$ in the 1p0h and 2p1h (0p1h and 1p2h) spaces for the $A + 1$ ($A - 1$) -body system. The matrix elements in such spaces are given in Appendix D.3 and D.4.

3.5   Actual Calculation Procedure

Here, we discuss the actual calculation procedures. Basically we truncates our formula at two-body level. The initial Hamiltonian is

$$H \simeq \sum_{i=1}^{A} t_i + \sum_{i<j}^{A} v_{ij}, \tag{3.77}$$

and the transformed Hamiltonian is

$$\widetilde{H} \simeq \sum_{i=1}^{A} \widetilde{h}_i + \sum_{i<j}^{A} \widetilde{v}_{ij}. \tag{3.78}$$

The auxiliary potential is $W \simeq \sum_{i=1}^{A} w_i$ and the transformed auxiliary potential is $\widetilde{W} \simeq \sum_{i=1}^{A} \widetilde{w}_i$. In this section, we introduce the two calculation methods. One is employed in former UMOA calculations which do not include the one-body correlation operator, named as *method I*. In *method I*, we employ the unitary transformation as $U \simeq e^{S^{(2)}}$. The other is employed in the recent UMOA calculations, named as *method II*. In *method II*, in addition to $S^{(2)}$, we introduce $S^{(1)}$ and the unitary transformation is defined as $U \simeq e^{S^{(1)}}e^{S^{(2)}}$.

3.5.1   *Method I*

Method I is employed in earlier UMOA works [39]. To obtain the converged results in the small model space, we adopt the two-step decoupling method in *method I*. The two-step decoupling method is commonly used, for example, in the G-matrix theory [63]. Fig. 3.3 shows how to decouple the model space. In the first-step decoupling, the original Hamiltonian is transformed so that our model space and its complement are decoupled, as shown by the dashed arrow in Fig. 3.3(a). Since the first-step decoupling is done in the huge space to take into account the short-range correlation of NN interaction, the decoupling equation is solved with the relative and CM coordinates. Thus, the first-step decoupling is very similar to the OLS transformations. Using the effective interaction, we decouple the 2p2h excitations with the reference state, as illustrated in Fig. 3.3(b).
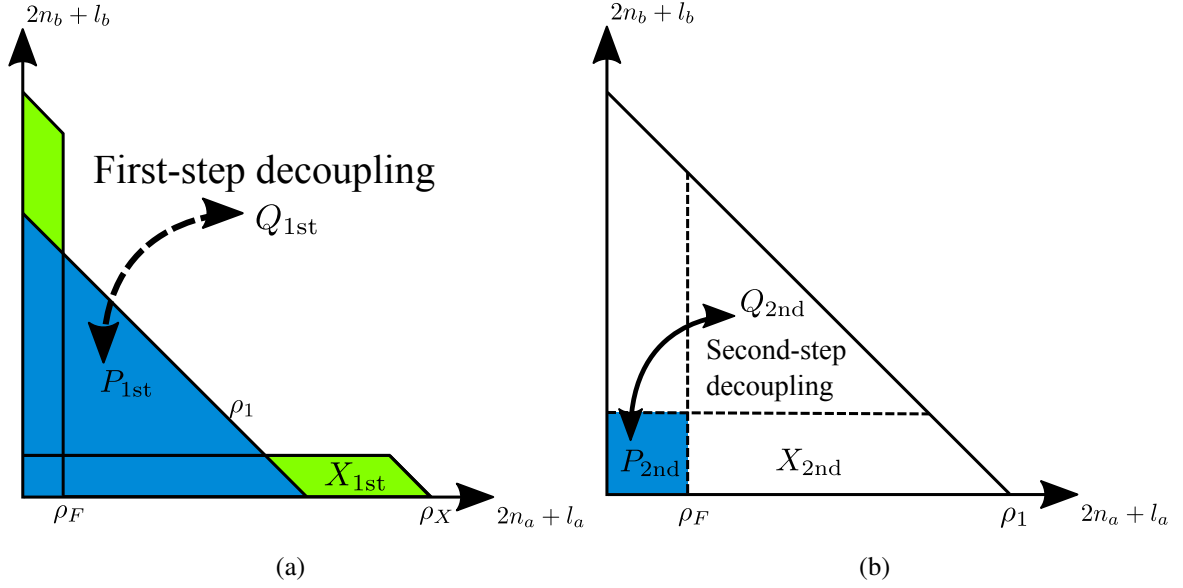
Figure 3.3: Illustrations of the model space employed in *method I*. The first-step decoupling (a) denotes the decoupling between the outside and inside of our model space. Our model space is defined by the two-body boundary number $\rho_1 = 2n_a + l_a + 2n_b + l_b$. The ρ_X is introduced so as to consider the Pauli exclusion principle. In this work, we use the fixed number $\rho_X = 20$. The second-step decoupling (b) is the decoupling of 2p2h excitations with 0p0h state.

First-Step Decoupling

Let $|ab: Z\rangle$ be antisymmetrized and normalized two-nucleon state. Here, Z means either proton-proton, proton-neutron, or neutron-neutron channel. As shown in the Fig. 3.3(a), we define our model space using the two-body boundary number $\rho_1 = 2n_a + l_a + 2n_b + l_b$ and consider the projection operators P_{1st}, X_{1st}, and Q_{1st}. The definitions of projection operators are

$$P_{1st} = \frac{1}{2} \sum_{ab} |ab: Z\rangle\langle ab: Z|, \text{ for } 2n_a + l_a + 2n_b + l_b \le \rho_1, \tag{3.79}$$

$$X_{1st} = \frac{1}{2} \sum_{ab} |ab: Z\rangle\langle ab: Z|, \text{ for } \rho_1 < 2n_a + l_a + 2n_b + l_b \le \rho_X,$$

$$\min(2n_a + l_a, 2n_b + l_b) \le \rho_F, \text{and } \max(2n_a + l_a, 2n_b + l_b) > \rho_F, \tag{3.80}$$

$$Q_{1st} = \frac{1}{2} \sum_{ab} |ab: Z\rangle\langle ab: Z|, \text{ otherwise.} \tag{3.81}$$

Note that X_{1st} is needed to take into account the Pauli exclusion principle and is defined with the fixed number $\rho_X = 20$. The condition $\min(2n_a + l_a, 2n_b + l_b) \le \rho_F$ and $\max(2n_a + l_a, 2n_b + l_b) > \rho_F$ mean that either a or b is the occupied state and the other one is unoccupied state. To consider the high-momentum component of the NN interaction, we have to span the huge HO space. In such a huge space, we cannot treat problems with $|ab: Z\rangle$ representation because the Talmi-Moshinsky transformation, introduced in Appendix A, demands the computational cost. Instead of $|ab: Z\rangle$, we

use $|nlS J_{rel} NL\colon Z\rangle$. Here, n, l, S, and J_{rel} are the nodal quantum number, orbital angular momentum, total spin, and total angular momentum ($J_{rel} = l + S$) of the relative motion of the NN system, respectively. The N and L are the nodal and azimuthal quantum number of CM motion, respectively. Owing to $|nlS J_{rel} NL\colon Z\rangle$ representation, we can solve the decoupling equation in the large space, typically $2n + l + 2N + L = 150$. Same as in the free-space OLS transformation, we solve the Schrödinger equation for the NN system:

$$\left(P_{1st} + \overline{Q}_{1st}\right)\left[\frac{\mathbf{p}_{rel}^2}{2\mu} + \overline{w} + V^{NN}\right]\left(P_{1st} + \overline{Q}_{1st}\right)|\psi_k\colon Z\rangle = E_k|\psi_k\colon Z\rangle. \tag{3.82}$$

Here, $\overline{Q}_{1st}$ is the projection operator onto the outside of P_{1st}, and $\overline{w}$ is one-body auxiliary potential transformed from single-particle to relative and CM coordinates. Because of $\overline{w}$, we obtain the two-body effective interaction taking into account the in-medium effect.

Before writing down $\overline{Q}_{1st}$ and $\overline{w}$, we mention about the two approximations taken in this first-step procedure. First, we assume that Eq. (3.82) be diagonal with respect to the CM motion. Due to the single-particle potential $\overline{w}$, the translational symmetry is supposed to be violated and Eq. (3.82) depends on N and L. We neglect this effect in this work. Secondary, we take the angle average approximations which is applied to $\overline{Q}_{1st}$ and $\overline{w}$. Because of the Pauli exclusion principle, the relative angular momentum J_{rel} cannot be a good quantum number. In the angle average approximation, $\overline{Q}_{1st}$ and $\overline{w}$ is averaged with respect to the CM angular momentum L. As a result, J_{rel} can be a good quantum number. The matrix element of $\overline{w}$ under the angle-average approximation is [37, 39, 64]

$$\langle nlS J_{rel}, NL\colon JZ|\overline{w}|n'lS J_{rel}, NL\colon JZ\rangle = \sum_{\lambda\lambda'J}\sum_{n_a n_a' n_b n_b'}\sum_{l_a j_a l_b j_b}(-1)^{\lambda+\lambda'}\begin{Bmatrix} l_a & 1/2 & j_a \\ l_b & 1/2 & j_b \\ \lambda & S & J \end{Bmatrix}\begin{Bmatrix} l_a & 1/2 & j_a \\ l_b & 1/2 & j_b \\ \lambda' & S & J \end{Bmatrix}$$

$$\times \frac{[\lambda][\lambda'][j_a][j_b][S][J]}{[L]}\begin{Bmatrix} L & l & \lambda \\ S & J & J_{rel} \end{Bmatrix}\begin{Bmatrix} L & l & \lambda' \\ S & J & J_{rel} \end{Bmatrix}$$

$$\times \langle nlNL\lambda|n_a l_a n_b l_b \lambda\rangle\langle n'lNL\lambda'|n_a' l_a n_b' l_b \lambda'\rangle \left(\langle n_a l_a j_a|w_{1st,1}|n_a' l_a j_a\rangle + \langle n_b l_b j_b|w_{1st,1}|n_b' l_b j_b\rangle\right).$$

$$\tag{3.83}$$

Here, $[x] = 2x + 1$ and J is the total angular momentum of NN system. The coefficients three by three $\{\cdots\}$, two by three $\{\cdots\}$, and $\langle nlNL\lambda|n_a l_a n_b l_b \lambda\rangle$ are the 9-j symbol, 6-j symbol, and the HO transformation brackets [65], respectively. The $w_{1st,1}$ is the single-particle potential represented in the laboratory frame and is determined self-consistently with the two-body effective interaction. The projection operator $\overline{Q}_{1st}$ is

$$\overline{Q}_{1st} = \sum_{nlNL\in Q_{1st}}\sum_{S J_{rel}}\theta_Z(n, l, N, L, S, J_{rel})|nlS J_{rel}NL\rangle\langle nlS J_{rel}NL|, \tag{3.84}$$
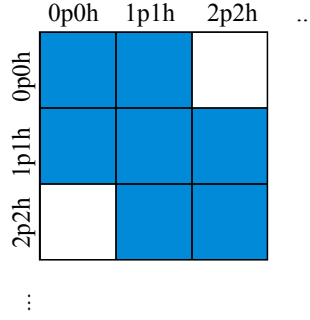
Figure 3.4: The schematic representation of the transformed Hamiltonian by *method I*.

with

$$
\theta_Z(n, l, N, L, S, J_{\text{rel}}) = 1 - \sum_{ab \in X_{1\text{st}}} \sum_{\lambda\lambda'J} (-1)^{\lambda+\lambda'} f_Z \begin{Bmatrix} l_a & 1/2 & j_a \\ l_b & 1/2 & j_b \\ \lambda & S & J \end{Bmatrix} \begin{Bmatrix} l_a & 1/2 & j_a \\ l_b & 1/2 & j_b \\ \lambda' & S & J \end{Bmatrix}
$$

$$
\times \frac{[\lambda][\lambda'][j_a][j_b][S][J]}{[L]} \begin{Bmatrix} L & l & \lambda \\ S & J & J_{\text{rel}} \end{Bmatrix} \begin{Bmatrix} L & l & \lambda' \\ S & J & J_{\text{rel}} \end{Bmatrix}
$$

$$
\times \langle nlNL\lambda | n_a l_a n_b l_b \lambda \rangle \langle n'lNL\lambda' | n'_a l_a n'_b l_b \lambda' \rangle. \tag{3.85}
$$

Here, f_Z is defined by

$$
f_Z \equiv \begin{cases} 1 - (-1)^{l+S} & \text{for} \quad Z = \text{proton-proton or neutron-neutron,} \\ 1 & \text{for} \quad Z = \text{proton-neutron.} \end{cases} \tag{3.86}
$$

Same as the free-space OLS transformation, we obtain the two-body effective interaction,

$$
\langle nlS\,J_{\text{rel}} | \widetilde{V}^{NN}_{\text{eff},1\text{st},12}(N, L) | n'l'S\,J_{\text{rel}} \rangle
$$

, by using Eq. (B.51). Note that the two-body effective interaction obtained here depends on CM quantum numbers N and L in contrast to the free-space OLS transformed effective interaction. Moreover, applying Eq. (A.14), the effective interaction can be transformed from relative and CM frame to laboratory frame. As mentioned above, the single-particle potential is determined with the effective interaction:

$$
\langle a | w_{1\text{st},1} | b \rangle = \sum_{m \le \rho_F} \langle am | \widetilde{V}^{NN}_{\text{eff},1\text{st},12} | bm \rangle. \tag{3.87}
$$

Since Eq. (3.82) includes $w_{1\text{st},1}$, we calculate the effective interaction $\widetilde{V}^{NN}_{\text{eff},1\text{st},12}$ iteratively untile $w_{1\text{st},1}$ converges.

Second-Step Decoupling

Using the effective interaction $\widetilde{V}^{NN}_{\text{eff},1\text{st},12}$, in the second-step calculation, we decouple the 2p2h excitations with the reference state. In the second step, we use up to two-body level:

$$H_{2\text{nd}} \approx \sum_{i<j}^{A} \frac{(\mathbf{p}_i - \mathbf{p}_j)^2}{2m} + \sum_{i<j}^{A} \widetilde{V}^{NN}_{\text{eff},1\text{st},ij} + H_{\text{CM}} = \sum_{i=1}^{A} t_i + \sum_{i<j}^{A} \widetilde{v}_{1\text{st},ij}, \tag{3.88}$$

$$\widetilde{H}_{2\text{nd}} \approx \sum_{i=1}^{A} \widetilde{h}_i + \sum_{i<j}^{A} \widetilde{v}_{2\text{nd},ij}, \tag{3.89}$$

$$U \approx e^{S^{(2)}}, \tag{3.90}$$

$$W \approx W^{(1)} = \sum_{i=1}^{A} w_{2\text{nd},i}, \tag{3.91}$$

$$\widetilde{W} \approx W. \tag{3.92}$$

Here, $H_{2\text{nd}}$ and $\widetilde{H}_{2\text{nd}}$ denote the initial and transformed Hamiltonian in the second-step calculations. Note that we add the CM Hamiltonian H_{CM},

$$H_{\text{CM}} = \frac{1}{2Am} \left(\sum_{i=1}^{A} \mathbf{p}_i \right)^2 + \frac{1}{2} Am\omega^2 \left(\frac{1}{A} \sum_{i=1}^{A} \mathbf{r}_i \right)^2 - \frac{3}{2}\hbar\omega, \tag{3.93}$$

in Eq. (3.88) to remove the spurious excitations from the CM motions [66]. The one-body part of the transformed Hamiltonian is $\widetilde{h}_i = t_i + w_i = t_i + \widetilde{w}_i$. We truncate the many-body interactions induced in the first-step calculations. The effect of such truncated interactions should be small when we increase the model-space size ρ_1, same as the free-space OLS transformation. The interaction coupling with the out side of our model space is already decoupled after the first-step decoupling. We consider only the inside of our model space defined by $\rho_1 = \max(2n_a + l_a + 2n_b + l_b)$ and treat the problem with the products of the single-particle basis states. In this step, we define the projection operator as

$$P_{2\text{nd}} = \frac{1}{2} \sum_{ab} |ab:Z\rangle\langle ab:Z|, \quad \text{both } a \text{ and } b \text{ are occupied state}, \tag{3.94}$$

$$X_{2\text{nd}} = \frac{1}{2} \sum_{ab} |ab:Z\rangle\langle ab:Z|, \quad \text{neither } a \text{ or } b \text{ is occupied state}, \tag{3.95}$$

$$Q_{2\text{nd}} = \frac{1}{2} \sum_{ab} |ab:Z\rangle\langle ab:Z|, \quad \text{both } a \text{ and } b \text{ are unoccupied state}. \tag{3.96}$$

The $P_{2\text{nd}}$ space is illustrated by the blue area in Fig. 3.3(b).

To decouple the 2p2h excitations, we have to determine the two-body correlation operator $S^{(2)}$ appeared in Eq. (3.14). As discussed in Sec. 3.2, we solve the two-body Schrödinger equation,

$$(P_{2\text{nd}} + Q_{2\text{nd}}) \left(\widetilde{h}_1 + \widetilde{h}_2 + \widetilde{v}_{1\text{st},12} \right) (P_{2\text{nd}} + Q_{2\text{nd}}) |\psi_k^{(2)}\rangle = E_k |\psi_k^{(2)}\rangle, \tag{3.97}$$

and obtain the two-body correlation operator $S^{(2)}$. Here, $|\psi_k^{(2)}\rangle$ is the two-body wave function. The matrix element of $\widetilde{w}_{2\text{nd},1}$ calculated in the second step is

$$\langle a|\widetilde{w}_{2\text{nd},1}|b\rangle = \sum_{m \leq \rho_F} \langle am|\widetilde{v}_{2\text{nd},12}|bm\rangle, \tag{3.98}$$

with the transformed two-body interaction $\widetilde{v}_{2\text{nd},12}$. Same as the first-step decoupling, $\widetilde{w}_{2\text{nd},1}$ and $\widetilde{v}_{2\text{nd},12}$ are determined self-consistently, and the calculations are done iteratively until $\widetilde{w}_{2\text{nd},1}$ converges.

After second-step decoupling, we construct the transformed Hamiltonian which is illustrated in Fig. 3.4. Then, the energy of the one- and two-body cluster term for the reference state is

$$E_0 = \langle \Phi|\widetilde{H}|\Phi\rangle \simeq \sum_{a_1 \leq \rho_F} \langle a_1|\widetilde{h}_1|a_1\rangle - \frac{1}{2!} \sum_{a_1 a_2 \leq \rho_F} \langle a_1 a_2|\widetilde{v}_{2\text{nd},12}|a_1 a_2\rangle. \tag{3.99}$$

As shown in Fig. 3.4, we have the non-zero coupling between the 0p0h and 1p1h states. To take into account such coupling, similar to the equation of motion approach, we diagonalize the transformed Hamiltonian in the 0p0h and 1p1h spaces. Let $E^{1\text{p1h}}$ be energy correction by the diagonalization. Then, the energy of the one- and two-body cluster term $E^{1+2\text{BC}}$ can be approximated by

$$E^{1+2\text{BC}} \approx E_0 + E^{1\text{p1h}}. \tag{3.100}$$

Note that the wave function is modified as

$$|\Psi\rangle = e^{S^{(2)}}\left(r_0 + \sum_{a > \rho_F} \sum_{i \leq \rho_F} r_i^a c_a^\dagger c_i\right)|\Phi\rangle. \tag{3.101}$$

To investigate the convergence of the cluster expansion, in addition to Eq. (3.99), we consider the energy of the three-body cluster term $E^{3\text{BC}}$:

$$E^{3\text{BC}} = \frac{1}{3!} \sum_{a_1 a_2 a_3 \leq \rho_F} \langle a_1 a_2 a_3|\widetilde{v}_{123}|a_1 a_2 a_3\rangle. \tag{3.102}$$

Since it is difficult to calculate the three-body term directly, we expand

$$\widetilde{v}_{123} = e^{-(s_{12}+s_{23}+s_{31})}(\widetilde{h}_1 + \widetilde{h}_2 + \widetilde{h}_3 + \widetilde{v}_{1\text{st},12} + \widetilde{v}_{1\text{st},23} + \widetilde{v}_{1\text{st},31})e^{s_{12}+s_{23}+s_{31}}$$
$$- (\widetilde{h}_1 + \widetilde{h}_2 + \widetilde{h}_3 + \widetilde{v}_{2\text{nd},12} + \widetilde{v}_{2\text{nd},23} + \widetilde{v}_{2\text{nd},31}), \tag{3.103}$$

in terms of $\widetilde{v}_{2\text{nd},12}$ and s_{12} and keep up to order of s_{12}^2. After the expansion, finally, we have [37]

$$E^{3\text{BC}} \simeq \frac{1}{4} \sum_{ab > \rho_F} \sum_{ijkl \leq \rho_F} \widetilde{v}_{ijkl}^{2\text{nd}} s_{abij} s_{abkl} + \sum_{abc > \rho_F} \sum_{ijk \leq \rho_F} \widetilde{v}_{iakc}^{2\text{nd}} s_{abjk} s_{bcij}. \tag{3.104}$$

Here, we use the shorted notations:

$$\widetilde{v}_{abcd}^{2\text{nd}} = \langle ab|\widetilde{v}_{2\text{nd},12}|cd\rangle, \quad s_{abcd} = \langle ab|s_{12}|cd\rangle. \tag{3.105}$$
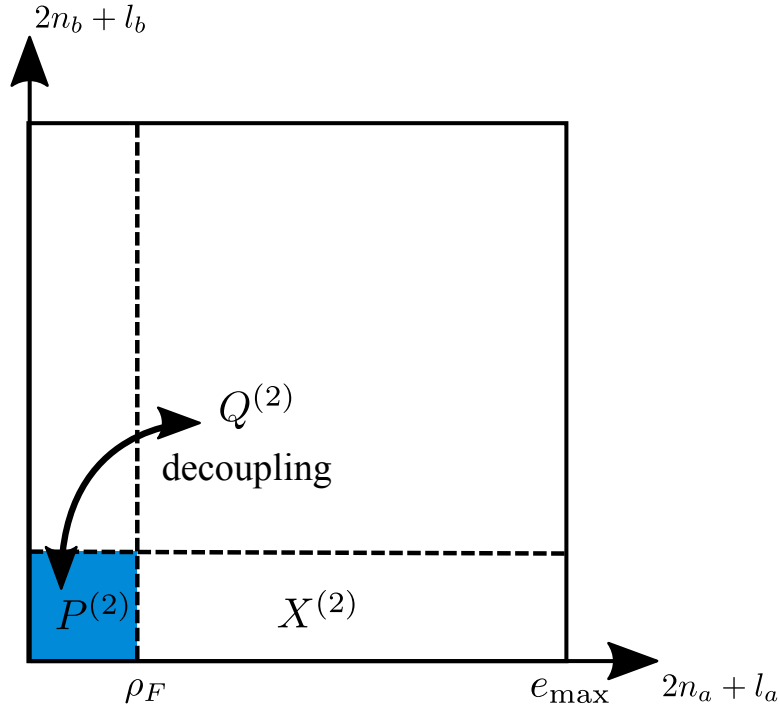
Figure 3.5: Illustrations of the model space employed in *method II*.

In *method I*, the ground-state energy by our calculation is

$$E_{\text{g.s.}} \simeq E^{1+2\text{BC}} + E^{3\text{BC}}. \tag{3.106}$$

The observables are calculated with the wave function (3.101). The expectation value is calculated up to order $S^{(2)2}$ [42],

$$\langle \Psi|O|\Psi \rangle \simeq \langle \Phi| \left(r_0^* + \sum_{a > \rho_F} \sum_{i \le \rho_F} r_i^{a*} c_i^\dagger c_a \right) \left\{ O + [O, S^{(2)}] + \frac{1}{2}[[O, S], S] \right\} \left(r_0 + \sum_{b > \rho_F} \sum_{j \le \rho_F} r_j^b c_b^\dagger c_j \right) |\Phi\rangle. \tag{3.107}$$

Finally, we summarize our calculation procedure of *method I* in Fig. 3.7.

3.5.2   *Method II*

As discussed in Sec. 4.1, the results with *method I* depends on $\hbar\omega$, even if our calculations are done in the large model space. Since the initial Hamiltonian does not include $\hbar\omega$, calculated observables should not depend on that. To reduce the $\hbar\omega$-dependence, we refer to the CCM calculations by Kohno and Okamoto [67] and change the UMOA calculation procedure. According to Ref. [67], the $\hbar\omega$-dependence was reduced by taking into account one-body correlation. Following this, in addition to $S^{(2)}$, we consider $S^{(1)}$ in *method II*.

Basically, we should compare results by the UMOA and by the other *ab initio* calculation methods to make sure the reliability of the UMOA. For this purpose, we do not employ the two-step

decoupling in *method II*. The first-step calculation can lead uncontrollable uncertainties, due to the approximations. The validity of angle-average approximation is not clear for finite nuclei. In nuclear matter calculations [68–70], at least, the angle-average approximation causes the non-negligible 0.4 - 0.5 MeV/*A* deviation at the saturation density. When we skip the first-step procedure, however, we encounter the problem about the convergence. As discussed in Sec. 2.1, it is practically impossible to treat bare *NN* interactions in the UMOA. Instead of using the two-step decoupling, we employ the *NN* interactions softened by $V_{\text{low k}}$ method or SRG in *method II*.

In *method II*, we decouple the 1p1h and 2p2h excitations with the reference state with the softened *NN* interaction. Then, the choice of the model space is no longer restricted to the triangle. In *method II*, we employ the simplest choice, where the model space is truncated by the square defined by $e_{\text{max}} = \max(2n_a + l_a)$, as shown in Fig. 3.5. The decoupling of 1p1h and 2p2h excitations are indicated by the solid arrow in Fig. 3.5. The square shape model space is more convenient and simpler than the triangle choice, and we can compare with HF results at the same e_{max} as discussed in Sec. 4.2.

Let us summarize the approximations used in *method II* are

$$H \approx H^{(1)} + H^{(2)} = \sum_{i=1}^{A} t_i + \sum_{i<j}^{A} v_{ij}, \tag{3.108}$$

$$\widetilde{H} \approx \widetilde{H}^{(1)} + \widetilde{H}^{(2)} = \sum_{i=1}^{A} \widetilde{h}_i + \sum_{i<j}^{A} \widetilde{v}_{ij}, \tag{3.109}$$

$$U \approx e^{S^{(1)}} e^{S^{(2)}}, \tag{3.110}$$

$$W \approx W^{(1)} = \sum_{i=1}^{A} w_i, \tag{3.111}$$

$$\widetilde{W} \approx \widetilde{W}^{(1)} = \sum_{i=1}^{A} \widetilde{w}_i, \tag{3.112}$$

Above approximations mean the UMOA at two-body level. The flow chart of the actual calculations are shown in Fig. 3.8. We employ the softened *NN* interactions as the input of the UMOA calculation. As mentioned in Sec. 3.2, we firstly solve the one-body Schrödinger equation and obtain the one-body correlation operator. In this process the projection operators are defined as

$$P^{(1)} = \sum_{a} |a\rangle\langle a|, \quad \text{for } 2n_a + l_a \leq \rho_F, \tag{3.113}$$

$$Q^{(1)} = \sum_{a} |a\rangle\langle a|, \quad \text{for } 2n_a + l_a > \rho_F. \tag{3.114}$$

Also, the Schrödinger equation which we should solve in this process is

$$(t_1 + w_1)|\psi^{(1)}\rangle = E_k^{(1)}|\psi_k^{(1)}\rangle. \tag{3.115}$$

Through Eq. (3.53), s_1 and e^{s_1} can be calculated. The transformed one-body auxiliary potential $\widetilde{w}_1 = e^{-s_1} w_1 e^{s_1}$ can be obtained. As the next step we solve the two-body Schrödinger equation and
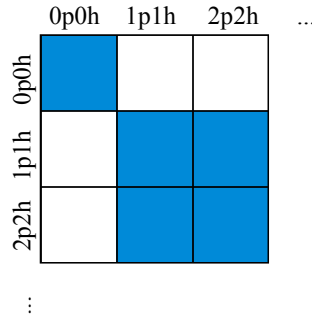
Figure 3.6: The schematic representation of the transformed Hamiltonian by *method II*.

determine the two-body correlation operator. The projection operators for the two-body system are

$$P^{(2)} = \frac{1}{2} \sum_{ab} |ab\colon Z\rangle\langle ab\colon Z|, \text{ both } a \text{ and } b \text{ are occupied state,} \tag{3.116}$$

$$X^{(2)} = \frac{1}{2} \sum_{ab} |ab\colon Z\rangle\langle ab\colon Z|, \text{ neither } a \text{ or } b \text{ is occupied state,} \tag{3.117}$$

$$Q_{(2)} = \frac{1}{2} \sum_{ab} |ab\colon Z\rangle\langle ab\colon Z|, \text{ both } a \text{ and } b \text{ are unoccupied state.} \tag{3.118}$$

The two-body Schrödinger equation which should be solved is

$$\left(P^{(2)} + Q^{(2)}\right)\left[e^{-(s_1+s_2)}(h_1 + h_2 + v_{12})e^{s_1+s_2}\right]\left(P^{(2)} + Q^{(2)}\right)|\psi_k^{(2)}\rangle = E_k|\psi_k^{(2)}\rangle. \tag{3.119}$$

After solving Eq. (3.119), s_{12} and $e^{s_{12}}$ can be determined with Eqs. (3.53) and (3.57), respectively. Taking the normal ordering of the transformed two-body interaction,

$$\widetilde{v}_{12} = e^{-s_{12}}e^{-(s_1+s_2)}(h_1 + h_2 + v_{12})e^{s_1+s_2}e^{s_{12}} - \left(\widetilde{h}_1 + \widetilde{h}_2\right),$$

we obtain the matrix element of the transformed auxiliary potential:

$$\langle a|w_1|b\rangle = \sum_{m\leq\rho_F} \langle am|\widetilde{v}_{12}|bm\rangle. \tag{3.120}$$

Applying the inversed transformation, non-transformed auxiliary potential can be obtained, $w_1 = e^{s_1}\widetilde{w}_1 e^{-s_1}$. This w_1 is used in Eq. (3.115) and the calculations are iterated until the difference between new and previous $\widetilde{w}_1$ become sufficiently small.

After the transformation, the transformed Hamiltonian does not induce the 1p1h and 2p2h excitations, as illustrated in Fig. 3.6. In contrast to the transformed Hamiltonian employed in *method I* (see Fig. 3.4), the coupling between 1p1h and 0p0h is suppressed. Owing to this decoupling, one- and two-body cluster term is

$$E^{1+2BC} = \sum_{a_1\leq\rho_F} \langle a_1|\widetilde{h}_1|a_1\rangle - \frac{1}{2} \sum_{a_1 a_2 \leq\rho_F} \langle a_1 a_2|\widetilde{v}_{12}|a_1 a_2\rangle, \tag{3.121}$$

$$= \sum_{a_1\leq\rho_F} \langle a_1|\widetilde{t}_1|a_1\rangle + \frac{1}{2} \sum_{a_1 a_2 \leq\rho_F} \langle a_1 a_2|\widetilde{v}_{12}|a_1 a_2\rangle, \tag{3.122}$$

and we do not need the extra diagonalization process. Moreover, we estimate the contribution of the three-body cluster term E^{3BC} to investigate the convergence with respect to the cluster expansion. Because two one-body correlation operator can commute, as in Eq. (3.20), we can hold Eq. (3.104) here. Totally, the ground-state energy in *method II* is

$$E_{\text{g.s.}} \simeq E^{\text{1+2BC}} + E^{\text{3BC}}. \tag{3.123}$$

The observables can be calculated with Eq. (3.66). In the actual calculations, we take up to two-body contribution:

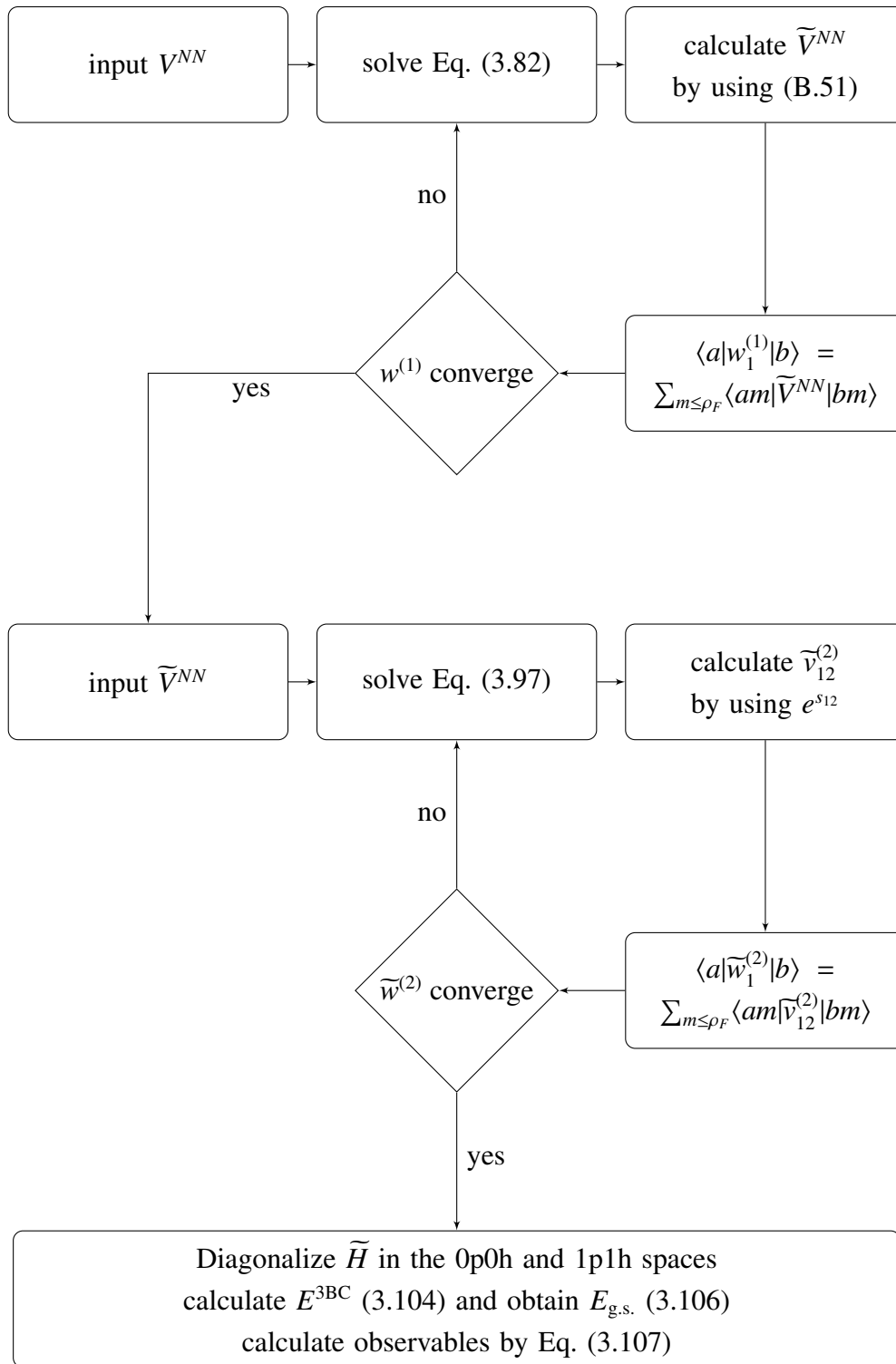$$\langle \Phi | \widetilde{O} | \Phi \rangle \simeq \sum_{a_1 \leq \rho_F} \langle a_1 | \widetilde{o}_1 | a_1 \rangle + \frac{1}{2!} \sum_{a_1 a_2 \leq \rho_F} \langle a_1 a_2 | \widetilde{o}_{12} | a_1 a_2 \rangle. \tag{3.124}$$
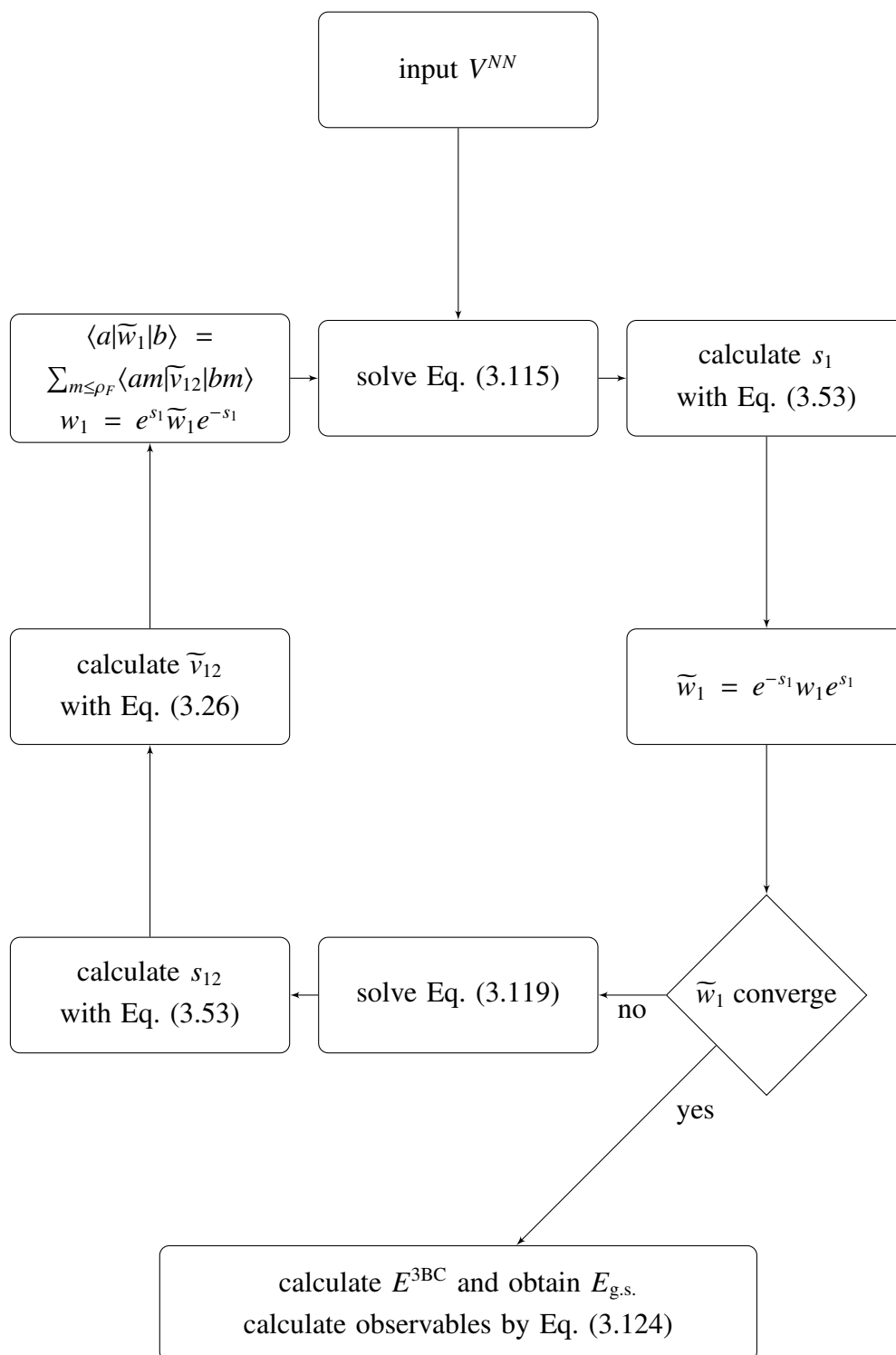
```
┌──────────────┐     ┌──────────────┐     ┌──────────────────┐
│  input V^NN  │ ──→ │ solve Eq.    │ ──→ │ calculate V͂^NN   │
│              │     │ (3.82)       │     │ by using (B.51)  │
└──────────────┘     └──────────────┘     └──────────────────┘
```

$\langle a | w_1^{(1)} | b \rangle = \sum_{m \leq \rho_F} \langle am | \widetilde{V}^{NN} | bm \rangle$

$w^{(1)}$ converge

$\langle a | \widetilde{w}_1^{(2)} | b \rangle = \sum_{m \leq \rho_F} \langle am | \widetilde{v}_{12}^{(2)} | bm \rangle$

$\widetilde{w}^{(2)}$ converge

input $\widetilde{V}^{NN}$

solve Eq. (3.97)

calculate $\widetilde{v}_{12}^{(2)}$ by using $e^{s_{12}}$

Diagonalize $\widetilde{H}$ in the 0p0h and 1p1h spaces
calculate E^{3BC} (3.104) and obtain $E_{\text{g.s.}}$ (3.106)
calculate observables by Eq. (3.107)

Figure 3.7: The flow chart of *method I*.

Figure 3.8: The flow chart of *method II*.

Chapter 4

Calculation Results in UMOA

In this Chapter, we show the calculation results by the UMOA. In Sec. 4.1, we employ *method I*, introduced in Sec. 3.5. The results shown in Sec. 4.1 are based on Ref. [42, 43]. In Sec. 4.2 - 4.4, we employ *method II*. Finally, we demonstrate the calculation results holding the three-body level in Sec. 4.5.

4.1 Ground-State Energies and Radii of Doubly Magic Nuclei

Here, we show the ground-state energies and charge radii for doubly magic nuclei, ^{4}He, ^{16}O, ^{40}Ca, and ^{56}Ni and attempt to understand the bulk property of finite nuclei based on Refs. [42, 43]. All the calculated results, exhibited in Sec. 4.1, are obtained with the CD-Bonn potential [9] and with *method I* introduced in the subsection 3.5.1. The UMOA calculations are performed with various model space defined by ρ_1 and the harmonic-oscillator energy $\hbar\omega$, and investigate the ρ_1- and $\hbar\omega$-dependence of the ground-state energies and charge radii.

Fig. 4.1 shows the ground-state energies of ^{4}He, ^{16}O, ^{40}Ca, and ^{56}Ni as functions of $\hbar\omega$. The ground-state energies lower with increasing ρ_1 except for ^{4}He. These nucleus-dependent behaviors are not surprising. Since the many-body cluster terms are truncated, our calculations do not have to be variational. Actually, our ground-state energy of ^{4}He, at $\rho_1 = 12$ and $\hbar\omega = 18$ MeV, is overbound a little compared with the Faddeev-Yakubovsky result (-26.26 MeV) [52] which is the exact solution with the CD-Bonn potential. The situation is similar to the calculation results with the free-space OLS transformed *NN* interactions (see e.g. Fig. 2.6). According to Fig. 4.1, our ground-state energies depend on $\hbar\omega$ even if the ρ_1-dependence practically vanishes. The $\hbar\omega$-dependence of the results should vanish in sufficiently large ρ_1, because our initial Hamiltonian does not include $\hbar\omega$. The reduction of $\hbar\omega$-dependence is important issue to obtain more reliable results. This topic will be discussed in Sec. 4.2, and in this section, we take the value at $\hbar\omega_{\min}$ minimizing the ground-state energy. The validity of this choice is discussed in the coupled-cluster method (CCM) [67]. Note that, in Fig. 4.1, we omit the results at $\hbar\omega$ where the iteration in the first-step decoupling does not converge. The final results of our ground-state energies are exhibited in Table 4.1. The $E^{1+2\mathrm{BC}}$ is the energy obtained from the one- and two-body cluster terms shown in Eq. (3.100). The contribution of
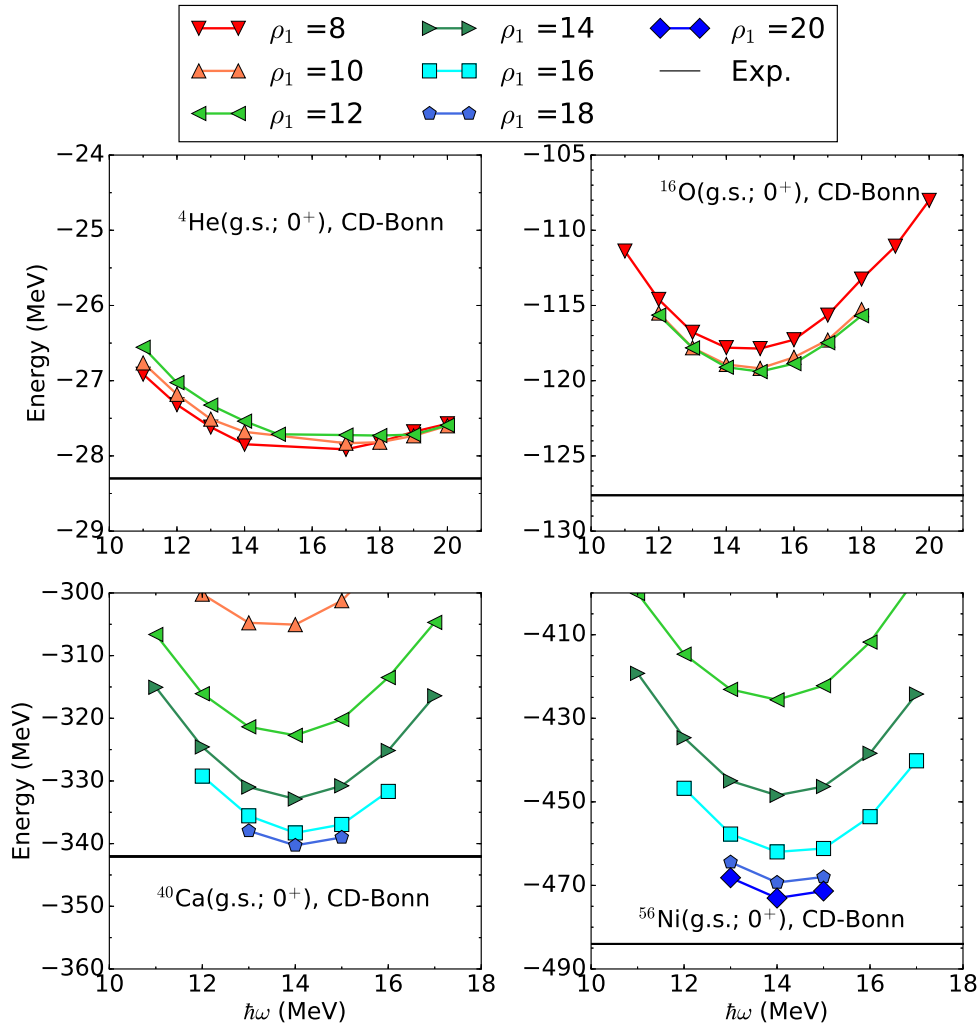
Figure 4.1: Ground-state energies of ^{4}He, ^{16}O, ^{40}Ca, and ^{56}Ni as functions of $\hbar\omega$. All the energies are calculated with the CD-Bonn potential and with the *method I*.

the three-body cluster term, E^{3BC}, is much smaller than E^{1+2BC} and attractive for all nuclei examined here. Since the contributions from the higher-body cluster terms would be less than those of the three-body cluster term, our ground-state energies, $E_{g.s.} = E^{1+2BC} + E^{3BC}$, are expected to almost converge with respect to the cluster expansion.

In addition to the ground-state energy, we calculate the charge radii r_{ch}. We use the definition [71],

$$r_{ch}^2 = \langle r_p^2 \rangle^{1/2} + R_p^2 + \frac{N}{Z}R_n^2. \tag{4.1}$$

Here, $\langle r_p^2 \rangle^{1/2}$ is the point-proton radius, and R_p and R_n are the charge radii evaluated from the charge distributions of the proton and neutron, respectively. In this work, we employ $R_p^2 = 0.832$ fm^2 [72] and $R_n^2 = -0.115$ fm^2 [73]. The higher order corrections coming from the relativistic effect can be expected to be small and do not included in this work. In Fig. 4.2, the charge radii of ^{4}He, ^{16}O, ^{40}Ca, and ^{56}Ni are shown as functions of $\hbar\omega$. The radii are not sensitive to ρ_1 and almost converge with

respect to ρ_1. On the other hand, for all cases, the charge radii decrease monotonically with increasing $\hbar\omega$ and strongly depend on $\hbar\omega$. This dependence is not likely vanished, if we enlarge the model-space size. To evaluate the charge radius in the UMOA, $\hbar\omega$ was formerly taken to $\hbar\omega_{\min}$ [27,38]. Moreover, it was demonstrated that the radius at $\hbar\omega_{\min}$ coincides the $\hbar\omega$-independent result in the recent CCM calculations [67]. Therefore, we can expect that the radius at $\hbar\omega_{\min}$ is close to $\hbar\omega$-independent results. In Table 4.2, the charge radius of each nucleus at $\hbar\omega_{\min}$ is tabulated. The contributions of the two-body correlation operator $S^{(2)}$ and the diagonalization coefficients r_i^a are also shown as the effects of 2p2h and 1p1h correlations, respectively. Since the effects of $S^{(2)}$ are much smaller than those of r_i^a, 1p1h excitations to the charge radius are more important than 2p2h excitations. In other words, for the radius, it can be expected that the consideration of the one-body correlation operator $S^{(1)}$ is more important than that of $S^{(2)}$. This is confirmed in Sec. 4.2. All the charge radii investigated here shrink compared with the experimental values as increasing the mass number. Note that the charge radius of ^{56}Ni has not been measured yet. Similar to the charge radius, we calculate the point-neutron and point-nucleon radii. The differences between the point-proton and point-neutron radii for the nuclei examined here are smaller than 0.02 fm. Therefore, we only discuss the point-proton (charge) radius here.

In Fig. 4.3, the saturation property of ^{4}He, ^{16}O, ^{40}Ca, and ^{56}Ni is illustrated. Note that our calculation results of ^{16}O and ^{40}Ca are consistent with the results by the earlier UMOA calculations, which were obtained with the realistic NN interactions at $\hbar\omega_{\min}$ [27, 38]. To understand relation between calculation results and data, we employ the empirical formulae for binding energies and radii. As for the binding energies, we use well known mass formula by Bethe and Weizsäcker [74],

$$E/A = -a_V + a_S A^{-1/3} + a_C Z^2/A^{4/3} + a_A \frac{(N-Z)^2}{A^2} - a_P A^{-7/4}. \tag{4.2}$$

Here, parameters a_V, a_S, a_C, a_A and a_P are coefficients for the volume, surface, coulomb, asymmetry, and pairing terms, respectively. We use a_S = 18.56 MeV, a_C = 0.717 MeV, a_A = 28.1 MeV, and a_P = 34.0 MeV as found in Ref. [74], and adjust a_V = 16.10 MeV to reproduce the experimental

Table 4.1: Ground-state energies for ^{4}He, ^{16}O, ^{40}Ca, and ^{56}Ni with the CD-Bonn potential. We take ρ_1 = 12 and $\hbar\omega_{\min}$ = 18 MeV for ^{4}He, ρ_1 = 14 and $\hbar\omega_{\min}$ = 15 MeV for ^{16}O, ρ_1 = 18 and $\hbar\omega_{\min}$ = 14 MeV for ^{40}Ca, and ρ_1 = 20 and $\hbar\omega_{\min}$ = 14 MeV for ^{56}Ni. The definitions of E^{1+2BC}, E^{3BC}, and $E_{\text{g.s.}}$ are given in Eqs. (3.100), (3.104), and (3.106). The experimental values are taken from Ref. [23]. All the energies are in units of MeV.

	^{4}He	^{16}O	^{40}Ca	^{56}Ni
E^{1+2BC}	-26.13	-115.58	-334.36	-454.84
E^{3BC}	-1.60	-3.82	-5.92	-18.20
$E_{\text{g.s.}}$	-27.73	-119.39	-340.28	-473.04
Exp.	-28.30	-127.62	-342.05	-483.99
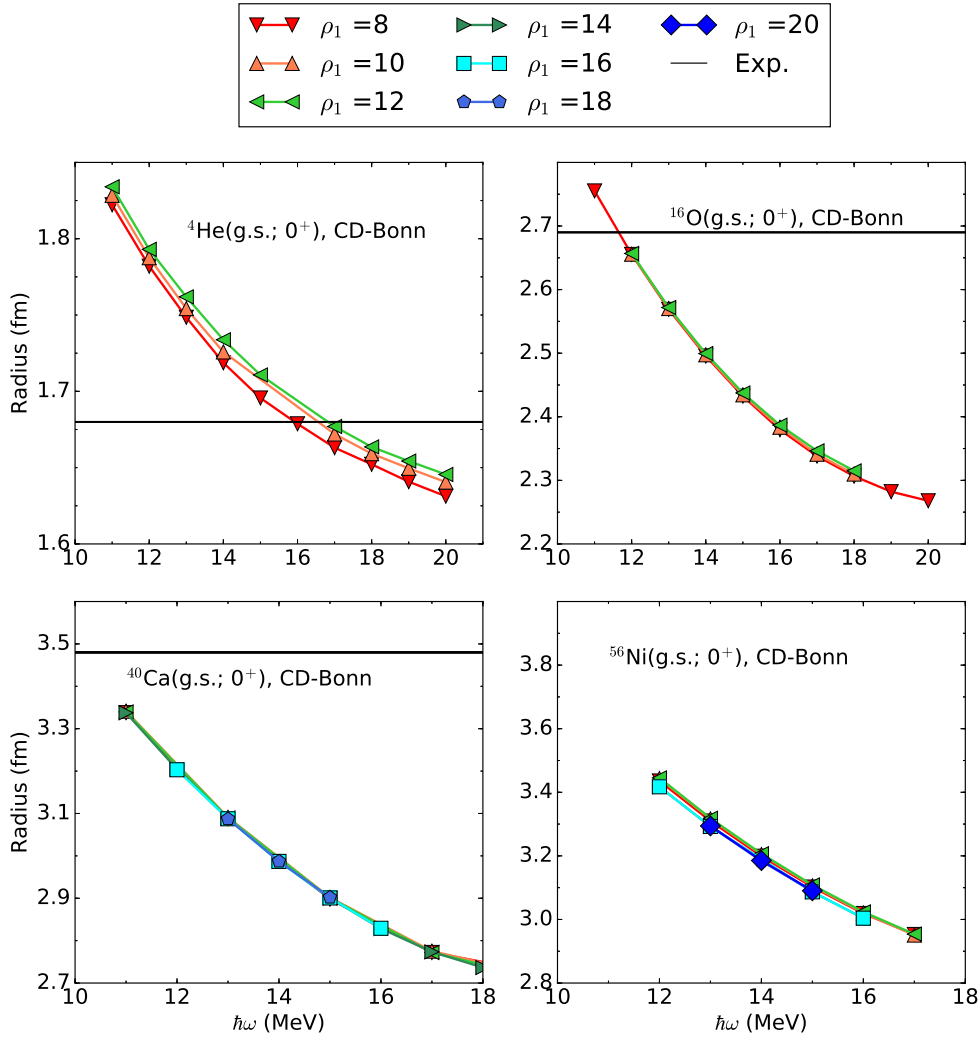
Figure 4.2: Charge radii of ^{4}He, ^{16}O, ^{40}Ca, and ^{56}Ni as functions of $\hbar\omega$. All radii are calculated with the CD-Bonn potential and with the *method I*. Note that the charge radius of ^{56}Ni has not been measured yet.

binding energies of ^{4}He, ^{16}O, ^{40}Ca, and ^{56}Ni. Note that the usual parameter sets of Eq. (4.2) is fitted to reproduce the data from medium- to heavy-mass nuclei. As for the charge radius, we employ [74],

$$r_{\mathrm{ch}} = r_0 A^{1/3}. \tag{4.3}$$

The r_0 is parameter and is fitted to $r_0 = 1.05$ fm. One may care that 1.05 fm is smaller than empirical value 1.2 fm. Since we discuss the root-mean-square radius, we should consider the factor, for example, $\sqrt{3/5}$. The factor $\sqrt{3/5}$ can be obtained by assuming the uniform charge density. Combining Eqs. (4.2) and (4.3), we obtain the dashed curve plotted in Fig. 4.3,

$$E/A = -a_{\mathrm{V}} + a_{\mathrm{S}}\frac{r_0}{r_{\mathrm{ch}}} + \frac{a_{\mathrm{C}}}{4}\left(\frac{r_{\mathrm{ch}}}{r_0}\right)^2 - a_{\mathrm{P}}\left(\frac{r_0}{r_{\mathrm{ch}}}\right)^{\frac{21}{4}}. \tag{4.4}$$

Note that we omit the asymmetry term, because we discuss the only $N = Z$ nuclei here. This curve gives the systematic behavior for light- and medium-mass $N = Z$ nuclei.

Our results show similar pattern to this empirical curve and reproduce the trend of the experimental data. However, taking a closer look at our results with the NN interaction only, all the binding energies are underbound and also all the charge radii are smaller than the experimental data. When we use the other realistic NN potentials, it can be expected that the binding energies increase (decrease) with decreasing (increasing) charge radii. In other words, the calculation results will distribute over the Coester line [74]. Actually, the former UMOA results [27, 38] show such a correlation between the binding energy and charge radius. Therefore, it is likely that the results do not approach the experimental data even if we employ the other modern high-precision NN interactions such as the AV18 [8] and chiral N³LO interactions [10]. The gap between calculated and experimental results might be filled by the effect of the genuine three-nucleon force ($3NF$), because it gives the attraction in light nuclei as shown in the Green's function Monte Carlo method [12]. Also, the $3NF$ through the relativistic framework stretches the nuclei as found in the comparison between the Brückner-Hartree-Fock and Dirac-Brückner-Hartree-Fock results [76]. Combining these facts, the $3NF$ seems to be necessary to reproduce simultaneously the binding energies and charge radiii. The discrepancy between the experimental data and the recent *ab initio* results still remains and needs to be further investigations [28, 33].

Our charge radii for ¹⁶O, ⁴⁰Ca, and ⁵⁶Ni, have sizable $\hbar\omega$-dependence. Thus, we cannot discuss these results accurately. It is necessary to obtain the practically $\hbar\omega$-independent results. To achieve this, the consideration of the one-body correlation operator is desirable.

4.2 Introduction of One-Body Correlation Operator

As discussed in the previous section, when the decoupling of the 2p2h excitations is only considered, i.e. $U = e^{S^{(2)}}$ in Eq. (3.12), results, especially radii, strongly depend on $\hbar\omega$. Due to the

Table 4.2: Charge radius r_{ch} for each nucleus. The entries of "r_{ch} w/o 1p1h and 2p2h correlations", "r_{ch} w/o 1p1h correlations", and "r_{ch} w/o 2p2h correlations" are the results from Eq. (3.107) with both of $S^{(2)} = 0$ and r_i^a, $r_i^a = 0$, and $S^{(2)} = 0$, respectively. The model-space size and $\hbar\omega_{\text{min}}$ are same as in Table 4.1. The experimental values are taken from Ref. [73]. All the radii are in units of fm.

	⁴He	¹⁶O	⁴⁰Ca	⁵⁶Ni
r_{ch} w/o 1p1h and 2p2h correlations	1.81	2.59	3.08	3.28
r_{ch} w/o 1p1h correlations	1.82	2.60	3.09	3.29
r_{ch} w/o 2p2h correlations	1.67	2.44	2.97	3.20
r_{ch}	1.67	2.44	2.97	3.19
Exp.	1.68	2.69	3.48	
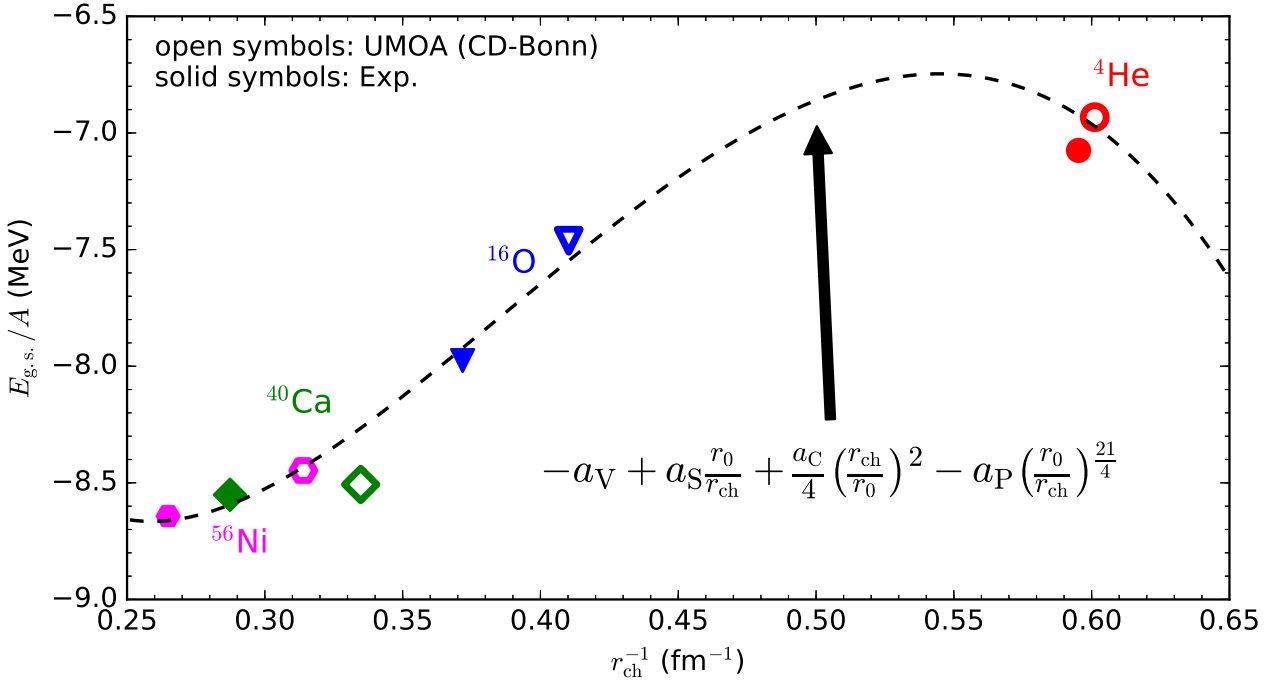
Figure 4.3: The saturation property of ^{4}He, ^{16}O, ^{40}Ca, and ^{56}Ni. The open and solid symbols are UMOA results with the CD-Bonn interaction and experimental values, respectively. The dashed curve is given by the combination of the empirical formulae.

$\hbar\omega$-dependence, it is difficult to obtain the reliable results. The main purposes in this section are to investigate the $\hbar\omega$-dependence in the UMOA and to examine the validity of the UMOA. To investigate the $\hbar\omega$-dependence, in this section, we introduce $S^{(1)}$ to the UMOA and demonstrate the role of $S^{(1)}$. To examine the validity of the UMOA, we compare the results in the UMOA and in the other *ab initio* calculation methods. Note that we do not employ *method I* due to the uncontrollable approximations, and so we, hereafter, employ *method II* introduced in Sec. 3.5.2. Since this is the first application of the UMOA including $S^{(1)}$, we compute the ground-state properties of the simplest closed shell ^{4}He nucleus.

4.2.1 Role of One-Body Correlation Operator

As the first attempt in the UMOA with $S^{(1)}$, the ground-state energies for ^{4}He are calculated with the bare AV18 and CD-Bonn interactions and are shown in Fig. 4.4. As shown in this figure, even though our energies almost converge with respect to the model-space size $e_{\max}$, they are not likely to converge to the Faddeev-Yakubovsky (FY) energies [52] for both AV18 and CD-Bonn potentials cases. To assess the reason of this discrepancy, let us focus on the contributions coming from each cluster terms. By using Eq. (3.123), our energy $E_{\text{g.s.}} = -14.88$ MeV can be decomposed into $E^{\text{1BC}} = -10.27$ MeV and $E^{\text{3BC}} = -4.61$ MeV, in the AV18 potential case at $\hbar\omega = 60$ MeV and $e_{\max} = 20$. The percentage of the energy of the three-body cluster term is $\sim 30\%$ and the difference between UMOA
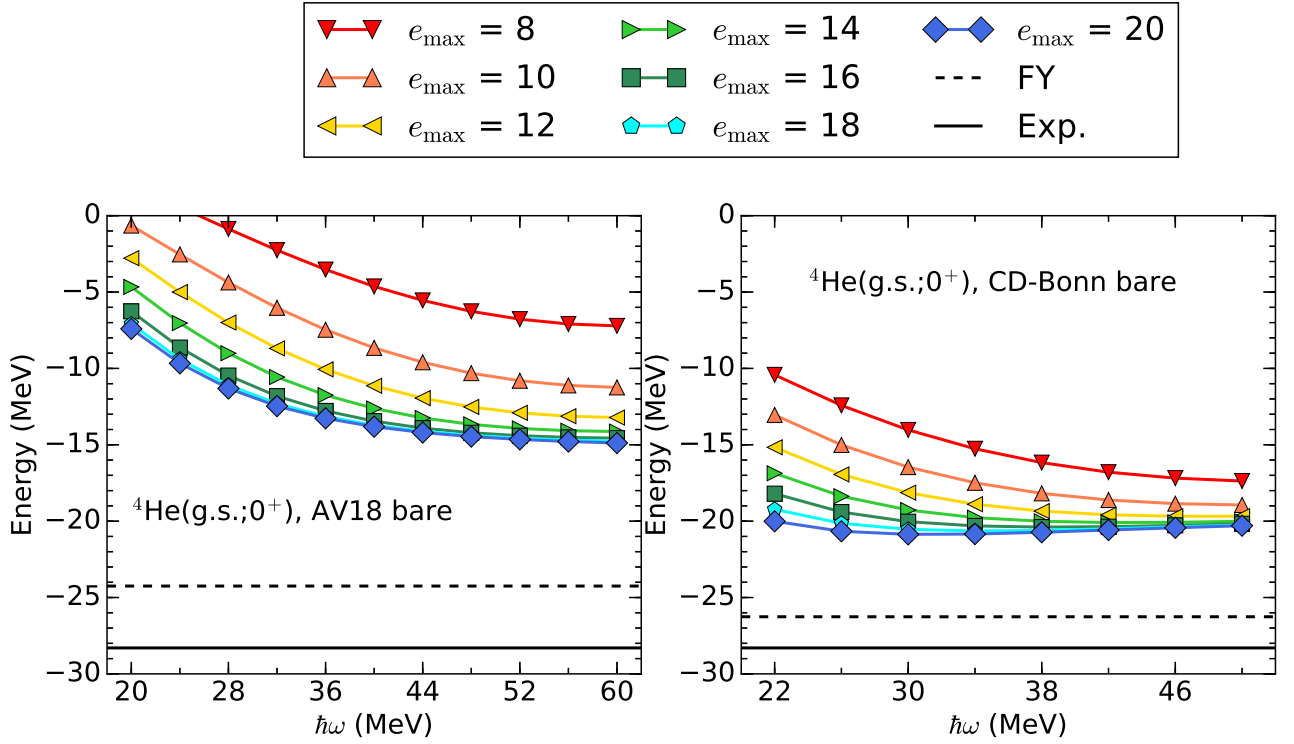
Figure 4.4: Ground-state energies of ^{4}He with the bare AV18 (left) and CD-Bonn (right) potentials as functions of $\hbar\omega$. The UMOA calculations are done with the *method II*. The results by the Faddeev-Yakubovsky (FY) method are taken from Ref. [52].

and FY energies, -9.37 MeV, is greater than $E^{3BC} = -4.61$ MeV. From those, the cluster expansion clearly breaks down. This is not surprising, because the strong short-range correlation of the bare *NN* interaction can be expected to induce the strong many-body correlations. Moreover, the convergence with respect to e_{max} is very slow. The calculations in the $e_{max} = 20$ model space would not be realistic for heavier nuclei such as ^{16}O or ^{40}Ca. It can be expected that we cannot reach the convergence for heavier or more loosely bound systems. Therefore, the current framework in the UMOA would not be applicable, when one employs "hard" *NN* interactions.

As another option, one can use the softened interactions introduced in Sec. 2.2.2 and 2.2.3. Here, we use the $V_{low\ k}$ interaction derived from AV18 interaction [8] with $\Lambda = 1.9$ fm^{-1}. The discussion given below would be valid for the other $V_{low\ k}$ interactions and for the SRG transformed interactions. Fig. 4.5 shows the convergence of the ground-state energies for ^{4}He with the $V_{low\ k}$ interaction as functions of $\hbar\omega$. In contrast to the case of bare interaction, left panel in Fig. 4.4, energies from $V_{low\ k}$ rapidly converge and are reasonably close to the coupled-cluster single and double (CCSD) [77] and exact Faddeev-Yakubovsky (FY) [78] results. Since, the results with the $V_{low\ k}$ interaction almost converges at $e_{max} = 12$, we discuss the role of one-body correlation operator with the $e_{max} = 12$ results.

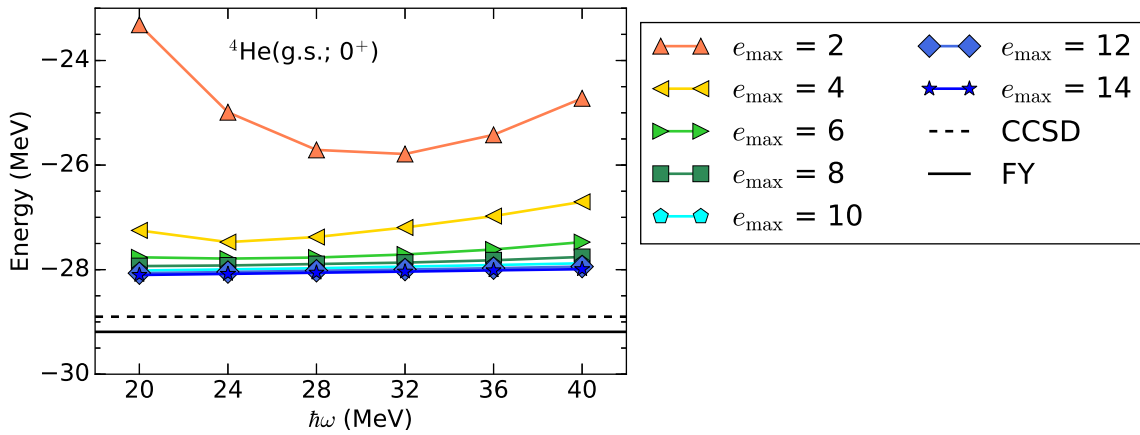Fig. 4.6 shows the ground-state energies and point-nucleon radii of ^{4}He as functions of $\hbar\omega$. In this

Figure 4.5: Ground-state energies and of ^{4}He as functions of $\hbar\omega$, using the $V_{\text{low k}}$ interaction derived at $\Lambda = 1.9$ fm^{-1}. The UMOA calculations are perfomed with the *method II*. The CCSD and FY results are taken from Refs. [77] and [77, 78].

figure, the calculation results are obtained with the HO 0p0h state (dashed curve), UMOA without $S^{(1)}$ (squares), diagonalization of the Hamiltonian (triangles), and UMOA with $S^{(1)}$ (circles). The diagonalization is done for the transformed Hamiltonian without $S^{(1)}$ in the 0p0h and 1p1h space. The UMOA without $S^{(1)}$ results (triangles) are almost parallel with the HO results (dashed line) for both of the ground-state energy and point-nucleon radius. The $S^{(2)}$ does not change the trend of the $\hbar\omega$-dependence coming from the original HO 0p0h state. After the diagonalization in the 0p0h and 1p1h space (squares), the $\hbar\omega$-dependence of the results is reduced compared to the UMOA without $S^{(1)}$ results (triangles) [42, 43]. The $\hbar\omega$-dependence of the results with the diagonalization is not negligible yet. However, if the transformation operator is constructed by the one- and two-body correlation operators, the situation is drastically changed. The results from the UMOA with $S^{(1)}$ (circles) are practically $\hbar\omega$-independent. This is the main result in this section. In the present framework, in contrast to the results in Sec. 4.1, we do not have to care about the choice of $\hbar\omega$, if the calculations are done in the sufficiently large model space.

Next, we discuss why the $\hbar\omega$-dependence of the results is reduced by introducing the one-body correlation operator. To assess the role of the one-body correlation operator, it is convenient to decompose the expectation value into the contributions coming from each cluster term. For the ground-state energy, it can be decomposed into energies of one-body kinetic term $\widetilde{t}_1$, two-body cluster term $\widetilde{v}_{12}$, and three-body cluster term $\widetilde{v}_{123}$. Fig. 4.7 shows the energies of the transformed one-, two-, and three-body cluster terms. In these figures, the dashed curve, dotted curve, triangles, and circles are obtained from the HO 0p0h state, HF state, UMOA without $S^{(1)}$, and UMOA with $S^{(1)}$, respectively. Let us focus on the kinetic energy part, the left panel in Fig. 4.7. When we ignore $S^{(1)}$ from the beginning of
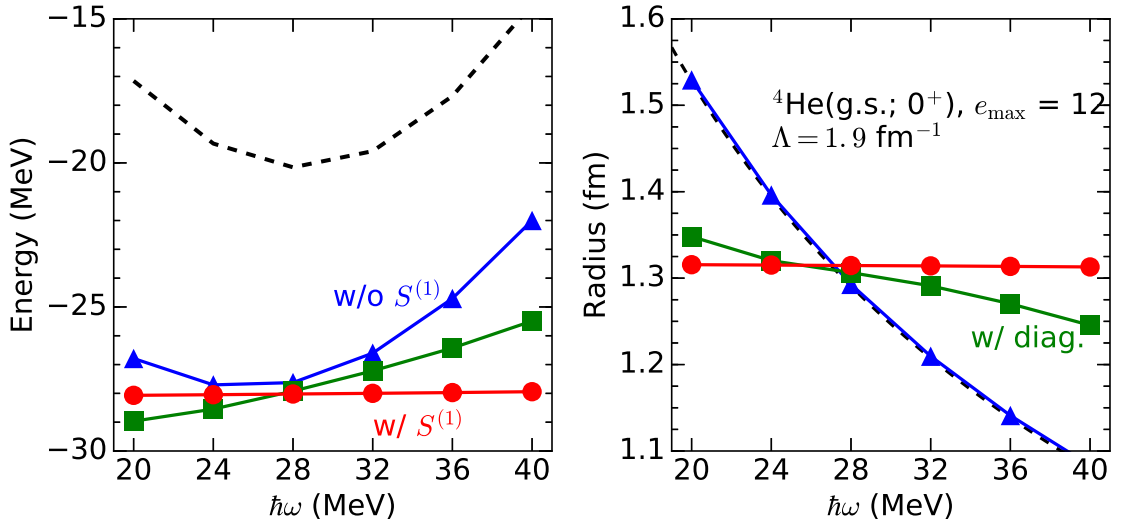
Figure 4.6: Ground state energies (left panel) and point-nucleon radii (right panel) of ^{4}He as functions of $\hbar\omega$, using the $V_{\text{low k}}$ interaction derived from the AV18 interaction at $\Lambda = 1.9$ fm^{-1}. Circle and triangle symbols are the results calculated in the UMOA with and without $S^{(1)}$, respectively. Squares are obtained after the diagonalization of the Hamiltonian derived without $S^{(1)}$ in the 0p0h and 1p1h space. The dashed curves are obtained with 0p0h reference state.

Figure 4.7: The energies of the one- (left), two- (middle), and three-body (right) cluster terms for ^{4}He as functions of $\hbar\omega$. Circles (triangles) are calculated with (without) $S^{(1)}$. The employed interaction is $V_{\text{low k}}$ interaction derived from the AV18 interaction at $\Lambda = 1.9$ fm^{-1}. The dashed and doted lines are calculated from the reference and HF states, respectively.

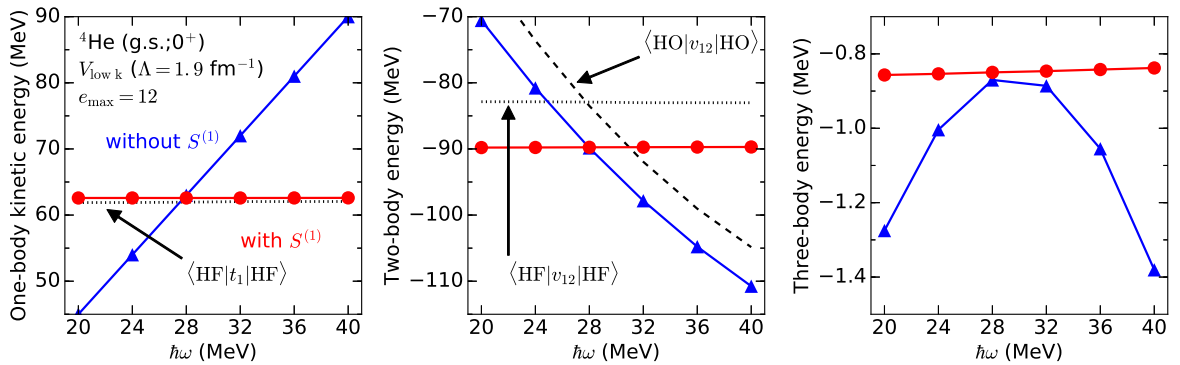calculations, $\langle t_1 \rangle$ is contributed solely by diagonal component of matrix $\langle a|t_1|b\rangle$. In this section, $\langle X \rangle$ means the expectation value of an operator X with respect to the HO reference state $|\text{HO}\rangle$. One can easily find that $\langle t_1 \rangle$ is proportional to $\hbar\omega$,

$$\langle t_1 \rangle = \left(1 - \frac{1}{A}\right) \sum_{a \leq \rho_F} \left(2n_a + l_a + \frac{3}{2}\right) \frac{\hbar\omega}{2}$$

$$= \frac{9\hbar\omega}{4}, \quad ((0s1/2)^4 \text{ for } {}^4\text{He}), \tag{4.5}$$

which can be found by UMOA without $S^{(1)}$ results (triangles) in the left panel in Fig. 4.7. On the other hand, when $S^{(1)}$ is introduced, $\widetilde{\langle t_1 \rangle} = \langle e^{-s_1} t_1 e^{s_1} \rangle$ can be affected by the off-diagonal component of the original matrix $\langle a|t_1|b\rangle$. As a result, $\widetilde{\langle t_1 \rangle}$ is practically $\hbar\omega$-independent as shown by circles in the left panel of Fig. 4.7. Also the results with $S^{(1)}$ (circles) are quite close to the dotted curve which is calculated by the HF method. Almost the same discussion can be done for the expectation value of the two-body cluster term. The HO 0p0h results (dashed line) in the middle panel in Fig. 4.7 show,

$$\langle v_{12} \rangle = \frac{1}{2} \sum_{a,b \leq \rho_F} \langle ab|v_{12}|ab\rangle, \tag{4.6}$$

the sum of the diagonal components of the original two-body matrix elements and strongly depends on $\hbar\omega$. While, the HF results (dotted curve) show the weak $\hbar\omega$-dependence. Similar correspondence can be seen in the results with and without $S^{(1)}$ (circles and triangles, respectively). The $\hbar\omega$-dependence is reduced by the effect of $S^{(1)}$, as shown by circles in the middle panel in Fig. 4.7. Similar to the one- and two-body cluster terms, the $\hbar\omega$-dependence of energy for the three-body cluster term is reduced (right panel). The inclusion of $S^{(1)}$ works well for reducing the $\hbar\omega$-dependence of ground-state energy. Moreover, the relation between the calculations with and without $S^{(1)}$ is similar to that between the results with the HF and reference states. Therefore, the introduction of $S^{(1)}$ relates with the HF basis states. In fact, if we ignore $S^{(2)}$ from the beginning of calculations, obtained ground-state energies coincides with the HF ground-state energies within a few keV level.

More directly, we investigate the role of $S^{(1)}$ by using the overlap of the wave functions. In Fig. 4.8, we show the three squared overlaps obtained between $|\text{HO}\rangle$ and HF$\rangle$ (dashed line), $|\text{UMOA}(S^{(1)} = 0)\rangle$ and $|\text{UMOA}(S^{(1)} \neq 0)\rangle$ (triangles), and $|\text{UMOA}(S^{(1)} \neq 0)\rangle$ and $|\text{HF}\rangle$ (circles), calculated at $e_{\max} = 12$. The $|\langle \text{HO}|\text{HF}\rangle|^2$ (dashed line) indicates the effect of the optimization of the single-particle basis states. In Fig. 4.8, the $|\langle \text{HO}|\text{HF}\rangle|^2$ (dashed line) and $|\langle \text{UMOA}(S^{(1)} \neq 0)|\text{UMOA}(S^{(1)} = 0)\rangle|^2$ (triangles) almost coincide. Therefore, the role of $S^{(1)}$ is to optimize the single-particle basis states, as expected in the previous discussion. Note that the $\hbar\omega$ maximizing the overlap gives the minimum of the ground-state energy (see Fig. 4.6). Since the HF results and UMOA with $S^{(1)}$ results do not depend on $\hbar\omega$ in Fig. 4.6, it can be expected that $|\langle \text{UMOA}(S^{(1)} \neq 0)|\text{HF}\rangle|^2$ is $\hbar\omega$-independent. As the check, we confirm that the circles, $|\langle \text{UMOA}(S^{(1)} \neq 0)|\text{HF}\rangle|^2$, do not depend on $\hbar\omega$.

Further insight can be obtained for $\widetilde{\langle t_1 \rangle}$ by looking the one-body density matrix γ. The definition of the element of the one-body density matrix γ_{ba} is

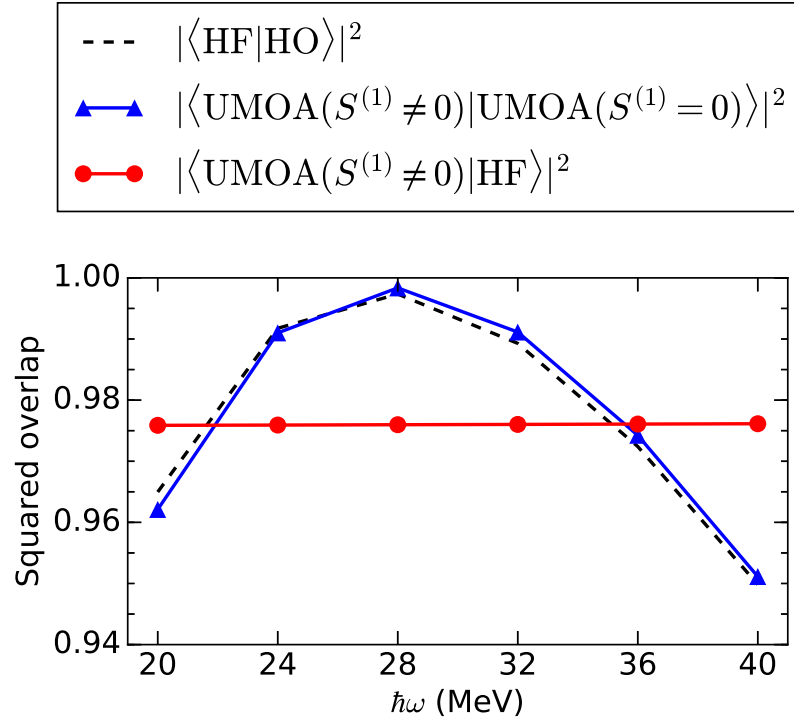$$\gamma_{ba} = \langle \Psi | c_a^\dagger c_b | \Psi \rangle, \tag{4.7}$$

Figure 4.8: The squared overlaps between the ground and reference states as functions of $\hbar\omega$. The employed *NN* interaction is the $V_{\text{low k}}$ interaction derived from the AV18 interaction at $\Lambda = 1.9$ fm^{-1}. Circles (triangles) are obtained with the UMOA with $S^{(1)}$ and HF (UMOA without $S^{(1)}$). The dashed line is given with the HF and HO reference states.

as found in the usual textbooks (see for example Ref. [74]). The γ_{ba} is calculated by using the cluster expansion, and we keep up to two-body cluster term (see Eq. (3.124)). Note that the expectation value of the one-body operator, $O = \sum_{ab}\langle a|o|b\rangle c_a^\dagger c_b$, can be obtained by

$$\langle\Psi|O|\Psi\rangle = \sum_{ab}\langle a|o|b\rangle\langle\Psi|c_a^\dagger c_b|\Psi\rangle = \sum_{ab} o_{ab}\gamma_{ab} = \text{Tr}(o\gamma). \tag{4.8}$$

Since the kinetic energy term, the effect of $S^{(2)}$ is very small, (see the difference between $\langle HF|t|HF\rangle$ (dotted line) and one-body kinetic energy in the UMOA (circles) in the left panel in Fig. 4.7), the kinetic energy in the UMOA can be approximated by $\text{Tr}(\gamma t_1)$. Fig. 4.9 shows the density matrices for the $s1/2$ orbitals with varying $\hbar\omega$ from 20 to 36 MeV. When $S^{(1)} = 0$, only $\gamma_{0s1/2,0s1/2}$ is dominant. This is consistent with the triangles in the left in Fig. 4.7. In contrast, the off-diagonal elements, especially $\gamma_{0s1/2,1s1/2}$, can have the large values, when $S^{(1)} \neq 0$. At $\hbar\omega = 20$ MeV, $\gamma_{0s1/2,1s1/2}$ is positive and increases $\langle\widetilde{t_1}\rangle$. Note that the off-diagonal component of $\langle a|t_1|b\rangle$ is always positive. On
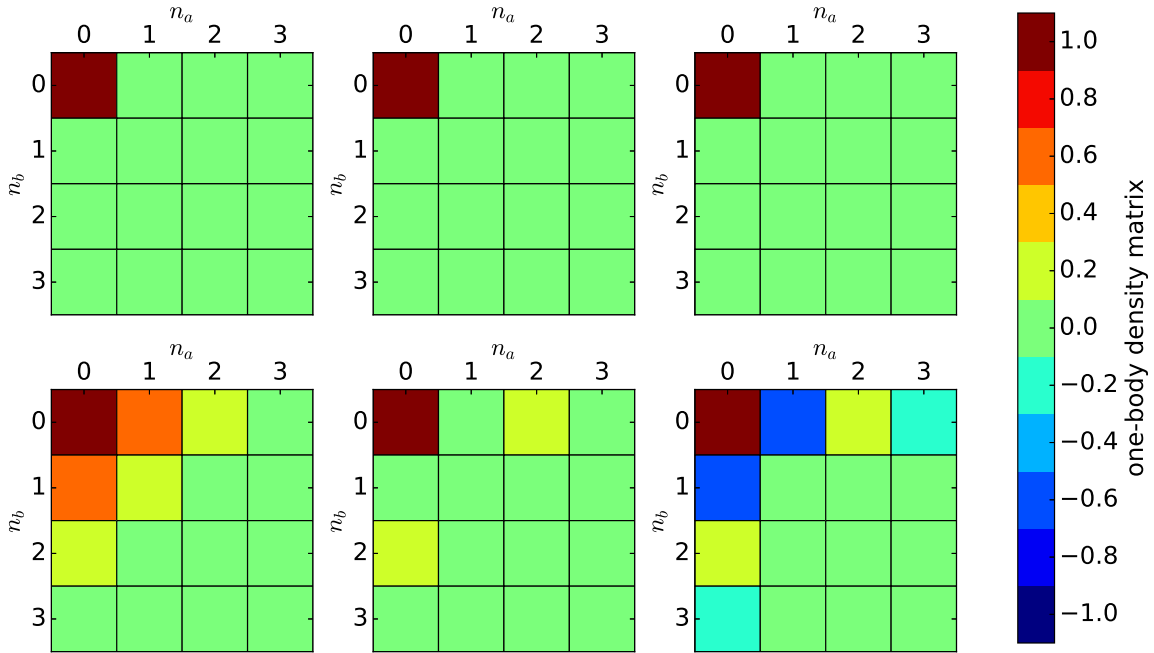
Figure 4.9: The one-body density matrix of $s1/2$ orbitals for ^{4}He calculated without (top) and with (bottom) the one-body correlation operator. The left, middle, and right panels are calculated at $e_{\max} = 12$ and $\hbar\omega = 20$, 28, and 36 MeV, respectively.

the other hand, $\gamma_{0s1/2,1s1/2}$ is negative and decreases $\langle \widetilde{t_1} \rangle$ at $\hbar\omega = 36$ MeV. The contribution to $\langle \widetilde{t_1} \rangle$ balances at $\hbar\omega = 28$ MeV, because $\gamma_{0s1/2,1s1/2}$ is almost zero. This discussion is consistent with the results shown in the left panel in Fig. 4.7. Since the radius is dominated by the one-body term, the reduction of the $\hbar\omega$-dependence for the radius is more understandable than energy. The point-nucleon radii of ^{4}He with respect to the reference state,

$$\langle r_{\mathrm{m}}^2 \rangle^{1/2} = \sqrt{\sum_a \frac{1}{A} \left(1 - \frac{1}{A}\right) \frac{(\hbar c)^2}{mc^2 \hbar\omega} \left(2n_a + l_a + \frac{3}{2}\right)}$$

$$\simeq \sqrt{\frac{9}{8} \times \frac{41.47}{\hbar\omega}} \ (\mathrm{fm}), \quad ((0s1/2)^4 \text{ for } {}^4\mathrm{He}), \tag{4.9}$$

are shown in the left panel in Fig. 4.6. Again, the off-diagonal components of the original matrix $\langle a | r_{\mathrm{m,1}}^2 | b \rangle$ affect to reduce the $\hbar\omega$-dependence. For these reasons, the $\hbar\omega$-dependence of the ground-state energies and matter radii are obviously reduced by introducing the one-body correlation operator, as discussed in Ref. [67]. From the density matrix in Fig. 4.9 and the negative off-diagonal component of $\langle a | r_{\mathrm{m,1}}^2 | b \rangle$, we can expect that the radius decreases (increases) in small (large) $\hbar\omega$ region compared to radius given in Eq. (4.9). This is consistent with the radii shown in the right panel in Fig. 4.6.

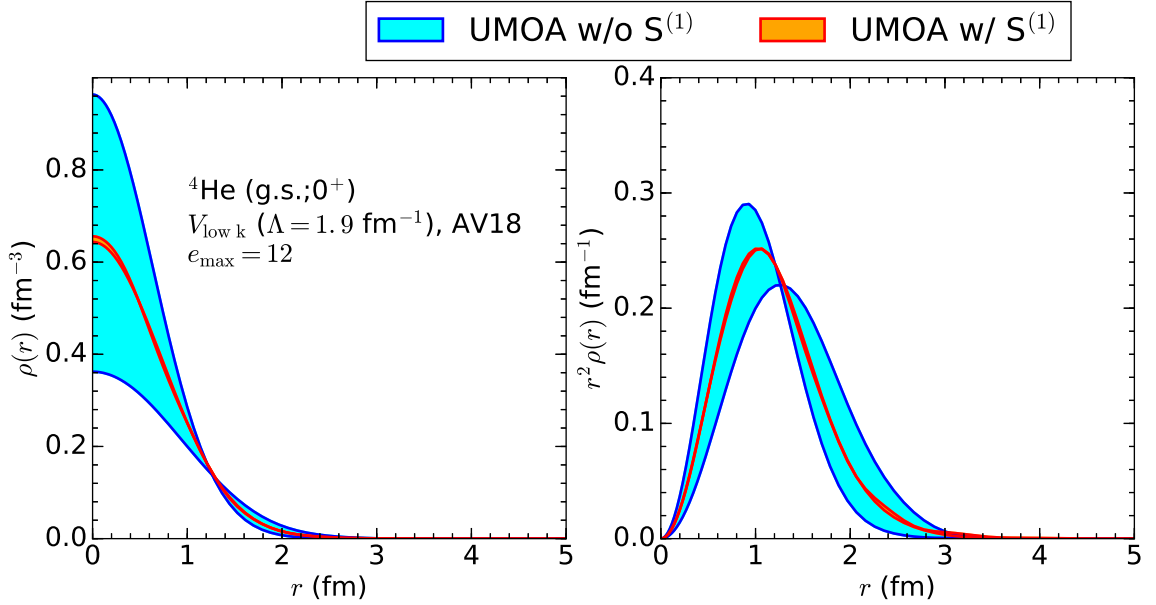As the final check, we plot the $\hbar\omega$-dependence of the translationally invariant radial point-nucleon

Figure 4.10: The translationally invariant point-nucleon density $\rho(r)$ (left panel) and $r^2\rho(r)$ (right panel) for ^{4}He. The results are calculated with the $V_{\text{low k}}$ interactions derived from AV18 interaction with $\Lambda = 1.9$ fm^{-1}. The shaded areas mean the $\hbar\omega$-dependence and are determined by changing from $\hbar\omega = 20$ MeV to 40 MeV.

density in left panel of Fig. 4.10. The definition of the translationally invariant is given in Appendix E.2. In this figure, the shaded areas denote the $\hbar\omega$-dependence of the density distribution and are determined by the difference between the density calculated with $\hbar\omega = 20$ MeV and 40 MeV. By the comparison between the results in the UMOA with and without $S^{(1)}$, one can confirm the significant reduction of the $\hbar\omega$-dependence. Similarly to the one-body density matrix, the expectation value of an arbitrary one-body operator $O = O(r)$ can be obtained with the density distribution:

$$\langle \Psi | O | \Psi \rangle \sim \int d^3\mathbf{r} O(r)\rho(r) = \int_0^\infty dr r^2 \rho(r) O(r). \tag{4.10}$$

According to the right panel of Fig. 4.10, $r^2\rho(r)$ is also $\hbar\omega$-independent in UMOA with $S^{(1)}$. As a result, the calculated observables are also $\hbar\omega$-independent.

4.2.2 Comparison with the Other *Ab Initio* Methods

Here, we compare our and the other *ab initio* calculations' results and examine the applicability of the UMOA. To compare with the published result in the other *ab initio* calculations, we employ the $V_{\text{low k}}$ interaction derived from AV18 interaction [8] at $\Lambda = 1.9$ fm^{-1}. In addition, we use the SRG transformed chiral N^{3}LO *NN* interaction [10] with the momentum cutoff $\lambda_{\text{SRG}} = 2.0$ fm^{-1},

which is widely used in the recent *ab initio* calculations. The results of ^{4}He energies are exhibited in Table 4.3 and are compared to the other *ab inito* calculation results. The convergence with respect to the model-space size is confirmed and the difference between $e_{\mathrm{max}} = 12$ and 14 results is (less than) the order of 10 keV for the $V_{\mathrm{low\ k}}$ (SRG transformed) interaction. As shown in Table 4.3, the contribution of the three-body cluster term, $E^{3\mathrm{BC}}$, is much smaller than those of one- and two-body cluster terms, $E^{1\mathrm{BC}}$ and $E^{2\mathrm{BC}}$. Therefore, our energy practically converges with respect to the cluster expansion. Moreover, our total energy, $E_{\mathrm{g.s.}}$, is reasonably close to the results by the other *ab initio* calculation methods, and the differences between them are comparable to the size the of $E^{3\mathrm{BC}}$. Since the contribution coming from the truncated terms is the order of $E^{3\mathrm{BC}}$, the error coming from the truncation of the cluster expansion is conservatively estimated by $E^{3\mathrm{BC}}$. The investigation of the higher contributions is discussed in Sec. 4.5.

Our results of the point-nucleon radius for the ^{4}He nucleus are also summarized in Table 4.4. According to Table 4.4, the contribution from the one-body cluster term, $\widetilde{r}_{\mathrm{m}}^{2(1\mathrm{BC})}$, is dominant. The effects of the higher-body cluster terms can be expected to be smaller than that of one-body cluster term. Similar to the Hamiltonian, the cluster expansion works well for the radius operator. The calculated radius is much smaller than the experimental radius 1.49 fm, which is consistent with the obtained large binding energy. Note that our charge radius for ^{4}He with the SRG transformed interaction, 1.65 fm is consistent with that from the in-medium similarity renormalization group approach [26]. The

Table 4.3: The calculated energies of the one-body cluster (kinetic) term, $E^{1\mathrm{BC}}$, two-body cluster (interaction) term, $E^{2\mathrm{BC}}$, the three-body cluster term, $E^{3\mathrm{BC}}$, and the total energy, $E_{\mathrm{g.s.}}$ for ^{4}He, respectively (see Eqs. (3.122) and (3.123)). The results in the section named "$V_{\mathrm{low\ k}}$" are calculated with the $V_{\mathrm{low\ k}}$ interaction derived from AV18 interaction with the sharp cutoff $\Lambda = 1.9$ fm^{-1}. Also, the results in section "V_{SRG}" are obtained with the SRG transformed chiral N^{3}LO *NN* interaction at $\lambda_{\mathrm{SRG}} = 2.0$ fm^{-1}. All the results are calculated at $e_{\mathrm{max}} = 14$ and $\hbar\omega = 20$ MeV. The results by the CCSD, FY, importance-truncated no-core shell model (IT-NCSM), and experiment are taken from Refs. [77], [77, 78], [79], and [23], respectively. All the energies are in MeV.

^{4}He		UMOA	CCSD	FY	Exp.
$V_{\mathrm{low\ k}}$	$E^{1\mathrm{BC}}$	62.60			
	$E^{2\mathrm{BC}}$	−89.84			
	$E^{3\mathrm{BC}}$	−0.86			
	$E_{\mathrm{g.s.}}$	−28.10	−28.9	−29.19(5)	−28.30
^{4}He		UMOA		IT-NCSM	Exp.
V_{SRG}	$E^{1\mathrm{BC}}$	53.50			
	$E^{2\mathrm{BC}}$	−80.47			
	$E^{3\mathrm{BC}}$	−0.76			
	$E_{\mathrm{g.s.}}$	−27.73		−28.25(1)	−28.30

UMOA works well and the results are consistent with the other *ab initio* calculation methods, at least, when one employs the soft *NN* interaction.

4.3 Results for Oxygen Isotopes

In the previous section, for light ^{4}He nucleus, we verified that the UMOA results are reasonably close to the results in the other *ab initio* calculation methods. As the next step, we can apply the UMOA to heavier mass region where the usual *ab initio* calculation methods, such as the NCSM and Green's function Monte Carlo, are not applicable. Since the ^{16}O is the second lightest doubly magic nucleus and is the spherical shape, the application to ^{16}O can be a good candidate for this purpose. Actually, in the other *ab initio* calculation methods such as coupled-cluster method (CCM) [77,81], self-consistent Green's function (SCGF) method [30], and in-medium similarity renormalization group (IM-SRG) approach [82, 83], the ground-state energy of ^{16}O were calculated as the benchmark. Also, in the earlier UMOA works [37, 60], ^{16}O calculations were done.

Another interest in the oxygen region is the limitation of neutron-rich oxygen isotope, i.e., the neutron drip line of the oxygen isotope. The heaviest oxygen having bound states is ^{24}O. ^{25}O and ^{26}O do not have bound states [84, 85]. On the other hand, ^{31}F is known as the most neutron-rich fluorine isotope with a bound state [86]. Adding one proton to oxygen, the drip line extend six neutrons. The mechanism of this anomaly was discussed with the shell-model calculations, and was explained by the effect of the three-nucleon (3N) interaction [13]. Moreover, in Ref. [13], it was discussed that the 3N interaction affects to the vanishment of the conventional neutron magic number $N = 20$ (filled up

Table 4.4: The calculated squared point-nucleon radii with the "one-body cluster term" $\widetilde{r}_{\mathrm{m}}^{2(1\mathrm{BC})}$, "two-body cluster term" $\widetilde{r}_{\mathrm{m}}^{2(2\mathrm{BC})}$, the "one- and two-body cluster term" $\widetilde{r}_{\mathrm{m}}^2$, and the root-mean-squared point-nucleon radii $(\widetilde{r}_{\mathrm{m}}^2)^{1/2}$ for ^{4}He. Note $\widetilde{r}_{\mathrm{m}}^2 = \widetilde{r}_{\mathrm{m}}^{2(1\mathrm{BC})} + \widetilde{r}_{\mathrm{m}}^{2(2\mathrm{BC})}$. The calculation set up is same as in Table 4.3. The experimental value is take from Ref. [80].

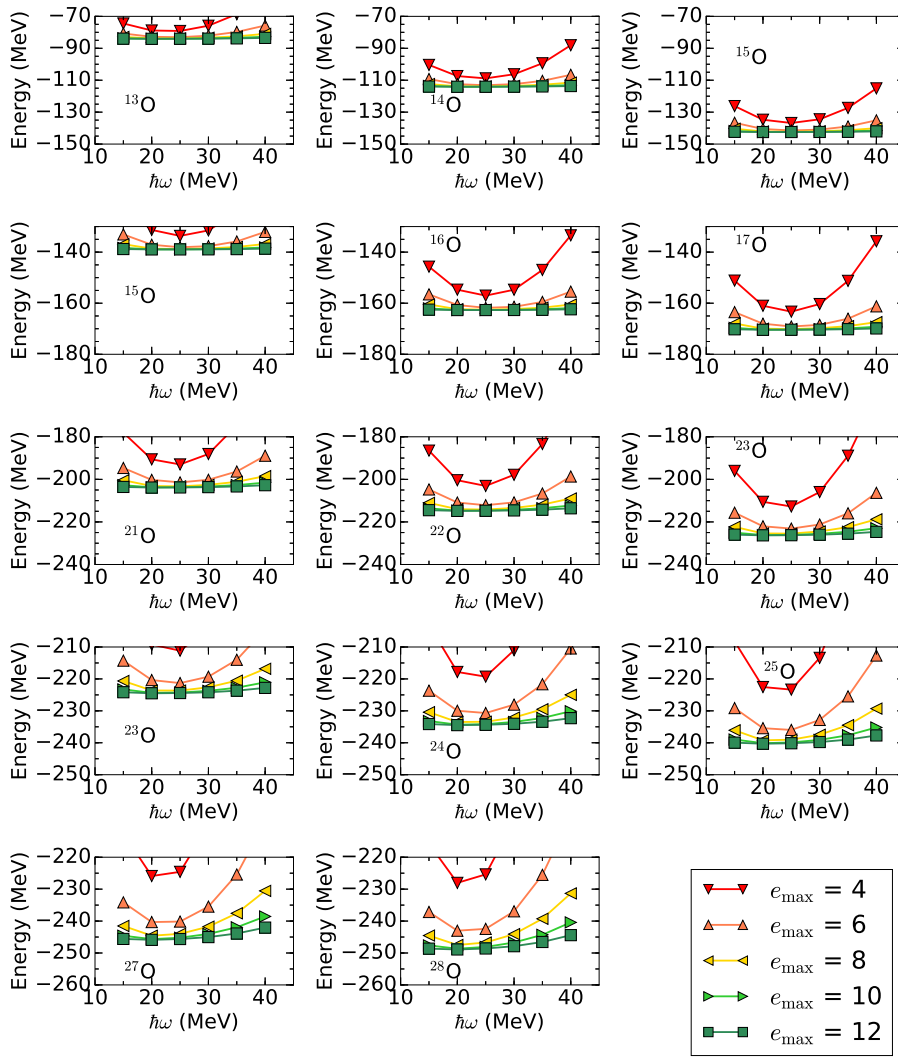| ^{4}He			UMOA	Exp.
$V_{\mathrm{low}\ k}$	$\widetilde{r}_{\mathrm{m}}^{2(1\mathrm{BC})}$	(fm^2)	1.70	
	$\widetilde{r}_{\mathrm{m}}^{2(2\mathrm{BC})}$	(fm^2)	0.04	
	$\widetilde{r}_{\mathrm{m}}^2$	(fm^2)	1.74	
	$(\widetilde{r}_{\mathrm{m}}^2)^{1/2}$	(fm)	1.32	1.49(3)
^{4}He			UMOA	Exp.
V_{SRG}	$\widetilde{r}_{\mathrm{m}}^{2(1\mathrm{BC})}$	(fm^2)	1.97	
	$\widetilde{r}_{\mathrm{m}}^{2(2\mathrm{BC})}$	(fm^2)	0.02	
	$\widetilde{r}_{\mathrm{m}}^2$	(fm^2)	1.99	
	$(\widetilde{r}_{\mathrm{m}}^2)^{1/2}$	(fm)	1.41	1.49(3)

Figure 4.11: The ground-state energies for oxygen isotopes as functions of $\hbar\omega$, using the chiral N^{3}LO (500 MeV) *NN* interaction [10] softened by the SRG transformation with $\lambda_{\mathrm{SRG}} = 2.0$ fm^{-1}. The left, middle, and right columns show the energies for nuclei, removing one neutron form the sub-shell closures, the sub-shell closures, and adding one neutron to sub-shell closures, respectively.

to $0d_{3/2}$ orbital) and appearing of the new magic number $N = 14$ (filled up to $0s_{1/2}$ orbital) and 16 (filled up to $0d_{3/2}$ orbital). Recently, the drip line of the oxygen isotope was reproduced in the *ab inito* calculations by introducing the 3*N* interactions [29–31].

The main purpose in this section is to investigate the applicability of the UMOA for the oxygen region. Here, we employ the chiral N^{3}LO *NN* interactions [10] evolved by the SRG transformation with $\lambda_{\mathrm{SRG}} = 1.88$ fm^{-1}, 2 fm^{-1}, 2.24 fm^{-1}. Note that the λ_{SRG}-dependence of the observables indicates the effect of the truncated many-body interactions, because the observables should not depend on resolution scale λ_{SRG}.

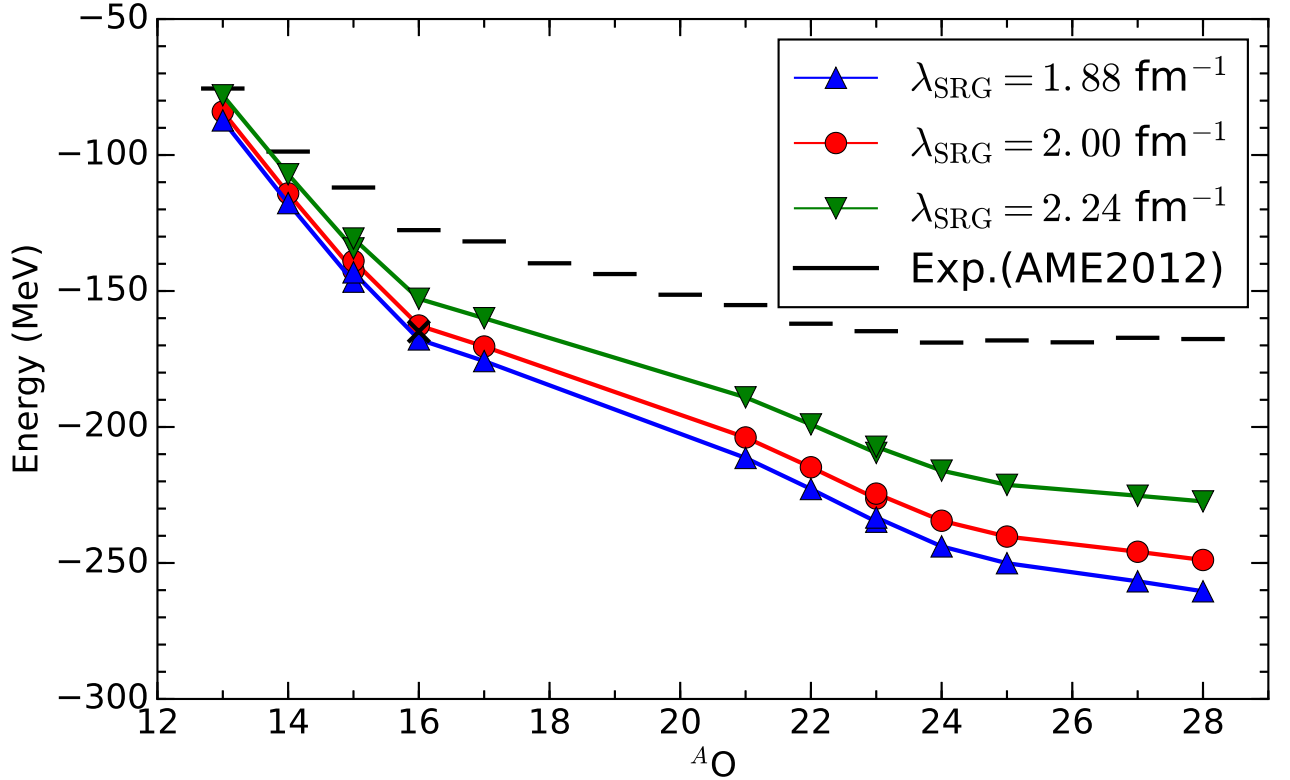Let us begin with discussing the convergence of the calculations. Fig. 4.11 shows the ground-

Figure 4.12: The ground-state energies for oxygen isotopes from the chiral N³LO (500 MeV) *NN* interaction [10] softened by the SRG transformation with λ_{SRG} = 1.88 fm⁻¹, 2 fm⁻¹, 2.24 fm⁻¹.

state energies of the oxygen isotopes, calculated with the λ_{SRG} = 2 fm⁻¹ interaction, as functions of $\hbar\omega$ with varying the model-space size e_{max}. The left, middle, and right columns show the ground-state energies for nuclei, removing one neutron from shell closures, shell closures, and attaching one neutron to shell closures, respectively. Note that the energy of odd-mass nuclei are calculated with the EOM approach. Since our energies with e_{max} = 12 practically converge, the results at e_{max} = 12 and $\hbar\omega$ = 20 MeV are used in the following discussions.

In Fig. 4.12, the ground-state energies of the oxygen isotopes are shown with varying λ_{SRG}. As for ¹⁵O and ²³O, the ground-state energies can be calculated by both of particle attachment (PA) and particle removing (PR) for sub-shell closures. The differences between them, $\Delta E_{g.s.} = E_{g.s.}^{PA} - E_{g.s.}^{PR}$, are $\Delta E_{g.s.}(^{15}O)$ = −3.29 MeV and $\Delta E_{g.s.}(^{23}O)$ = −1.82 MeV. The $\Delta E_{g.s.}$ should reflect the truncation error in the UMOA and they are a few percent level in the total ground-state energy. This agreement between PR and PA approaches means that our approximations, such as the truncation of the many-body cluster term and the restriction of the space of diagonalization, are reasonable. Our energies show a good agreement with the SCGF energies [87]. Particularly, our ¹⁶O energy with λ_{SRG} = 2 fm⁻¹ shows a good agreement with the importance-truncated no-core shell model (IT-NCSM) results (cross) [79]. Our results show sizable λ_{SRG}-dependence. Since the observables should not depend on the resolution scale, this λ-dependence suggests the contributions of the truncated
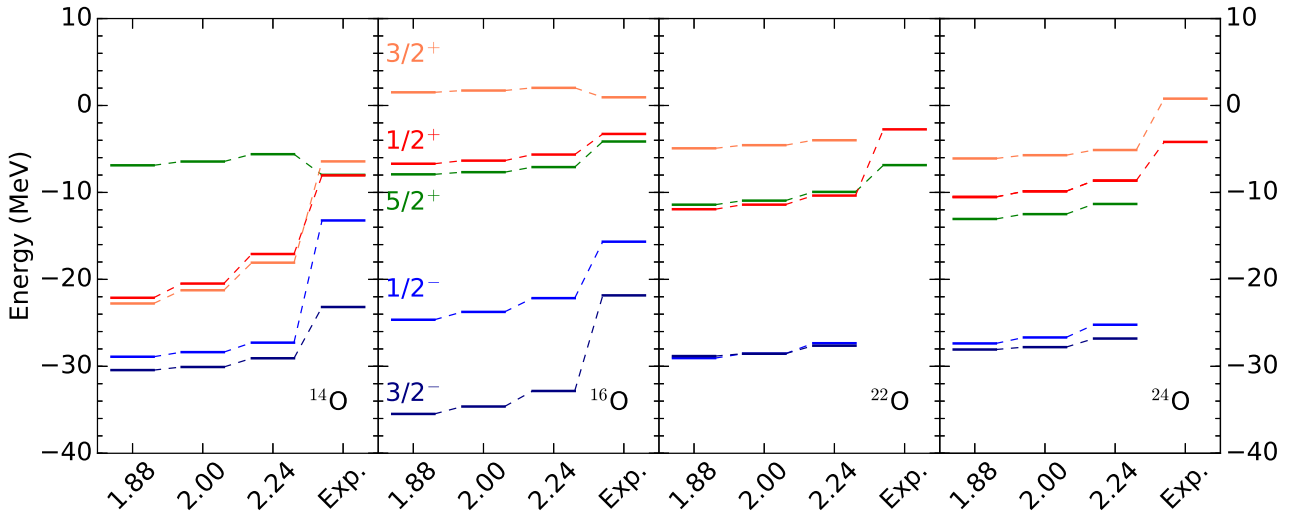
Figure 4.13: The neutron single-particle energies for ^{14}O, ^{16}O, ^{22}O, and ^{24}O from the chiral N^{3}LO (500 MeV) *NN* interaction [10] softened by SRG transformation with $\lambda_{\mathrm{SRG}} = 1.88$ fm^{-1}, 2 fm^{-1}, 2.24 fm^{-1}.

many-body interactions. Our ground-state energies become overbound compared to the experimental data with increasing the mass number and do not reproduce the neutron drip line. As found in the recent works [13, 29–31], the ground-state energies of the oxygen isotopes can be reproduced well by introducing the 3*N* interaction.

To pay attention to the single-particle energy is useful for understanding the structure. The definition of the single-particle energy cannot be determined uniquely as discussed in Ref. [87]. In this thesis, the single-particle energy ϵ_k for *A*-body sub-shell closure is defined by $\epsilon_k = \pm(E_{\mathrm{g.s.}}^A - E_k^{A\mp 1})$. Fig. 4.13 shows the neutron single-particle energies for ^{14}O, ^{16}O, ^{22}O and ^{24}O with $\lambda_{\mathrm{SRG}} = 1.88$ fm^{-1}, 2 fm^{-1}, 2.24 fm^{-1}. The calculated levels are consistent with those in the SCGF method [87]. Therefore, the UMOA works well including the excitation energies of neighbors of sub-shell closure. For ^{14}O and ^{16}O, one can find the many experimental data [88, 89]. Comparing to the experimental data, our spectra are much stretched than the experimental spectra and the shell gaps are overestimated. The change of λ_{SRG} seems to give the overall shift and is not significant to the shell structure. Therefore, we need to include the 3*N* interaction to reproduce the experimental data.

4.4   Towards Heavier Nuclei

The UMOA works well similarly to the other *ab initio* methods, as demonstrated in Sec. 4.2 and 4.3. Following these, we can apply the UMOA to heavier system. Then, one will encounter the problem that the three- and many-body interactions can be critical to reproduce the data for heavier system, as pointed out in Sec. 4.3. Even if we employ only the *NN* interactions, however, it is significant to complete the whole mass region with the systematic *ab initio* calculations. It is interesting, especially,
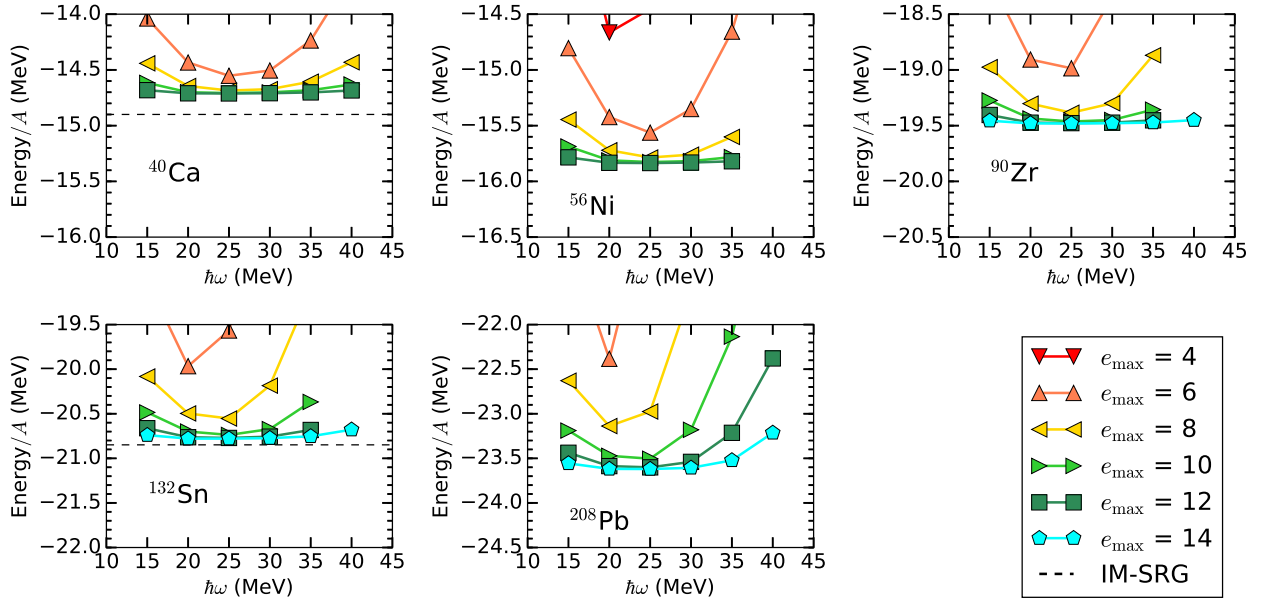
Figure 4.14: The 0^+ ground-state energies per nucleon for ^{40}Ca, ^{56}Ni, ^{90}Zr, ^{132}Sn, and ^{208}Pb as functions of $\hbar\omega$. The chiral N^{3}LO (500 MeV) *NN* interaction [10] softened by SRG transformation with $\lambda_{\text{SRG}} = 2.0$ fm^{-1} is employed. The IM-SRG results are taken from Ref. [26].

whether certain nuclear properties can be determined by the *NN* interactions. In this section, we investigate the ground-state properties of closed shell nuclei across the nuclear chart and discuss the bulk properties of many-nucleon system.

4.4.1 Convergence

Since it can be easily expected that the convergence becomes worse in the heavier or loosely bound systems, before discussing the results, let us see the convergence of the UMOA calculations for the heavier systems. In Fig. 4.14, the ground-state energies per nucleon for ^{40}Ca, ^{56}Ni, ^{90}Zr, ^{132}Sn, and ^{208}Pb are shown as the functions of $\hbar\omega$ and e_{max}. Since the difference of energies at $e_{\text{max}} = 12$ and $e_{\text{max}} = 14$, at $\hbar\omega = 20$ MeV, are less than 10 keV/A , 20 keV/A, and 30 keV/A for ^{90}Zr, ^{132}Sn, and ^{208}Pb, respectively, our energies almost converge at $e_{\text{max}} = 12$. The ratio to the three-body cluster term correction to the total energy, $|E^{\text{3BC}}/E_{\text{g.s.}}|$, is less than 0.05 and our results practically converge with respect to the cluster expansion. Moreover, our energies for ^{40}Ca and ^{132}Sn are consistent with the IM-SRG energies [26].

Similarly to the energy, the point-nucleon radii for ^{40}Ca, ^{56}Ni, ^{90}Zr, ^{132}Sn, and ^{208}Pb are shown in Fig. 4.15 as functions of $\hbar\omega$ and e_{max}. The radii are also practically converged at $e_{\text{max}} = 12$ with fixed $\hbar\omega = 20$ MeV. Therefore, our discussions given in Sec. 4.4.2 are based on at $e_{\text{max}} = 12$ and $\hbar\omega = 20$ MeV. Note that our charge radii for ^{16}O and ^{40}Ca are consistent with the IM-SRG results found in Ref. [26]. In addition to $\lambda_{\text{SRG}} = 2$ fm^{-1} interaction, we employ $\lambda_{\text{SRG}} = 1.88$ fm^{-1}, 2.24 fm^{-1}
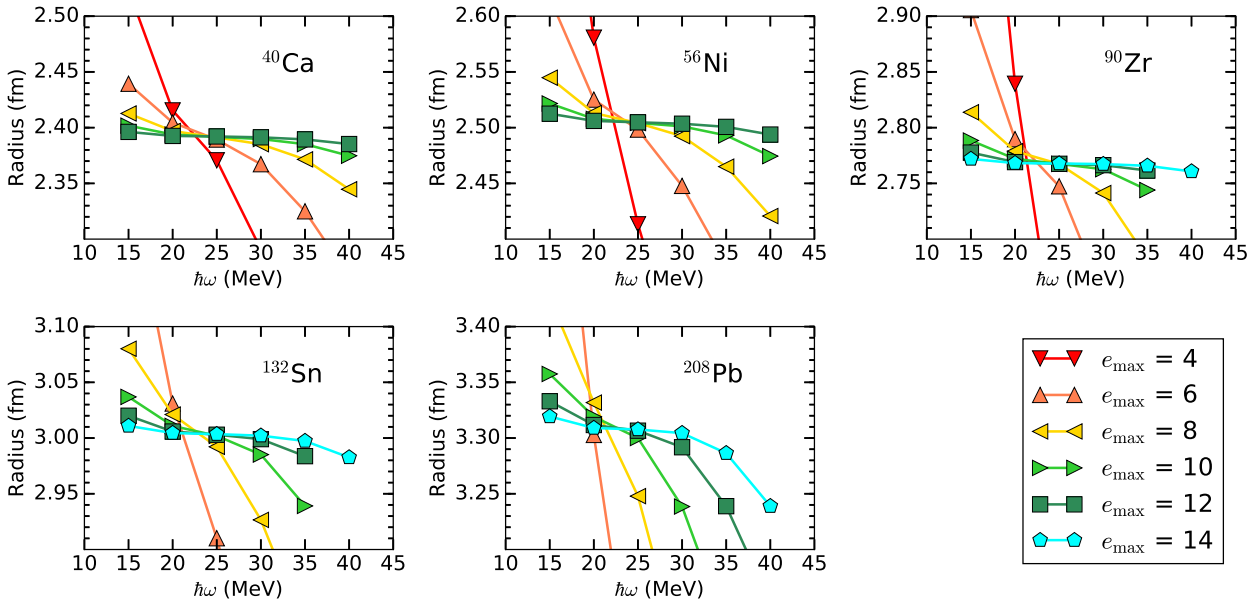
Figure 4.15: Same as Fig. 4.15 except for the point-nulceon radii.
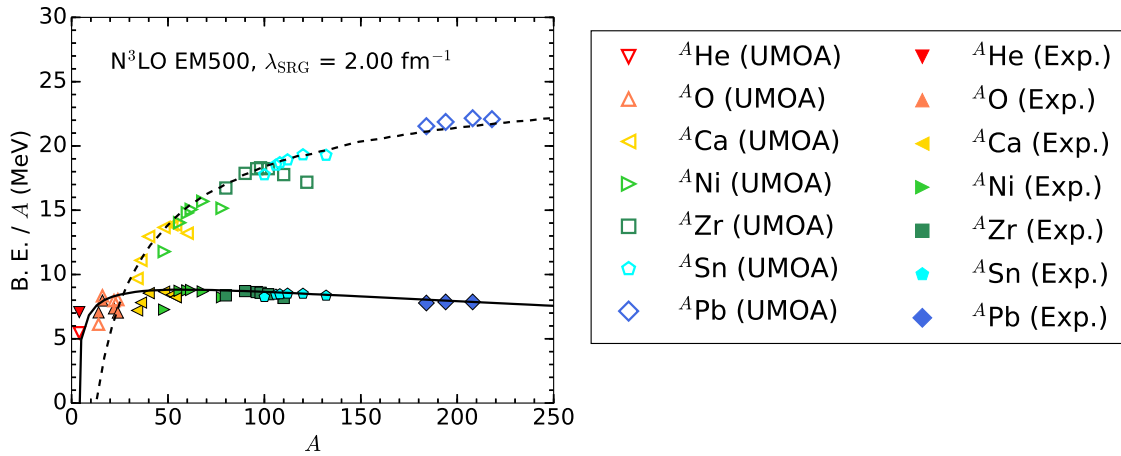
Figure 4.16: The binding energies per nucleon with the chiral N^{3}LO (500 MeV) *NN* interaction [10] softened by SRG transformation with λ_{SRG} = 2.0 fm^{-1}. The experimental data (solid symbols) are taken from Ref. [23]. The dashed (solid) line is given by the Bethe-Weizäcker's mass formula fitted to the UMOA (experimental) results.

interactions. The final results are exhibited in Table F.1, F.2, and F.3 in Appendix F.

4.4.2   Bulk Properties of Many-Nucleon System

Fig. 4.16 shows the binding energies per nucleon calculated with the chiral NN N^{3}LO interaction evolved to $\lambda_{\text{SRG}} = 2$ fm^{-1} as functions of mass number. The experimental data shown in Fig. 4.16 are taken from Ref. [23]. Comparing to the experimental energies, our energies become much larger than the experimental data as the mass number increases. Since the initial interactions employed in our calculations are short-range interactions, it is worth fitting to the semi-empirical mass formula,

$$B/A = a_{\text{V}} - a_{\text{S}}A^{-1/3} - a_{\text{C}}\frac{Z^2}{A^{4/3}} - a_{\text{A}}\frac{(N-Z)^2}{A^2}. \tag{4.11}$$

Here, B/A is the binding energy per nucleon. Coefficients a_{V}, a_{S}, a_{C}, and a_{A} are for the volume, surface, coulomb, and asymmetry terms, respectively. The resulting parameters are exhibited in Table 4.5. Since it is well known that the liquid drop model works for heavier system, fitting is done by using data heavier than oxygen region. Our a_{V} and a_{S} are much larger than those obtained with the experimental energies and strongly depend on λ_{SRG} and are far from the results with the experimental data. Our a_{C} results are smaller than a_{C} from experimental data. This is consistent with our A-dependence of radii (see next discussion). Interestingly, our a_{A} are less sensitive to the change of λ_{SRG}. This suggests that the observables originated by proton-neutron asymmetry can be independent of λ_{SRG}. Moreover, a_{A} from the UMOA results are close to the result with the experimental data.

In addition to the binding energy, the size of nucleus is the fundamental observable and important to discuss the saturation property of finite nuclei. Fig. 4.17 shows the calculated and experimental charge radii. Note that the definition of charge radii are given in Eq. (4.1). The experimental data are taken from Ref. [73]. We also show the solid (dashed) line given by fitting the experimental (calculated) radii heavier than oxygen region with $r_{\text{ch}} = r_0 A^x$. Here, r_0 and x are fitting parameters. After fitting, $r_{0,\text{exp}} = 1.12(4)$ fm, $x_{\text{exp}} = 0.299(7)$ and $r_{0,\text{cal}} = 1.28(5)$ fm, $x_{\text{cal}} = 0.177(9)$ are obtained from the experimental and calculated radii, respectively. As well known, the experimental data are proportional to $A^{1/3}$, i.e. $x_{\text{exp}} \sim 1/3$ for experimental radii. In contrast, our radii are not proportional to $A^{1/3}$ and become much smaller than the experimental radii as A increases. The density ρ_0 of nucleus can be easily obtained as a function of A by assuming the uniform density,

$$\rho_0 \sim \frac{3}{4\pi r_0^3}A^{1-3x}. \tag{4.12}$$

Table 4.5: Coefficients in Eq. (4.11) fitted to the UMOA and experimental results. The number in parenthesis means the error and given from the standard deviation of fitting. All the units are in MeV.

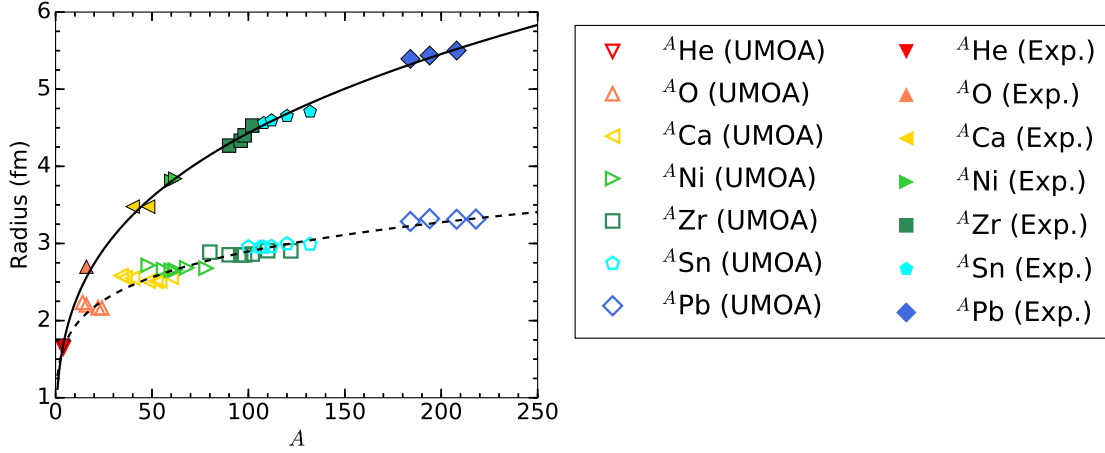|	$\lambda_{\text{SRG}} = 1.88$ fm^{-1}	$\lambda_{\text{SRG}} = 2$ fm^{-1}	$\lambda_{\text{SRG}} = 2.24$ fm^{-1}	Exp.
a_{V}	44.1(1.5)	41.6(1.3)	36.6(1.1)	14.9(2)
a_{S}	97.9(3.9)	91.0(3.5)	76.8(2.9)	15.1(4)
a_{C}	0.32(0.14)	0.38(0.13)	0.48(0.10)	0.65(2)
a_{A}	26.4(4.3)	26.6(3.9)	26.5(3.2)	21.1(6)

Figure 4.17: The charge radii for closed sub-shell nuclei. The experimental data are taken from Ref. [73]. The solid (dashed) line is given by fitting the experimental (calculated) radii heavier than oxygen region with $r_{\mathrm{ch}} = r_0 A^x$. The resulting parameters with the experimental and calculated radii are $r_{0,\mathrm{exp}} = 1.12(4)$ fm, $x_{\mathrm{exp}} = 0.299(7)$ and $r_{0,\mathrm{cal}} = 1.28(5)$ fm, $x_{\mathrm{cal}} = 0.177(9)$, respectively.

Obviously, one can obtain nucleus-independent ρ_0 for $x = 1/3$ and can define the density for infinite nuclear matter. According to the fitting results with the calculation values, however, we have A-dependent density and obtain infinite density as A goes infinity. This result is consistent with the recent nuclear matter calculation results with the softened NN interactions [90]. To confirm the nucleus-dependence of density, we calculate the nucleon translationally invariant density $\rho_{\mathrm{m}}(r)$. In Fig. 4.18, $\rho_{\mathrm{m}}(r)$ is plotted for some selected shell closed nuclei from ^{4}He to ^{208}Pb with the $\lambda_{\mathrm{SRG}} = 2$ fm^{-1} interaction. One can clearly see the increases of the density as A increases. For both binding energy and density, we cannot reproduce the saturation property with only the NN interaction.

The simplest observable coming from proton-neutron asymmetry is the difference between point-neutron and point-proton radii, $\langle r_n^2 \rangle^{1/2}$ and $\langle r_p^2 \rangle^{1/2}$, respectively, i.e.,

$$\Delta r_{np} = \langle r_n^2 \rangle^{1/2} - \langle r_p^2 \rangle^{1/2}. \tag{4.13}$$

The calculated numbers of Δr_{np} are also displayed in Table F.1, F.2, and F.3. Fig. 4.19 shows Δr_{np} as functions of mass number. The error bars come from the SRG scale variation $\lambda_{\mathrm{SRG}} = 1.88$ fm^{-1}, 2 fm^{-1} and 2.24 fm^{-1}. This small λ_{SRG}-dependence means that Δr_{np} results are not affected by induced many-body interactions. Combining with the universality of the SRG transformed interactions, our results do not depend on choice of initial interactions. Moreover, our results show good agreement with the empirical formula (blue bands) [91,92], $\Delta r_{np} = (0.90 \pm 0.15)(N - Z)/A + (-0.03 \pm 0.02)$ fm, which shows trend of the experimental Δr_{np} for the 26 stable nuclei from ^{40}Ca and ^{238}U deduced from the antiprotonic atom data. Our results are consistent with the recent CCM results (hatched area), including the $3N$ force effect, for ^{48}Ca.

The determination of Δr_{np} is an important issue because the correlation between Δr_{np} and sym-
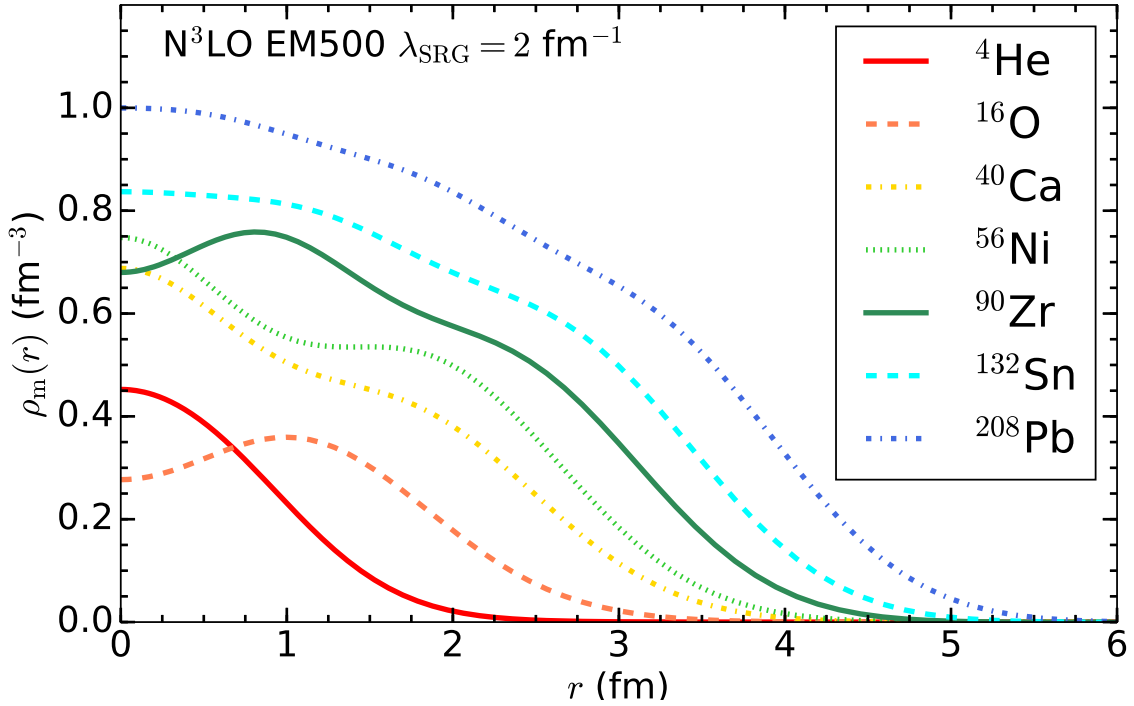
Figure 4.18: The calculated nucleon translationally invariant density $\rho_{\mathrm{m}}(r)$ for selected nuclei from ^{4}He to ^{208}Pb as functions of r. The employed interaction is chiral N^{3}LO *NN* interaction softened by SRG transformation with $\lambda_{\mathrm{SRG}} = 2$ fm^{-1}.

metry energy of infinite nuclear matter is well known in the mean-field calculations [93–95]. In order to discuss such a topic in the UMOA, further developments and investigations are needed.

4.5 UMOA at Three-Body Level

So far, our calculations are done with the only *NN* interactions. To reproduce the data quantitatively, at least, the inclusion of the 3*N* interactions are needed. The simplest way is to extend the UMOA framework and to complete the three-body cluster term. In this section, we show the first results for ^{4}He with the UMOA at three-body level. To compare to the UMOA at two-body level, at first, we begin with the numerical calculation with the *NN* interaction. The employed *NN* interaction in this section is chiral N^{3}LO interaction SRG evolved to $\lambda_{\mathrm{SRG}} = 2$ fm^{-1}.

As discussed in Sec. 3.1, the extension of the framework is rather straightforward. Since the current UMOA code is written in the *J*-coupled basis, however, the antisymmetrization and derivations of the matrix elements in the three-body state are much more complicated than those in the two-body state. The details for such issues are discussed in Appendix G.

To investigate the effect of the truncation in the UMOA, we attempt several options. In this section,
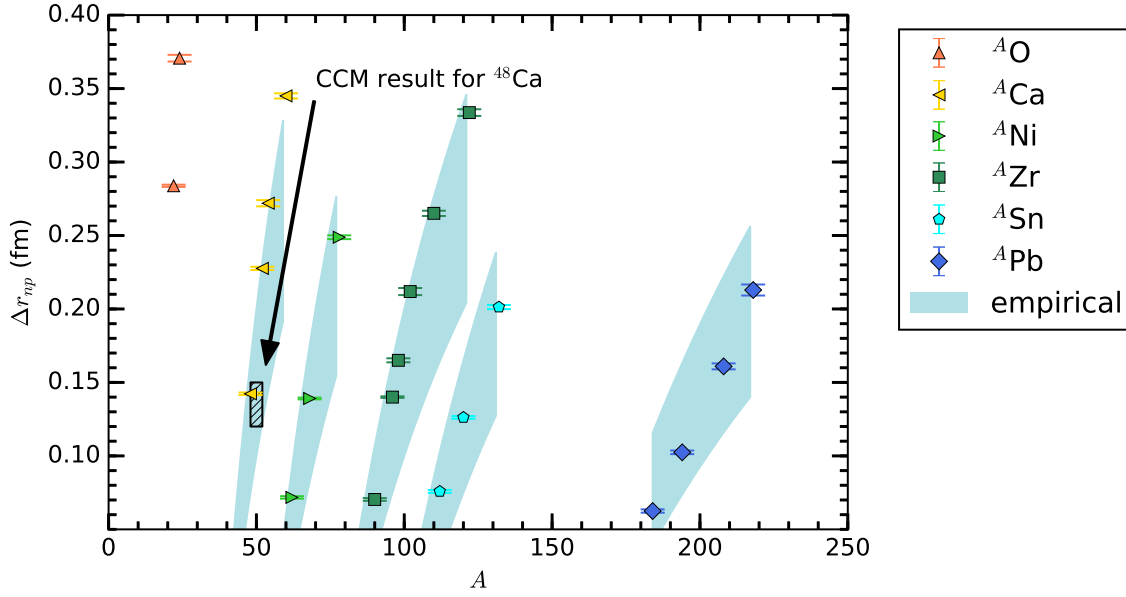
Figure 4.19: The $\Delta r_{np} = \langle r_n^2 \rangle^{1/2} - \langle r_p^2 \rangle^{1/2}$ for closed sub-shell nuclei. The error bars come from the SRG cut off variation $\lambda_{\rm SRG} = 1.88$ fm^{-1}, 2 fm^{-1}, and 2.24 fm^{-1}. The blue bands are given by the empirical formula based on the experimental data [91, 92]. The CCM result for ^{48}Ca are taken from Ref. [41].

we classify the calculation rank by UMOA(m, n) which means the calculation with

$$ U = e^{S^{(1)}} \cdots e^{S^{(m)}}, \quad \widetilde{H} \approx \sum_{i=1}^{n} H^{(i)}. \tag{4.14} $$

Moreover, the perturbative correction of the n-body cluster term is denoted by $\{n\}$. The results presented so far, therefore, are based on UMOA(2, {3}).

Fig. 4.20 shows the ground-state energies for ^{4}He as functions of $\hbar\omega$ with varying $e_{\rm max}$. For all the UMOA calculations, energies become more $\hbar\omega$-independent values with increasing $e_{\rm max}$. The almost converged results can be found at $e_{\rm max} = 6$ and $\hbar\omega = 25$ MeV and are summarized in Table 4.6. The displayed energies, $E^{\rm 1BC}$, $E^{\rm 2BC}$, and $E^{\rm 3BC}$ are contributions of one-, two-, and three-body cluster terms, respectively. For UMOA(2,{3}), UMOA(2, 3), and UMOA(3, 3) cases, the $E^{\rm 3BC}$ are much smaller than $E^{\rm 1BC}$ and $E^{\rm 2BC}$, which means the good convergence of the cluster expansion. The UMOA(2, 3) energy shows excellent agreement with the IT-NCSM result [79], while the UMOA(3, 3) energy is overbound to it by a hundred keV. Note that the IT-NCSM energy can be thought of as the exact solution of NN interaction employed here. Then, the size of the four-body cluster term correction $E^{\rm 4BC}$ can be estimated as a few or less than hundred keV level. This is very reasonable with respect to the size of $E^{\rm 3BC}$ because of $E^{\rm 4BC}/E^{\rm 3BC} \sim 10\%$. Our promising results, exhibited here, are consistent with the IT-NCSM result. Owing to this extension of the UMOA framework, a $3N$ interaction can be directly introduced to the initial Hamiltonian and can be treated consistently. The calculations with
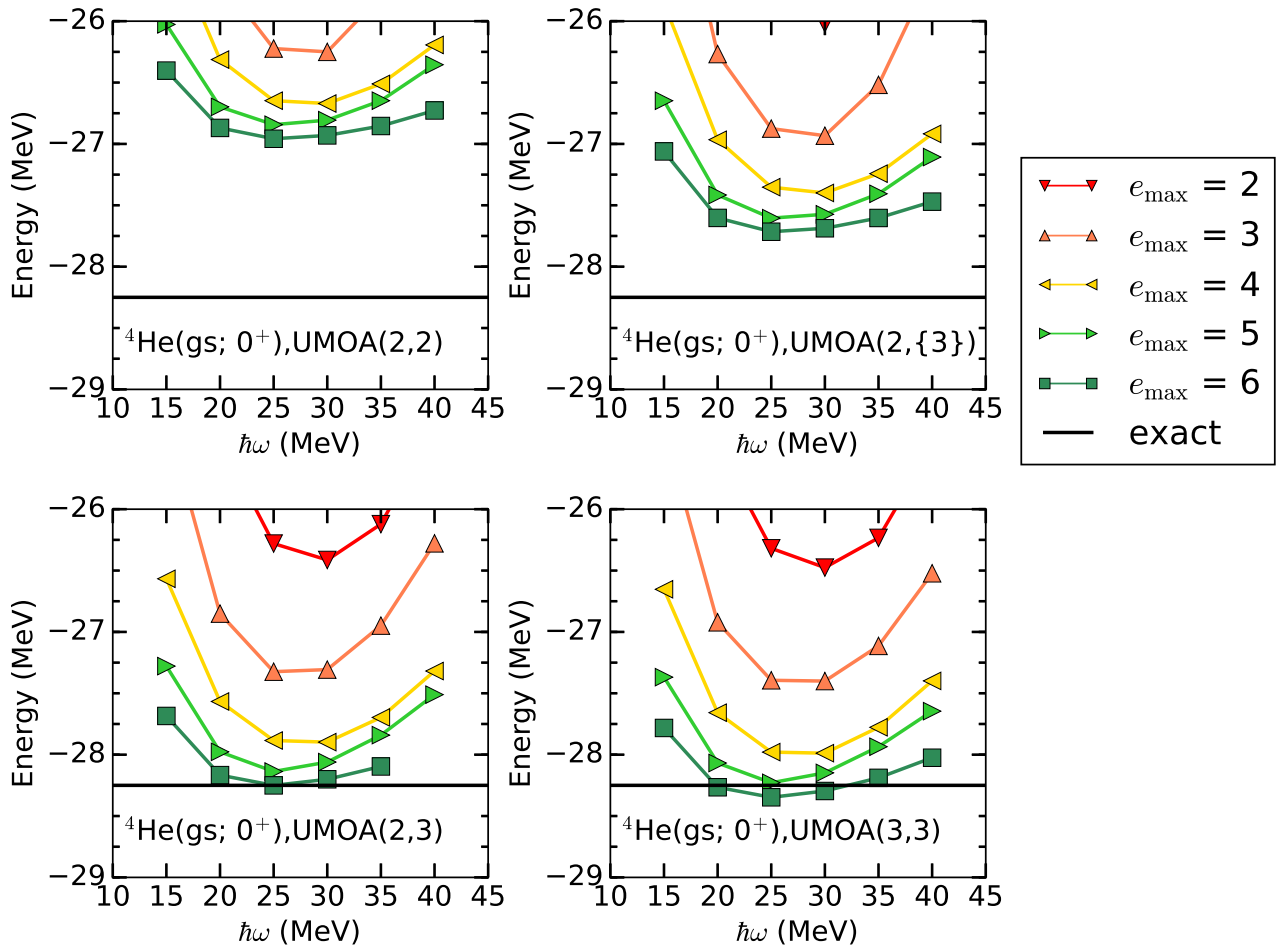
Figure 4.20: The 0^+ ground-state energies for ^{4}He as functions of $\hbar\omega$. The chiral N^{3}LO (500 MeV) *NN* interaction [10] softened by SRG transformation with $\lambda_{\mathrm{SRG}} = 2$ fm^{-1} is employed. The UMOA(2, 2), UMOA(2, {3}), UMOA(2, 3), and UMOA(3, 3) results are displayed.

NN and 3*N* interactions are future work.

Table 4.6: Ground-state energies for ^{4}He with the UMOA(2, 2), UMOA(2, {3}), UMOA(2, 3), and UMOA(3, 3). The employed interaction is N^{3}LO *NN* interaction with the SRG transformation evolved to $\lambda_{\text{SRG}} = 2$ fm^{-1}. All the results are given at $e_{\text{max}} = 6$ and $\hbar\omega = 25$ MeV. The IT-NCSM and experimental results are taken from Ref. [79] and [23], respectively. All the energies are in units of MeV.

	UMOA(2, 2)	UMOA(2, {3})	UMOA(2, 3)	UMOA(3, 3)	IT-NCSM	Exp.
E^{1BC}	−107.41	−107.41	−102.85	−102.07		
E^{2BC}	80.45	80.45	72.97	72.39		
E^{3BC}		−0.76	1.63	1.34		
$E_{\text{g.s.}}$	−26.96	−27.72	−28.25	−28.35	−28.25(1)	−28.30

Chapter 5

Summary and Outlook

In order to investigate the nuclear structure, one encounters two major obstacles. One is the nuclear interactions which are inputs of the nuclear structure calculations. The other is the many-body calculation method. As for the interactions, in this work, we mainly use the nucleon-nucleon (NN) interactions softened with the SRG transformation or $V_{\mathrm{low\ k}}$ approach, because the bare interactions, such as AV18 and CD-Bonn interactions, often cause the slow convergence of the numerical calculations. The acceleration of the convergence for the numerical calculations is confirmed in the triton ground-state energies. Our main focus is to solve the many-body Schrödinger equation based on such underlying nuclear interactions and to obtain the ground-state energies and radii for finite nuclei. To investigate the medium-mass nuclei in the *ab initio* calculations, one can employ several methods. In the present work, we use the unitary-model-operator approach (UMOA), which is based on the Hermitian effective-interaction theory. The essential point in the UMOA is to construct the effective Hamiltonian which does not induce the particle-hole excitations. In this thesis, we introduce the *method I* and *method II* to fulfill the actual calculations. In the *method I*, we decouple the 2p2h excitations with the reference state. Then, the calculated results depend on $\hbar\omega$ which is a parameter characterising the harmonic-oscillator single-particle basis. Since the initial Hamiltonian does not include $\hbar\omega$, this $\hbar\omega$-dependence of the results should be vanished if the numerical calculations are done in the sufficiently large model space. To investigate and reduce the $\hbar\omega$-dependence of the results, we decouple 1p1h, in addition to 2p2h, excitations with the reference state in the *method II* which is developed in this work for the first time. Using the UMOA, we calculate the ground-state energies and radii for 35 closed shell nuclei including the lead region. Although the importance of the three-nucleon ($3N$) interaction is reported in many recent works, we employ only the NN interactions in this work. Since the studies for heavy nuclei have been mainly done with the mean-field calculations and there are no systematic *ab initio* calculations for lead region, it is worth doing the UMOA calculations across the nuclear chart even if one employs only the NN interactions.

We show the numerical results of the ground-state energies and charge radii for ^{4}He, ^{16}O, ^{40}Ca, and ^{56}Ni from the CD-Bonn interaction in the *method I*. Then, the size of the three-body cluster term correction is estimated perturbatively. From the calculated ground-state energies, the one- and two-body cluster terms are dominant and the cluster expansion almost converges. In the *method I*, the

$\hbar\omega$-dependence of the results is not negligible even if the calculations are done in our largest model space. Following the recent CCM calculations, we determine the results by taking $\hbar\omega$ minimizing the ground-state energy. By comparing with the empirical formulae, we find that our results can reproduce the trend of the experimental data. To reproduce the data quantitatively, however, our calculations need the introduction of the genuine $3N$ interaction.

To investigate and reduce the $\hbar\omega$-dependence of the results, we introduce the one-body correlation operator to the UMOA and perform the numerical calculations with the *method II*. The reduction of the $\hbar\omega$-dependence of the results can be observed through the ^{4}He ground-state calculations with the $V_{\text{low k}}$ interaction derived from the AV18 interaction at $\Lambda = 1.9$ fm^{-1}. We conclude that the role of the one-body correlation operator is the optimization of the single-particle basis state similarly to the HF method. The convergence of the cluster expansion is also observed in the *method II* as long as we use the softened NN interactions. Our ^{4}He results are reasonably close to the results from the other *ab initio* calculations.

Moreover, we calculate the energies for the oxygen isotopes with the SRG transformed chiral N^{3}LO NN interactions with the resolution scales $\lambda_{\text{SRG}} = 1.88$ fm^{-1}, 2 fm^{-1}, 2.24 fm^{-1} to examine the applicability of the UMOA in the *method II*. We confirm a good agreement between the results in the UMOA and in the other *ab initio* calculations. Our ground-state energies depend on λ_{SRG} and are much larger than the data. These mean that we need to include the $3N$ interaction induced by the SRG transformation.

We apply the *method II* to the 35 closed shell nuclei from ^{4}He to ^{218}Pb with the SRG transformed chiral N^{3}LO NN interactions with the resolution scales $\lambda_{\text{SRG}} = 1.88$ fm^{-1}, 2 fm^{-1}, 2.24 fm^{-1}. The converged results can be obtained when we take 13 major shells as the model space. Our ground-state energies and radii become overbound and smaller than the experimental data, respectively, as the mass number increases. The saturation property cannot be reproduced with our binding energies and radii. From these facts, at least, the inclusion of the $3N$ interaction is needed to reproduce the data. In our calculation results, it is be found that the observables originated by proton-neutron asymmetry can be independent of λ_{SRG} and can be determined almost uniquely. This is confirmed in the asymmetry term of the ground-state energy and in the difference between point-proton and point-neutron radii, Δr_{np}. Interestingly, our Δr_{np} results are consistent with the experimental trend and the recent CCM result with the $NN + 3N$ interactions.

As shown in this and recent works, the inclusion of the $3N$ interaction is needed for understanding of the nuclear structure. To introduce the $3N$ interaction to the UMOA, we have to extend the current framework. In this work, we explicitly treat the three-body cluster term and investigate the effect of the many-body cluster terms through the calculations for the ^{4}He ground-state energies with the NN interaction. The cluster expansion works well and our ^{4}He energies show a good agreement with the energy from the no-core shell model. Owing to the iterative treatment of the three-body cluster term, we will deal directly with the $3N$ interaction in the new UMOA framework. Through the systematic calculations of the energies and radii with the $NN + 3N$ interactions, it can be expected to lead the quantitative and systematic understanding of the nuclear structure.

Acknowledgments

Appendix A

Two Body Matrix Element

In general, the nucleon-nucleon (NN) interactions are given as a function of the relative coordinate or momenta. Since our calculations are done in the product of the single-particle HO basis states, we need transformations from given expressions to required two-body matrix elements (TBMEs). To obtain the TBME, we apply two-step transformation. First, we transform the NN interaction from relative and CM coordinate space (or momentum space) expression $|\mathbf{r}, \mathbf{R}_{\text{CM}}\rangle$ (or $|\mathbf{q}, \mathbf{Q}_{\text{CM}}\rangle$) to HO relative and CM basis expression $|nlS J_{\text{rel}} NL: JMT\rangle$. Here, $\mathbf{r}$ and $\mathbf{R}_{\text{CM}}$ ($\mathbf{q}$ and $\mathbf{Q}_{\text{CM}}$) are coordinate (momentum) vectors of relative and CM motions, respectively, for the two nucleons. As for the HO relative state, n, l, S, and J_{rel}, are the nodal quantum number, orbital angular momentum, total spin, and total angular momentum ($J_{\text{rel}} = l + S$) for the relative motion, respectively. The N and L are the nodal quantum number, orbital angular momentum for the CM motion, respectively. The J and M are the total angular momentum of NN system and its third component, respectively. The T distinguishes the proton-proton, proton-neutron, or neutron-neutron channels. Second, such a NN interaction is transformed to product of the single-particle basis state $|ab: JMT\rangle$. The second transformation is known as the Talmi-Moshinsky transformation. In Appendix A, the HO basis state is denoted by alphabetical letters, for example $a = \{n_a, l_a, s_a, j_a, m_a, t_a\}$. Here, n_a, l_a, s_a, j_a, m_a, and t_a are the nodal quantum number, orbital angular momentum, spin, total angular momentum, third component of total angular momentum, and label distinguishing the proton and neutron, respectively.

A.1 Matrix Element in HO Relative and CM Basis State

Here, we show the transformation of the NN interactions from given original expression to the HO relative and CM basis state. There are local and non-local NN interactions, for example, the AV18 [8] and CD-Bonn [9] interactions, respectively. Due to the locality, the transformation is slightly different. The transformations are shown for local and non-local interaction in Sec. A.1.1 and Sec. A.1.2, respectively.

A.1.1 Local *NN* Interaction

To do the transformation, we will need the overlap between the $|\mathbf{r}, \mathbf{R}_{\text{CM}}\rangle$ and $|nlS J_{\text{rel}} NL \colon JMT\rangle$,

$$\langle \mathbf{r}, \mathbf{R}_{\text{CM}} | nlS J_{\text{rel}} NL \colon JMT \rangle = \sum_{m_l m_S, m_L, m_{J_{\text{rel}}}} C^{lS J_{\text{rel}}}_{m_l m_S m_{J_{\text{rel}}}} C^{J_{\text{rel}} LJ}_{m_{J_{\text{rel}}} m_L M} R_{nl}(r/b) Y_{l m_l}(\hat{\mathbf{r}}) \chi_{S m_S}$$

$$\times R_{NL}(R_{\text{CM}}/b) Y_{L m_L}(\hat{\mathbf{R}}_{\text{CM}}) \tag{A.1}$$

with the Clebsch-Gordan coeficient $C^{lsj}_{m_l m_s m_j}$, the spinor $\chi_{S m_S}$, spherical harmonics $Y_{l m_l}(\hat{\mathbf{r}})$, and radial function $R_{nl}(r/b)$. Here, $R_{nl}(x)$ is

$$R_{n_a l_a}(x) = b^{-3/2} \sqrt{\frac{2\Gamma(n_a + 1)}{\Gamma(n_a + l_a + 3/2)}} x^{l_a} e^{-x^2/2} L^{l_a + 1/2}_{n_a}(x^2), \tag{A.2}$$

with the Gamma function $\Gamma(x)$ and associated Laguerre polynomial $L^{\alpha}_n(x)$. The oscillator length b is defined as $b = \sqrt{\hbar/\mu\omega}$. For the local *NN* interaction, the matrix element with such basis state is

$$\langle nlS J_{\text{rel}} NL \colon JMT | V_{NN} | n'l'S' J'_{\text{rel}} N'L' \colon J'M'T' \rangle = \int d^3\mathbf{r} d^3\mathbf{r}' d^3\mathbf{R}_{\text{CM}} d^3\mathbf{R}'_{\text{CM}} \langle nlS J_{\text{rel}} NL \colon JMT | \mathbf{r}, \mathbf{R}_{\text{CM}} \rangle$$

$$\times \langle \mathbf{r} | V_{NN} | \mathbf{r}' \rangle \delta(\mathbf{r} - \mathbf{r}') \delta(\mathbf{R}_{\text{CM}} - \mathbf{R}'_{\text{CM}}) \langle \mathbf{r}', \mathbf{R}'_{\text{CM}} | n'l'S' J'_{\text{rel}} N'L' \colon J'M'T' \rangle$$

$$= \int dr r^2 R^*_{nl}(r/b) V_{ll'S J_{\text{rel}}}(r) R_{n'l'}(r/b) \delta_{SS'} \delta_{J_{\text{rel}} J'_{\text{rel}}} \delta_{NN'} \delta_{LL'} \delta_{JJ'} \delta_{MM'} \delta_{TT'}, \tag{A.3}$$

where, $V_{ll'S J_{\text{rel}}}(r)$ is *NN* interaction after the partial wave decomposition and is

$$V_{ll'S J_{\text{rel}}}(r) = \sum_{m_l m_S m'_S m'_{l'}} C^{lS J_{\text{rel}}}_{m_l m_S m_{J_{\text{rel}}}} C^{l'S J_{\text{rel}}}_{m'_{l'} m'_S m_{J_{\text{rel}}}} \int d\hat{\mathbf{r}} Y^*_{l m_l}(\hat{\mathbf{r}}) \chi^{\dagger}_{S m_S} \langle \mathbf{r} | V_{NN} | \mathbf{r} \rangle \chi_{S m'_S} Y_{l' m'_{l'}}(\hat{\mathbf{r}}) \tag{A.4}$$

Note that $\delta_{SS'} \delta_{J_{\text{rel}} J'_{\text{rel}}} \delta_{NN'} \delta_{LL'} \delta_{JJ'} \delta_{MM'}$ is required by symmetries of *NN* system, i.e. the rotational and translational symmetries. Since we ignore the week interaction, $\delta_{TT'}$ also holds. Therefore,

$$\langle nlS J_{\text{rel}} NL \colon JMT | V_{NN} | n'l'S' J'_{\text{rel}} N'L' \colon J'M'T' \rangle$$

can be rewritten as

$$\langle nlS J_{\text{rel}} NL \colon JMT | V_{NN} | n'l'S' J'_{\text{rel}} N'L' \colon J'M'T' \rangle = \langle nlS J_{\text{rel}} T | V_{NN} | n'l'S J_{\text{rel}} T \rangle. \tag{A.5}$$

A.1.2 Non-Local *NN* Interaction

Same as in Sec. A.1.2, we begin with the overlap between $|\mathbf{q}, \mathbf{Q}_{\text{CM}}\rangle$ and $|nlS J_{\text{rel}} NL \colon JMT\rangle$, which is given by the Fourier transformation of Eq. (A.1),

$$\langle \mathbf{q}, \mathbf{Q}_{\text{CM}} | nlS J_{\text{rel}} NL \colon JMT \rangle = \int d^3\mathbf{r} d^3\mathbf{R}_{\text{CM}} \langle \mathbf{q}, \mathbf{Q}_{\text{CM}} | \mathbf{r}, \mathbf{R}_{\text{CM}} \rangle \langle \mathbf{r}, \mathbf{R}_{\text{CM}} | nlS J_{\text{rel}} NL \colon JMT \rangle$$

$$= i^{2n+2N+l+L} \sum_{m_l m_S, m_L, m_{J_{\text{rel}}}} C^{lS J_{\text{rel}}}_{m_l m_S m_{J_{\text{rel}}}} C^{J_{\text{rel}} LJ}_{m_{J_{\text{rel}}} m_L M} R_{nl}(bq) Y_{l m_l}(\hat{\mathbf{q}}) \chi_{S m_S}$$

$$\times R_{NL}(bQ_{\text{CM}}) Y_{L m_L}(\hat{\mathbf{q}}_{\text{CM}}). \tag{A.6}$$

Similar to the local *NN* interaction case, the matrix element for the non-local *NN* interaction is

$$\langle nlS\, J_{\text{rel}} NL\colon JMT | V_{NN} | n'l'S'J'_{\text{rel}} N'L'\colon J'M'T'\rangle$$

$$= (-1)^{n+n'} \int dq\, dq'\, q^2 q'^2 R^*_{nl}(bq) V_{ll'S\,J_{\text{rel}}}(q,q') R_{n'l'}(bq') \delta_{SS'} \delta_{J_{\text{rel}}J'_{\text{rel}}} \delta_{NN'} \delta_{LL'} \delta_{JJ'} \delta_{MM'} \delta_{TT'}. \quad \text{(A.7)}$$

Here, $V_{ll'S\,J_{\text{rel}}}(q,q')$ is the non-local interaction after the partial wave decomposition and is

$$V_{ll'S\,J_{\text{rel}}}(q,q') = i^{l+l'} \sum_{m_l m_S m'_S m'_{l'}} C^{lS\,J_{\text{rel}}}_{m_l m_S m_{J_{\text{rel}}}} C^{l'S\,J_{\text{rel}}}_{m'_{l'} m'_S m_{J_{\text{rel}}}} \int d\hat{\mathbf{q}}\, d\hat{\mathbf{q}}'\, Y^*_{lm_l}(\hat{\mathbf{r}}) \chi^\dagger_{Sm_S} \langle \mathbf{q} | V_{NN} | \mathbf{q}' \rangle \chi_{Sm'_S} Y_{l'm'_{l'}}(\hat{\mathbf{q}}'). \quad \text{(A.8)}$$

Note that the relation in Eq. (A.5) is also satisfied.

A.2 Talmi-Moshinsky Transformation

Next task is to transform from $|nlS\, J_{\text{rel}} NL\colon JMT\rangle$ to $|ab\colon JMT\rangle$ which is known as the Talmi-Moshinsky transformation. First, we recouple the angular momenta from $j_a + j_b = J$ to $\lambda + S = J$, i.e. separating the orbital and spin parts. Here, λ is total orbital angular momentum. Such a recoupling can be done by using the $9j$ symbol [65],

$$|a(n_a l_a j_a) b(n_b l_b j_b)\colon JMT\rangle = \sum_{\lambda S} |(n_a l_a n_b l_b)\lambda(s_a s_b)S\colon JMT\rangle$$

$$\times \langle (n_a l_a n_b l_b)\lambda(s_a s_b)S\colon JMT | a(n_a l_a j_a) b(n_b l_b j_b)\colon JMT\rangle$$

$$= \sum_{\lambda S} \sqrt{[\lambda][S][j_a][j_b]} \begin{Bmatrix} l_a & l_b & \lambda \\ s_a & s_b & S \\ j_a & j_b & J \end{Bmatrix} |(n_a l_a n_b l_b)\lambda(s_a s_b)S\colon JMT\rangle \quad \text{(A.9)}$$

Next, we expand $|(n_a l_a n_b l_b)\lambda(s_a s_b)S\colon JMT\rangle$ in the basis $|(nlNL)\lambda S\colon JMT\rangle$. Then, we have

$$|(n_a l_a n_b l_b)\lambda(s_a s_b)S\colon JMT\rangle = \sum_{nlNL} \langle nlNL; \lambda | n_a l_a n_b l_b; \lambda\rangle |(nlNL)\lambda S\colon JMT\rangle, \quad \text{(A.10)}$$

where, $\langle nlNL; \lambda | n_a l_a n_b l_b; \lambda\rangle$ is the HO transformation bracket [65, 96]. In the next step, we decouple the CM part with $|(nlNL)\lambda S\colon JMT\rangle$ by using the $6j$ symbol [65],

$$|(nlNL)\lambda S\colon JMT\rangle = \sum_{J_{\text{rel}}} |nlS\, J_{\text{rel}} NL\colon JMT\rangle \langle nlS\, J_{\text{rel}} NL\colon JMT | (nlNL)\lambda S\colon JMT\rangle$$

$$= \sum_{J_{\text{rel}}} (-1)^{L+l+S+J} \sqrt{[\lambda][J_{\text{rel}}]} \begin{Bmatrix} L & l & \lambda \\ S & J & J_{\text{rel}} \end{Bmatrix} |nlS\, J_{\text{rel}} NL\colon JMT\rangle \quad \text{(A.11)}$$

Combining Eqs. (A.9)-(A.11), we obtain the transformation from $|ab\colon JMT\rangle$ basis to $|nlS\, J_{\text{rel}} NL\colon JMT\rangle$ basis,

$$|ab\colon JMT\rangle = N_{ab} \sum_{\lambda S} \sum_{nlNL} \sum_{J_{\text{rel}}} (-1)^{L+l+S+J} \frac{f_T}{\sqrt{2}} [\lambda] \sqrt{[S][j_a][j_b][J_{\text{rel}}]}$$

$$\times \langle nlNL; \lambda | n_a l_a n_b l_b; \lambda\rangle \begin{Bmatrix} l_a & l_b & \lambda \\ s_a & s_b & S \\ j_a & j_b & J \end{Bmatrix} \begin{Bmatrix} L & l & \lambda \\ S & J & J_{\text{rel}} \end{Bmatrix} |nlS\, J_{\text{rel}} NL\colon JMT\rangle, \quad \text{(A.12)}$$

with the normalization factor $N_{ab} = 1/\sqrt{\delta_{n_a n_b}\delta_{l_a l_b}\delta_{j_a j_b}\delta_{t_a t_b}}$. Also, f_T is defined as

$$
f_T \equiv \begin{cases} 1 - (-1)^{l+S} & \text{for} \quad T = \text{proton-proton or neutron-neutron,} \\ 1 & \text{for} \quad T = \text{proton-neutron.} \end{cases} \tag{A.13}
$$

Finally we have the TBME,

$$
\begin{aligned}
\langle ab : JMT|V_{NN}|cd : JMT\rangle = N_{ab}N_{cd} \sum_{\lambda\lambda'S} \sum_{nln'l'} \sum_{NLJ_{\text{rel}}} (-1)^{l+l'} f_T [\lambda][\lambda'][J_{\text{rel}}][S] \sqrt{[j_a][j_b][j_c][j_d]} \\
\times \langle nlNL; \lambda|n_a l_a n_b l_b; \lambda\rangle\langle n'l'NL; \lambda'|n_c l_c n_d l_d; \lambda'\rangle \\
\times \begin{Bmatrix} l_a & l_b & \lambda \\ s_a & s_b & S \\ j_a & j_b & J \end{Bmatrix} \begin{Bmatrix} l_c & l_d & \lambda' \\ s_c & s_d & S \\ j_c & j_d & J \end{Bmatrix} \begin{Bmatrix} L & l & \lambda \\ S & J & J_{\text{rel}} \end{Bmatrix} \begin{Bmatrix} L & l' & \lambda' \\ S & J & J_{\text{rel}} \end{Bmatrix} \\
\times \langle nlS J_{\text{rel}}T|V_{NN}|n'l'S J_{\text{rel}}T\rangle,
\end{aligned} \tag{A.14}
$$

which can be applied directly our calculations.

Appendix B

Effective-Interaction Theories

The basic idea in the effective-interaction theory is to renormalize the high-energy physics into the low-energy regime which we are interest in. Mathematically, we employ the similarity transformation of the Hamiltonian matrix so that the coupling between the P and Q spaces are suppressed. Here, P and Q spaces are physically interesting model space and its complement, respectively. Since the P space is decoupled with the Q, small P-space Hamiltonian matrix reproduce parts of eigenvalues of the original Hamiltonian. Generally, the effective interactions cannot be determined uniquely, because they depend on the choice of the similarity transformation. One can categorize the effective interactions according to energy-dependence and Hermiticity. In this appendix, we discuss, especially energy-independent, effective-interaction theories and relation between Hermitian and non-Hermitian effective-interaction theories. First, we begin with the non-Hermitian effective-interaction theory which is simpler than Hermitian theory. Since the non-Hermitian effective interaction does not preserve the variational principle and can provide the practical problem, we, next, introduce the Hermitian effective-interaction theory.

B.1   Non-Hermitian Effective-Interaction Theory

At first, we define two projection operators onto the P and Q space. The projection operators satisfy $P + Q = 1$, $PQ = QP = 0$, $P^2 = P$ and $Q^2 = Q$. The original Hamiltonian in the matrix form is

$$H = \begin{pmatrix} PHP & PHQ \\ QHP & QHQ \end{pmatrix} \equiv \begin{pmatrix} PH_0P + PVP & PVQ \\ QVP & QH_0Q + QVQ \end{pmatrix}, \tag{B.1}$$

where H_0 and V are the unperturbative Hamiltonian and the bare interaction, respectively. Note that the mathematical definition of projection operators are

$$P = \sum_{\alpha \leq \Lambda_{\mathrm{cut}}} |\alpha\rangle\langle\alpha|, \quad Q = \sum_{\alpha > \Lambda_{\mathrm{cut}}} |\alpha\rangle\langle\alpha|, \tag{B.2}$$

with a certain boundary Λ_{cut} and

$$H_0|\alpha\rangle = E_\alpha|\alpha\rangle. \tag{B.3}$$

In the non-Hermitian effective-interaction theory, the original Hamiltonian is transformed by e^ω:

$$\overline{H} = e^{-\omega} H e^\omega. \tag{B.4}$$

Since Eq. (B.4) is similarity transformation, eigenvalues of $\overline{H}$ coincide with those of the original Hamiltonian. Here, the operator ω acts as the mapping between the P and Q spaces. The operator ω satisfies

$$\omega = Q\omega P, \tag{B.5}$$

$$P\omega = \omega Q = 0, \tag{B.6}$$

$$\omega^2 = 0. \tag{B.7}$$

The ω in the matrix form is

$$\omega = \begin{pmatrix} 0 & 0 \\ \omega & 0 \end{pmatrix}. \tag{B.8}$$

From Eq. (B.7), e^ω can be expanded into

$$e^\omega = 1 + \omega, \tag{B.9}$$

or

$$e^\omega = \begin{pmatrix} 1 & 0 \\ \omega & 1 \end{pmatrix}. \tag{B.10}$$

The ω is determined so that the coupling between Q and P spaces vanishes, i.e.,

$$Q e^{-\omega} H e^\omega P = 0. \tag{B.11}$$

By using Eq. (B.9), we have

$$Q(1 - \omega)H(1 + \omega)P = 0. \tag{B.12}$$

Note that the adjoint condition $P e^{-\omega} H e^\omega Q = 0$ is not satisfied in the non-Hermitian effective-interaction theory. If ω is determined, the P-space Schrödinger equation is written as

$$PH_0 P|\phi'_k\rangle + PRP|\phi'_k\rangle = E|\phi'_k\rangle, \tag{B.13}$$

with the P-space wave function $|\phi'_k\rangle$. The operator R is the non-Hermitian effective interaction given by

$$R = PVP + PVQ\omega. \tag{B.14}$$

Note that the problem is reduced to the diagonalization in the model space.

Since Eq. (B.12) is non-linear equation, to obtain ω is generally difficult. However, the decoupling condition, Eq. (B.12), is satisfied when ω is determined as follows. Let $|\psi_k\rangle$ be the eigenstate of the original Hamiltonian. This eigenstate satisfies the following Schrödinger equation,

$$H|\psi_k\rangle = E_k|\psi_k\rangle. \tag{B.15}$$

We decompose $|\psi_k\rangle$ into the P-space component $P|\psi_k\rangle$ ($\equiv |\phi_k\rangle$) and Q-space component $Q|\psi_k\rangle$. Suppose that Q-space component of the eigenstate can be generated by acting ω to $|\phi_k\rangle$, i.e.,

$$|\psi_k\rangle = |\phi_k\rangle + \omega|\phi_k\rangle. \tag{B.16}$$

A solution of ω is

$$\omega = \sum_{k=1}^{d} Q|\psi_k\rangle\langle\widetilde{\phi_k}|P, \tag{B.17}$$

where $\langle\widetilde{\phi_k}|$ is the bi-orthogonal state of $|\phi_k\rangle$, and $\langle\widetilde{\phi_k}|$ is determined by the orthogonal relation,

$$\langle\widetilde{\phi_i}|\phi_j\rangle = \delta_{ij}. \tag{B.18}$$

By acting $|\psi_k\rangle$ from the right of Eq. (B.12) and substituting Eq. (B.17) to Eq. (B.12), one can examine that Eq. (B.17) satisfies the decoupling condition Eq. (B.12).

B.2   Hermitian Effective-Interaction Theory

We, here, discuss the Hermitian effective-interaction theories. To obtain the unique solution, we choose the correlation operator S satisfying the condition, $PSP = QSQ = 0$. Since S is antihermitian, S can be decomposed into

$$S = i(\chi + \chi^{\dagger}) = i(Q\chi P + P\chi^{\dagger}Q), \tag{B.19}$$

with the operator χ [98]. For simplicity, we also define the P-space Hermitian operator,

$$T^2 = \chi^{\dagger}\chi. \tag{B.20}$$

By using χ, e^S can be expanded into

$$e^S = e^{i(\chi^{\dagger}+\chi)} = \sum_{n=0} \frac{i^n}{n!}(\chi^{\dagger} + \chi)^n. \tag{B.21}$$

By the definition of χ, one can obtain the relation, $\chi\chi = \chi^{\dagger}\chi^{\dagger} = 0$. Therefore, we find that, for even n ($n = 2, 4, 6, \cdots$), the nonvanishing terms are

$$\chi^{\dagger}\chi\cdots\chi^{\dagger}\chi = P(T^2)^{n/2}P, \tag{B.22}$$

and

$$\chi\chi^{\dagger}\cdots\chi\chi^{\dagger} = Q\chi(T^2)^{(n-2)/2}\chi^{\dagger}Q. \tag{B.23}$$

For odd n ($n = 1, 3, 5, \cdots$), the nonvanishing terms are

$$\chi\chi^{\dagger}\cdots\chi^{\dagger}\chi = Q\chi P(T^2)^{(n-1)/2}P, \tag{B.24}$$

and

$$\chi^{\dagger}\chi\cdots\chi\chi^{\dagger} = P(T^2)^{(n-1)/2}P\chi^{\dagger}Q. \tag{B.25}$$

We then have

$$
e^S = P\left\{1 + \sum_{n:even} \frac{i^n}{n!}(T^2)^{n/2}\right\}P + P\left\{\sum_{n:odd} \frac{i^n}{n!}(T^2)^{(n-1)/2}\chi^\dagger\right\}Q
$$
$$
+ Q\left\{\chi \sum_{n:odd} \frac{i^n}{n!}(T^2)^{(n-1)/2}\right\}P + Q\left\{1 + \sum_{n:even} \chi\frac{i^n}{n!}(T^2)^{(n-2)/2}\chi^\dagger\right\}Q. \tag{B.26}
$$

Eq. (B.26) can be simplified by using the trigonometric function as

$$
e^S = P\cos T P + iQ\chi T^{-1}\sin T P + iPT^{-1}\sin T\chi^\dagger Q + Q(1 + \chi T^{-1}(\cos T - P)T^{-1}\chi^\dagger)Q, \tag{B.27}
$$

or

$$
e^S = \begin{pmatrix} \cos T & iT^{-1}(\sin T)\chi^\dagger \\ i\chi T^{-1}\sin T & 1 + \chi T^{-1}(\cos T - 1)T^{-1}\chi^\dagger \end{pmatrix}, \tag{B.28}
$$

in the matrix form. The *P*-space effective Hamiltonian can be written as

$$
P\widetilde{H}P = \cos T PHP \cos T + i\cos T PHQ\chi\{T^{-1}\sin T\} - i\{T^{-1}\sin T\}\chi^\dagger QHP \cos T
$$
$$
+ \{T^{-1}\sin T\}\chi^\dagger QHQ\chi\{T^{-1}\sin T\}, \tag{B.29}
$$

and the component between the *P* and *Q* space is written as

$$
Q\widetilde{H}P = QHP \cos T + \chi\{T^{-1}(\cos T - P)T^{-1}\}\chi^\dagger QHP \cos T
$$
$$
- i\chi\{T^{-1}\sin T\}PHP \cos T + iQHQ\chi\{T^{-1}\sin T\}
$$
$$
+ i\chi\{T^{-1}(\cos T - P)T^{-1}\}\chi^\dagger QHQ\chi\{T^{-1}\sin T\} + \chi\{T^{-1}\sin T\}PHQ\chi\{T^{-1}\sin T\}. \tag{B.30}
$$

The decoupling condition is $Q\widetilde{H}P = 0$. When $Q\widetilde{H}P$ vanishes, $\chi^\dagger Q\widetilde{H}P$ also vanishes. Therefore, we have

$$
\chi^\dagger Q\widetilde{H}P = \cos T\chi^\dagger QHP \cos T - iT^2\{T^{-1}\sin T\}PHP \cos T + i\cos T\chi^\dagger QHQ\chi T^{-1}\sin T
$$
$$
+ T^2\{T^{-1}\sin T\}PHQ\chi\{T^{-1}\sin T\} = 0. \tag{B.31}
$$

We can solve for $\chi^\dagger QHP \cos T$ by operating $\sec T$ from the left. By substituting $\chi^\dagger QHP \cos T$ to Eq. (B.30), we obtain

$$
Q[1 - i\chi \sec T\{T^{-1}\sin T\}]H[1 + i\chi \sec T\{T^{-1}\sin T\}]P = 0. \tag{B.32}
$$

Reminding Eq. (B.12), χ can be related with ω.

$$
\omega = i\chi[\sec T\{T^{-1}\sin T\}] = i\chi[T^{-1}\tan T]. \tag{B.33}
$$

This equation also relate Hermitian and non-Hermitian effective-interaction theories. Then, some useful equations can be derived

$$
\omega^\dagger\omega = \tan^2 T, \tag{B.34}
$$
$$
(P + \omega^\dagger\omega)^{1/2} = \sec T, \tag{B.35}
$$
$$
(P + \omega^\dagger\omega)^{-1/2} = \cos T. \tag{B.36}
$$

Through Eqs. (B.33) - (B.36), we obtain

$$S = i(\chi + \chi^\dagger) = \omega \frac{\arctan \sqrt{\omega^\dagger \omega}}{\sqrt{\omega^\dagger \omega}} - \frac{\arctan \sqrt{\omega^\dagger \omega}}{\sqrt{\omega^\dagger \omega}} \omega^\dagger. \tag{B.37}$$

By using the following expansion formula,

$$\mathrm{arctanh}x = \sum_{n=0}^{\infty} \frac{(-1)^n}{2n+1} x^{2n+1}, \tag{B.38}$$

Eq. (B.37) can be simplified as [97–99]

$$S = \sum_{n=0}^{\infty} \frac{(-1)^n}{2n+1} \left\{ \omega(\omega^\dagger \omega)^n - (\omega^\dagger \omega)^n \omega^\dagger \right\} = \mathrm{arctanh}(\omega - \omega^\dagger). \tag{B.39}$$

Eq. (B.39) gives the relation between the non-Hermitian and Hermitian effective-interaction theories. The unitary transformation operator in Eq. (B.28) can be also written in terms of the operator ω and its adjoint

$$e^S = \begin{pmatrix} (1 + \omega^\dagger \omega)^{-1/2} & -\omega^\dagger(1 + \omega \omega^\dagger)^{-1/2} \\ \omega(1 + \omega^\dagger \omega)^{-1/2} & (1 + \omega \omega^\dagger)^{-1/2} \end{pmatrix} \tag{B.40}$$

or

$$e^S = (1 + \omega - \omega^\dagger)(1 + \omega^\dagger \omega + \omega \omega^\dagger)^{-1/2}. \tag{B.41}$$

Moreover, the Hermitian effective interaction defined by $P\widetilde{V}P = P(\widetilde{H} - H_0)P$ is

$$\widetilde{V} = (P + \omega^\dagger \omega)^{-1/2}(PHP + PVQ\omega + \omega^\dagger QVP + \omega^\dagger QHQ\omega)(P + \omega^\dagger \omega)^{-1/2} - PH_0P. \tag{B.42}$$

By using the decoupling condition, Eq. (B.12), we obtain

$$\widetilde{V} = (P + \omega^\dagger \omega)^{1/2}(PHP + PVQ\omega)(P + \omega^\dagger \omega)^{-1/2} - PH_0P. \tag{B.43}$$

The Hermiticy of Eq. (B.43) is not clear. Let us consider clearer expression. The operator $\omega^\dagger$ satisfies the adjoint decoupling condition,

$$P(1 + \omega^\dagger)H(1 - \omega^\dagger)Q = 0. \tag{B.44}$$

By using Eqs. (B.12) and (B.44), we can eliminate the term, $\omega^\dagger QHQ\omega$. We then have

$$(PHP + \omega^\dagger QVP)(P + \omega^\dagger \omega) = (P + \omega^\dagger \omega)(PHP + PVQ\omega). \tag{B.45}$$

From Eqs. (B.43) and (B.45), we obtain

$$\widetilde{V} = (P + \omega^\dagger \omega)^{-1/2}(PHP + \omega^\dagger QVP)(P + \omega^\dagger \omega)^{1/2} - PH_0P. \tag{B.46}$$

From Eqs. (B.43) and (B.46), we have the explicitly Hermitian effective interaction,

$$\widetilde{V} = \frac{1}{2} \left\{ (P + \omega^\dagger \omega)^{1/2}(PHP + PVQ\omega)(P + \omega^\dagger \omega)^{-1/2} + \mathrm{h.c.} \right\} - PH_0P. \tag{B.47}$$

In order to obtain the matrix element of $\widetilde{V}$ and the e^S, we solve the eigenvalue equation for $\omega^\dagger \omega$ in the
P space as

$$\omega^\dagger \omega |\alpha_i\rangle = \mu_i^2 |\alpha_i\rangle, \tag{B.48}$$

and define the Q-space vector $|\nu_i\rangle$ as

$$|\nu_i\rangle = \frac{1}{\mu_i} \omega |\alpha_i\rangle. \tag{B.49}$$

By using Eqs. (B.48) and (B.49), the matrix elements of Eqs. (B.43) and (B.46) are

$$
\begin{aligned}
\langle \alpha_i | \widetilde{V} | \alpha_j \rangle &= \sqrt{\frac{1+\mu_i^2}{1+\mu_j^2}} \langle \alpha_i | R | \alpha_j \rangle - \langle \alpha_i | H_0 | \alpha_j \rangle + \sqrt{\frac{1+\mu_i^2}{1+\mu_j^2}} \langle \alpha_i | H_0 | \alpha_j \rangle \\
&= \sqrt{\frac{1+\mu_j^2}{1+\mu_i^2}} \langle \alpha_i | R^\dagger | \alpha_j \rangle - \langle \alpha_i | H_0 | \alpha_j \rangle + \sqrt{\frac{1+\mu_j^2}{1+\mu_i^2}} \langle \alpha_i | H_0 | \alpha_j \rangle.
\end{aligned}
\tag{B.50}
$$

From Eq. (B.50), we obtain the matrix element of the effective interaction [27, 37, 60, 100, 101]

$$\langle p' | \widetilde{V} | p \rangle = \sum_{ij} \langle p' | \alpha_i \rangle \frac{\sqrt{1+\mu_i^2}\langle \alpha_i | R | \alpha_j \rangle + \sqrt{1+\mu_j^2}\langle \alpha_i | R^\dagger | \alpha_j \rangle}{\sqrt{1+\mu_i^2} + \sqrt{1+\mu_j^2}} \langle \alpha_j | p \rangle, \tag{B.51}$$

where $|p\rangle$ and $|p'\rangle$ are basis states in the P space. We can obtain the matrix elements of the unitary
transformation operator in the same way,

$$\langle p' | e^S | p \rangle = \langle p' | (1 + \omega^\dagger \omega)^{-1/2} | p \rangle = \sum_{i=1}^{d} \frac{1}{\sqrt{1+\mu_i^2}} \langle p' | \alpha_i \rangle \langle \alpha_i | p \rangle, \tag{B.52}$$

$$\langle q | e^S | p \rangle = \langle q | \omega (1 + \omega^\dagger \omega)^{-1/2} | p \rangle = \sum_{i=1}^{d} \frac{\mu_i}{\sqrt{1+\mu_i^2}} \langle q | \nu_i \rangle \langle \alpha_i | p \rangle, \tag{B.53}$$

$$\langle p | e^S | q \rangle = \langle p | \omega^\dagger (1 + \omega \omega^\dagger)^{-1/2} | q \rangle = - \sum_{i=1}^{d} \frac{\mu_i}{\sqrt{1+\mu_i^2}} \langle p | \alpha_i \rangle \langle \nu_i | q \rangle, \tag{B.54}$$

$$\langle q' | e^S | q \rangle = \langle q' | (1 + \omega \omega^\dagger)^{-1/2} | q \rangle = \sum_{i=1}^{d} \left(\frac{1}{\sqrt{1+\mu_i^2}} - 1 \right) \langle q' | \nu_i \rangle \langle \nu_i | q \rangle + \delta_{q'q}, \tag{B.55}$$

where $|q\rangle$ and $|q'\rangle$ are basis states in the Q space.

Appendix C

Similarity Transformation in Coupled-Cluster Method

Similar to the UMOA, the coupled-cluster theory is based on the similarity transformation,

$$\overline{H} = e^{-T} H e^{T}, \tag{C.1}$$

with the Hamiltonian H. Here, H is normal ordered with respect to a single Slater-determinant reference state $|\Phi\rangle$. The operator T is sum of the particle-hole cluster operator,

$$T = T^{(1)} + T^{(2)} + \cdots + T^{(A)}, \tag{C.2}$$

defined with respect to the reference state. The n-particle-n-hole (npnh) cluster operator is defined as

$$T^{(n)} = \frac{1}{(n!)^2} \sum_{i_1 \cdots i_n \leq \rho_F} \sum_{a_1 \cdots a_k > \rho_F} t^{a_1 \cdots a_k}_{i_1 \cdots i_k} a^\dagger_{a_1} \cdots a^\dagger_{a_k} a_{i_k} \cdots a_{i_1}, \tag{C.3}$$

in the second quantization form. Note $T^\dagger \neq -T$ because the cluster operator T includes only the excitation operators. As a result transformation (C.1) is not unitary transformation. The important properties of $T^{(n)}$ is

$$[T^{(n)}, T^{(m)}] = 0, \text{ for } 1 \leq m, n \leq A. \tag{C.4}$$

Eq. (C.4) can be directly proved:

$$
\begin{aligned}
[T^{(n)}, T^{(m)}] &= \left(\frac{1}{m!n!}\right)^2 \sum_{i_1 \cdots i_n \leq \rho_F} \sum_{a_1 \cdots a_n > \rho_F} \sum_{i_{n+1} \cdots i_{n+m} \leq \rho_F} \sum_{a_{n+1} \cdots a_{m+n} > \rho_F} t^{a_1 \cdots a_n}_{i_1 \cdots i_n} t^{a_{n+1} \cdots a_{n+m}}_{i_{n+1} \cdots i_{n+m}} \\
&\quad \times \Big[(a^\dagger_{a_1} \cdots a^\dagger_{a_n})(a_{i_1} \cdots a_{i_n})(a^\dagger_{a_{n+1}} \cdots a^\dagger_{a_{n+m}})(a_{i_{n+1}} \cdots a_{i_{n+m}}) \\
&\quad\quad - (a^\dagger_{a_{n+1}} \cdots a^\dagger_{a_{n+m}})(a_{i_{n+1}} \cdots a_{i_{n+m}})(a^\dagger_{a_1} \cdots a^\dagger_{a_n})(a_{i_1} \cdots a_{i_n}) \Big] \\
&= \left[1 - (-1)^{2nm} \right] \left(\frac{1}{m!n!}\right)^2 \sum_{i_1 \cdots i_n \leq \rho_F} \sum_{a_1 \cdots a_n > \rho_F} \sum_{i_{n+1} \cdots i_{n+m} \leq \rho_F} \sum_{a_{n+1} \cdots a_{m+n} > \rho_F} t^{a_1 \cdots a_n}_{i_1 \cdots i_n} t^{a_{n+1} \cdots a_{n+m}}_{i_{n+1} \cdots i_{n+m}} \\
&\quad \times (a^\dagger_{a_1} \cdots a^\dagger_{a_n})(a_{i_1} \cdots a_{i_n})(a^\dagger_{a_{n+1}} \cdots a^\dagger_{a_{n+m}})(a_{i_{n+1}} \cdots a_{i_{n+m}}) \\
&= 0. \tag{C.5}
\end{aligned}
$$

Eq. (C.4) is very useful to expand $\overline{H}$. Assuming H includes up to the two-body interaction, the transformed Hamiltonian $\overline{H}$ can be written with Baker-Campbell-Hausdorff expansion as

$$\overline{H} = H + [H, T] + \frac{1}{2}[[H, T], T] + \frac{1}{3!}[[[H, T], T], T] + \frac{1}{4!}[[[[H, T], T], T], T]. \tag{C.6}$$

Since T not contracted with H is vanish, the expansion terminates with the four-fold commutator.

The most commonly used approximation is coupled-cluster with single-and-double (CCSD) where $T \approx T^{(1)} + T^{(2)}$. The cluster operators $T^{(1)}$ and $T^{(2)}$ are determined by coupled-cluster equations,

$$\langle 1p1h | \overline{H} | 0p0h \rangle = 0, \tag{C.7}$$

$$\langle 2p2h | \overline{H} | 0p0h \rangle = 0, \tag{C.8}$$

with the 0p0h state $|0p0h\rangle$, 1p1h state $|1p1h\rangle$, and 2p2h state $|2p2h\rangle$. Once the cluster operator is determined, the ground state energy $E_{\text{g.s.}}$ is given as

$$E_{\text{g.s.}} = \langle 0p0h | \overline{H} | 0p0h \rangle. \tag{C.9}$$

Appendix D

Matrix Elements for Equation of Motion Approach

As mentioned in Sec. 3.4, we diagonalize the transformed Hamiltonian to obtain the energies of excited states. Moreover, we diagonalize the transformed Hamiltonian in the 1p0h and 2p1h (0p1h and 1p2h) space to obtain the energies of $A + 1$ ($A - 1$) -body system. Here, the explicit expressions for the matrix elements are shown.

D.1   Normal Ordering with respect to the Reference State

First, let us remind the normal ordered transformed Hamiltonian with respect to the reference state.

$$\widetilde{H} \simeq E_0 + \sum_{ab}\langle a|\widetilde{h_1}|b\rangle : c_a^\dagger c_b : +\frac{1}{4}\sum_{abcd}\langle ab|\widetilde{v}_{12}|cd\rangle : c_a^\dagger c_b^\dagger c_d c_c : . \tag{D.1}$$

Here, Eq. (D.1) is given in terms of creation $c_a^\dagger$ and annihilation c_a operators of nucleon. To consider the matrix elements with the states around the reference state, let us define the creation and annihilation operators of particle and hole states as

$$c_a^\dagger = (1 - \rho_a)a_a^\dagger + \rho_a(-1)^{j_a+m_a}b_a, \tag{D.2}$$

$$c_a = (1 - \rho_a)a_a + \rho_a(-1)^{j_a+m_a}b_a^\dagger. \tag{D.3}$$

Here, $a_a^\dagger$ and a_a are the creation and annihilation operators of the particle state a, respectively. Also, $b_a^\dagger$ and b_a are the creation and annihilation operators of the hole state a, respectively. The ρ_a is equal to 1 (0) for the occupied (unoccupied) state, i.e., the occupation number of the reference state. By definition, the one-body operator can be written as

$$\langle a|o_1|b\rangle : c_a^\dagger c_b : \ =\langle a|o_1|b\rangle a_a^\dagger a_b + \langle \overline{a}|o_1|b\rangle b_a a_b(-1)^{j_a+m_a}$$
$$+ \langle a|o_1|\overline{b}\rangle a_a^\dagger b_b^\dagger(-1)^{j_b+m_b} - \langle \overline{a}|o_1|\overline{b}\rangle b_b^\dagger b_a(-1)^{j_a+m_a}(-1)^{j_b+m_b}, \tag{D.4}$$

Here, $\bar{a}$ means $\{n_a, l_a, j_a, -m_a, z_a\}$. Moreover, the two-body operator is

$$\langle ab|o_2|cd\rangle \colon c_a^\dagger c_b^\dagger c_d c_c \colon = \langle ab|o_2|cd\rangle a_a^\dagger a_b^\dagger a_d a_c + 2\langle ab|o_2|c\bar{d}\rangle a_a^\dagger a_b^\dagger b_d^\dagger a_c (-1)^{j_d+m_d}$$

$$+ \langle ab|o_2|\bar{c}\bar{d}\rangle a_a^\dagger a_b^\dagger b_d^\dagger b_c^\dagger (-1)^{j_c+m_c}(-1)^{j_d+m_d} + 2\langle a\bar{b}|o_2|cd\rangle a_a^\dagger b_b a_d a_c (-1)^{j_b+m_b}$$

$$+ \langle \bar{a}\bar{b}|o_2|cd\rangle b_a b_b a_d a_c (-1)^{j_a+m_a}(-1)^{j_b+m_b} - 4\langle a\bar{b}|o_2|c\bar{d}\rangle a_a^\dagger b_d^\dagger b_b a_c (-1)^{j_b+m_b}(-1)^{j_d+m_d}$$

$$+ 2\langle \bar{a}\bar{b}|o_2|c\bar{d}\rangle b_d^\dagger b_a b_b a_c (-1)^{j_a+m_a}(-1)^{j_b+m_b}(-1)^{j_d+m_d}$$

$$+ 2\langle a\bar{b}|o_2|\bar{c}\bar{d}\rangle a_a^\dagger b_d^\dagger b_c^\dagger b_b (-1)^{j_b+m_b}(-1)^{j_c+m_c}(-1)^{j_d+m_d}$$

$$+ \langle \bar{a}\bar{b}|o_2|\bar{c}\bar{d}\rangle b_d^\dagger b_c^\dagger b_a b_b (-1)^{j_a+m_a}(-1)^{j_b+m_b}(-1)^{j_c+m_c}(-1)^{j_d+m_d}. \tag{D.5}$$

D.2 Matrix Elements for the A-Body Closed Shell System

Here, we show the matrix elements for the excitation states of the A-body closed shell system. What we want to derive here is the explicit expression of

$$\langle \Phi^A|\widetilde{H}|\Phi^A\rangle, \tag{D.6}$$

$$\langle \Phi^A|\widetilde{H}|a_1 a_2^{-1} \colon J\rangle, \tag{D.7}$$

$$\langle a_1 a_2^{-1} \colon J|\widetilde{H}a_{a_3}^\dagger b_{a_4}^\dagger|a_3 a_4^{-1} \colon J\rangle, \tag{D.8}$$

$$\langle \Phi^A|\widetilde{H}|(a_1 a_2 \colon J_{a_1 a_2})(a_3^{-1} a_4^{-1} \colon J_{a_3 a_4})J\rangle, \tag{D.9}$$

$$\langle a_1 a_2^{-1} \colon J|\widetilde{H}|(a_3 a_4 \colon J_{a_3 a_4})(a_5^{-1} a_6^{-1} \colon J_{a_5 a_6})J\rangle, \tag{D.10}$$

$$\langle (a_1 a_2 \colon J_{a_1 a_2})(a_3^{-1} a_4^{-1} \colon J_{a_3 a_4})J|\widetilde{H}|(a_5 a_6 \colon J_{a_5 a_6})(a_7^{-1} a_8^{-1} \colon J_{a_7 a_8})J\rangle. \tag{D.11}$$

We use notations:

$$|a_1 a_2^{-1} \colon J\rangle = \sum_{m_{a_1} m_{a_2}} C^{j_{a_1} j_{a_2} J}_{m_{a_1} m_{a_2} M} a_{a_1}^\dagger b_{a_2}^\dagger|\Phi^A\rangle, \tag{D.12}$$

$$|(a_1 a_2 \colon J_{a_1 a_2})(a_3^{-1} a_4^{-1} \colon J_{a_3 a_4})J\rangle = \frac{1}{\Delta_{a_1 a_2} \Delta_{a_3 a_4}} \sum_{m_{a_1} m_{a_2} m_{a_3} m_{a_4}} C^{j_{a_1} j_{a_2} J_{a_1 a_2}}_{m_{a_1} m_{a_2} M_{a_1 a_2}} C^{j_{a_3} j_{a_4} J_{a_3 a_4}}_{m_{a_3} m_{a_4} M_{a_3 a_4}} C^{J_{a_1 a_2} J_{a_3 a_4} J}_{M_{a_1 a_2} M_{a_3 a_4} M}$$

$$\times a_{a_1}^\dagger a_{a_2}^\dagger b_{a_3}^\dagger b_{a_4}^\dagger|\Phi^A\rangle. \tag{D.13}$$

The $J_{a_1 a_2}$ and J denote the intermediate and total angular momentum. The coefficient $C^{j_1 j_2 J}_{m_1 m_2 M}$ is Clebsh-Gordan coefficient. Note that $|\Phi^A\rangle$ has total angular momentum 0. The Δ_{ab} means $\sqrt{(1 + \delta_{n_a n_b l_a l_b j_a j_b z_a z_b})}$. The Hamiltonian in Eq. (3.70) is

$$\widetilde{H}(A) = \begin{pmatrix} \text{Eq. (D.6)} & \text{Eq. (D.7)} & \text{Eq. (D.9)} & \cdots \\ \text{Eq. (D.7)} & \text{Eq. (D.8)} & \text{Eq. (D.10)} & \cdots \\ \text{Eq. (D.9)} & \text{Eq. (D.10)} & \text{Eq. (D.11)} & \cdots \\ \vdots & \vdots & \vdots & \ddots \end{pmatrix}. \tag{D.14}$$

Due to the normal ordering, the matrix element for the reference state can be derived as

$$\langle \Phi^A|\widetilde{H}|\Phi^A\rangle = E_0. \tag{D.15}$$

Eq. (D.7) is

$$\langle\Phi^A|\widetilde{H}|a_1a_2^{-1}: J\rangle = \sqrt{[j_{a_1}]}\,\widetilde{h}_{a_1a_2}\delta_{J0},\qquad(D.16)$$

with $\widetilde{h}_{ab} = \langle a|\widetilde{h}_1|b\rangle$. Since the reference state has 0^+ state, J takes only 0 for the coupling between 0p0h and 1p1h. Note that the vanishment of this coupling introduced in *method II* as shown in Sec. 3.5. Eq. (D.8) is

$$\langle a_1a_2^{-1}: J|\widetilde{H}|a_3a_4^{-1}: J\rangle = \widetilde{h}_{a_1a_3}\delta_{a_2a_4} - \widetilde{h}_{a_2a_4}\delta_{a_1a_3} - \sum_K[K]\left\{\begin{array}{ccc} j_{a_1} & j_{a_4} & K \\ j_{a_3} & j_{a_2} & J \end{array}\right\}\widetilde{v}^K_{a_1a_4a_3a_2}.\qquad(D.17)$$

The notation $\widetilde{v}^J_{abcd} = \langle ab: J|\widetilde{v}|cd: J\rangle$ is used. Eq. (D.9) is

$$\langle\Phi^A|\widetilde{H}|(a_1a_2: J_{a_1a_2})(a_3^{-1}a_4^{-1}: J_{a_3a_4})J\rangle = 0.\qquad(D.18)$$

Because the 2p2h excitations are already decoupled by the unitary-transformation. Eq. (D.10) is

$$\langle a_1a_2^{-1}: J|\widetilde{H}|(a_3a_4: J_{a_3a_4})(a_5^{-1}a_6^{-1}: J_{a_5a_6})J\rangle$$
$$= A(a_3a_4)A(a_5a_6)\frac{(-1)^{j_{a_1}+j_{a_3}+J_{a_3a_4}}\delta_{a_1a_4}\delta_{a_2a_6}}{\Delta_{a_3a_4}\Delta_{a_5a_6}}\sqrt{[J_{a_3a_4}][J_{a_5a_6}]}\widetilde{h}_{a_3a_5}\left\{\begin{array}{ccc} J_{a_3a_4} & j_{a_6} & j_{a_3} \\ j_{a_4} & J_{a_5a_6} & J \end{array}\right\}$$
$$- A(a_5a_6)\frac{1}{\Delta_{a_5a_6}}\widetilde{v}^{J_{a_3a_4}}_{a_1a_5a_3a_4}\delta_{a_2a_6}\sqrt{[J_{a_3a_4}][J_{a_5a_6}]}\left\{\begin{array}{ccc} j_1 & J_{a_3a_4} & j_5 \\ J_{a_5a_6} & j_2 & J \end{array}\right\}$$
$$- A(a_3a_4)\frac{(-1)^{j_{a_1}+j_{a_3}+J_{a_3a_4}}}{\Delta_{a_3a_4}}\widetilde{v}^{J_{a_5a_6}}_{a_5a_6a_3a_2}\delta_{a_1a_4}\sqrt{[J_{a_3a_4}][J_{a_5a_6}]}\left\{\begin{array}{ccc} J_{a_5a_6} & j_2 & j_3 \\ j_1 & J_{a_3a_4} & J \end{array}\right\}.\qquad(D.19)$$

Here, $A(ab)$ acts as $A(ab)f(ab) = f(ab) - (-1)^{j_a+j_b+J_{ab}}f(ba)$ for an arbitrary function $f(ab)$. Finally, Eq. (D.11) is

$$\langle(a_1a_2: J_{a_1a_2})(a_3^{-1}a_4^{-1}: J_{a_3a_4})J|\widetilde{H}|(a_5a_6: J_{a_5a_6})(a_7^{-1}a_8^{-1}: J_{a_7a_8})J\rangle$$
$$= A(a_1a_2)A(a_3a_4)A(a_5a_6)\frac{\widetilde{h}_{a_1a_5}\delta_{a_3a_7}\delta_{a_4a_8}\delta_{a_2a_6}\delta_{J_{a_1a_2}J_{a_5a_6}}\delta_{J_{a_3a_4}J_{a_7a_8}}}{\Delta^{a_1a_2}\Delta_{a_5a_6}\Delta^2_{a_3a_4}}$$
$$- A(a_1a_2)A(a_3a_4)A(a_7a_8)\frac{\widetilde{h}_{a_3a_7}\delta_{a_1a_5}\delta_{a_2a_6}\delta_{a_4a_8}\delta_{J_{a_1a_2}J_{a_5a_6}}\delta_{J_{a_3a_4}J_{a_7a_8}}}{\Delta^2_{a_1a_2}\Delta_{a_3a_4}\Delta_{a_7a_8}}$$
$$+ A(a_3a_4)\frac{\delta_{a_3a_7}\delta_{a_4a_8}\delta_{J_{a_1a_2}J_{a_5a_6}}\delta_{J_{a_3a_4}J_{a_7a_8}}}{\Delta^2_{a_3a_4}}\widetilde{v}^{J_{a_1a_2}}_{a_1a_2a_5a_6}$$
$$+ A(a_1a_2)\frac{\delta_{a_1a_5}\delta_{a_2a_6}\delta_{J_{a_1a_2}J_{a_5a_6}}\delta_{J_{a_3a_4}J_{a_7a_8}}}{\Delta^2_{a_1a_2}}\widetilde{v}^{J_{a_3a_4}}_{a_3a_4a_7a_8}$$
$$+ \sum_{IK}\frac{A(a_1a_2)A(a_3a_4)A(a_5a_6)A(a_7a_8)(-1)^{j_{a_1}+j_{a_2}+j_{a_4}+j_{a_5}}(-1)^{J_{a_3a_4}+J_{a_7a_8}+K+I+J}\delta_{a_4a_8}\delta_{a_2a_6}}{\Delta_{a_1a_2}\Delta_{a_3a_4}\Delta_{a_5a_6}\Delta_{a_7a_8}}[I][K]$$
$$\times\left\{\begin{array}{ccc} j_{a_1} & J_{a_1a_2} & j_{a_2} \\ J_{a_5a_6} & j_{a_5} & I \end{array}\right\}\left\{\begin{array}{ccc} j_{a_3} & J_{a_3a_4} & j_{a_4} \\ J_{a_7a_8} & j_{a_7} & I \end{array}\right\}\left\{\begin{array}{ccc} J_{a_1a_2} & J_{a_5a_6} & I \\ J_{a_7a_8} & J_{a_3a_4} & J \end{array}\right\}$$
$$\times\left\{\begin{array}{ccc} j_{a_1} & j_{a_7} & K \\ j_{a_3} & j_{a_5} & I \end{array}\right\}\widetilde{v}^K_{a_1a_7a_5a_3}.\qquad(D.20)$$

D.3 Matrix Elements for the Closed Shell Plus-One-Body System

Similarly to Sec. D.2, we show explicit expressions of following matrix element:

$$\langle a_1 : J | \widetilde{H} | a_2 : J \rangle, \tag{D.21}$$

$$\langle a_1 : J | \widetilde{H} | (a_2 a_3 : J_{a_2 a_3}) a_4^{-1} : J \rangle, \tag{D.22}$$

$$\langle (a_1 a_2 : J_{a_1 a_2}) a_3^{-1} : J | \widetilde{H} | (a_4 a_5 : J_{a_4 a_5}) a_6^{-1} : J \rangle. \tag{D.23}$$

Here, we use

$$|a_1 : J \rangle = a_{a_1}^\dagger \delta_{j_{a_1} J} | \Phi^A \rangle, \tag{D.24}$$

$$|(a_1 a_2 : J_{a_1 a_2}) a_3^{-1} : J \rangle = \frac{1}{\Delta_{a_1 a_2}} \sum_{m_{a_1} m_{a_2} m_{a_3}} C^{j_{a_1} j_{a_2} J_{a_1 a_2}}_{m_{a_1} m_{a_2} M_{a_1 a_2}} C^{J_{a_1 a_2} j_{a_3} J}_{M_{a_1 a_2} m_{a_3} M} a_{a_1}^\dagger a_{a_2}^\dagger b_{a_3}^\dagger | \Phi^A \rangle. \tag{D.25}$$

The Hamiltonian in Eq. (3.75) is

$$\widetilde{H}(A+1) = \begin{pmatrix} \text{Eq. (D.21)} & \text{Eq. (D.22)} & \cdots \\ \text{Eq. (D.22)} & \text{Eq. (D.23)} & \cdots \\ \vdots & \vdots & \ddots \end{pmatrix}. \tag{D.26}$$

Eq. (D.21) is

$$\langle a_1 : J | \widetilde{H} | a_2 : J \rangle = \sqrt{[j_{a_1}]} \, \widetilde{h}_{a_1 a_2}. \tag{D.27}$$

Eq. (D.22) is

$$\langle a_1 : J | \widetilde{H} | (a_2 a_3 : J_{a_2 a_3}) a_4^{-1} : J \rangle = -(-1)^{J_{a_2 a_3} + j_{a_4} - J} \frac{\sqrt{[J_{a_2 a_3}]}}{\sqrt{[J]}} \widetilde{v}^{J_{a_2 a_3}}_{a_1 a_4 a_2 a_3}. \tag{D.28}$$

Eq. (D.23) is

$$\langle (a_1 a_2 : J_{a_1 a_2}) a_3^{-1} : J | \widetilde{H} | (a_4 a_5 : J_{a_4 a_5}) a_6^{-1} : J \rangle$$

$$= A(a_1 a_2) A(a_4 a_5) \frac{\delta_{J_{a_1 a_2} J_{a_4 a_5}} \delta_{a_2 a_5} \delta_{a_3 a_6}}{\Delta_{a_1 a_2} \Delta_{a_4 a_5}} \widetilde{h}_{a_1 a_4} - A(a_1 a_2) \frac{\delta_{J_{a_1 a_2} J_{a_4 a_5}} \delta_{a_1 a_4} \delta_{a_2 a_5}}{\Delta_{a_1 a_2}^2} \widetilde{h}_{a_3 a_6} + \delta_{J_{a_1 a_2} J_{a_4 a_5}} \delta_{a_3 a_6} \widetilde{v}^{J_{a_1 a_2}}_{a_1 a_2 a_4 a_5}$$

$$- A(a_1 a_2) A(a_4 a_5) \sum_{IK} \frac{(-1)^{j_{a_3} + j_{a_6} + J_{a_1 a_2} + J_{a_4 a_5}} \delta_{a_2 a_5}}{\Delta_{a_1 a_2} \Delta_{a_4 a_5}} [I][K] \sqrt{[J_{a_1 a_2}][J_{a_4 a_5}]} \begin{Bmatrix} j_{a_1} & j_{a_2} & J_{a_1 a_2} \\ J & j_{a_3} & K \end{Bmatrix}$$

$$\times \begin{Bmatrix} j_{a_4} & j_{a_5} & J_{a_4 a_5} \\ J & j_{a_6} & K \end{Bmatrix} \begin{Bmatrix} j_{a_1} & j_{a_6} & I \\ j_{a_4} & j_{a_3} & K \end{Bmatrix} \widetilde{v}^I_{a_1 a_6 a_4 a_3}. \tag{D.29}$$

D.4 Matrix Elements for the Closed Shell Minus-One-Body System

Similarly to previous sections, we show explicit expressions of following matrix element:

$$\langle a_1^{-1} : J | \widetilde{H} | a_2^{-1} : J \rangle, \tag{D.30}$$

$$\langle a_1^{-1} : J | \widetilde{H} | a_2 (a_3^{-1} a_4^{-1} : J_{a_3 a_4}) : J \rangle, \tag{D.31}$$

$$\langle a_1 (a_2^{-1} a_3^{-1} : J_{a_2 a_3}) : J | \widetilde{H} | a_4 (a_5^{-1} a_6^{-1} : J_{a_5 a_6}) : J \rangle. \tag{D.32}$$

Here, we use

$$|a_1^{-1} : J\rangle = b_{a_1}^\dagger \delta_{j_{a_1} J} |\Phi^A\rangle, \tag{D.33}$$

$$|a_1(a_2^{-1} a_3^{-1} : J_{a_2 a_3}) : J\rangle = \frac{1}{\Delta_{a_2 a_3}} \sum_{m_{a_1} m_{a_2} m_{a_3}} C_{m_{a_1} M_{a_2 a_3} M}^{j_{a_1} J_{a_2 a_3} J} C_{m_{a_2} m_{a_3} M_{a_2 a_3}}^{j_{a_2} j_{a_2} J_{a_2 a_3}} a_{a_1}^\dagger b_{a_2}^\dagger b_{a_3}^\dagger |\Phi^A\rangle. \tag{D.34}$$

The Hamiltonian in Eq. (3.76) is

$$\widetilde{H}(A-1) = \begin{pmatrix} \text{Eq. (D.30)} & \text{Eq. (D.31)} & \cdots \\ \text{Eq. (D.31)} & \text{Eq. (D.32)} & \cdots \\ \vdots & \vdots & \ddots \end{pmatrix}. \tag{D.35}$$

Eq. (D.30) is

$$\langle a_1^{-1} : J | \widetilde{H} | a_2^{-1} : J\rangle = -\sqrt{[j_{a_1}]}\, \widetilde{h}_{a_1 a_2}. \tag{D.36}$$

Eq. (D.31) is

$$\langle a_1^{-1} : J | \widetilde{H} | a_2(a_3^{-1} a_4^{-1} : J_{a_3 a_4}) : J\rangle = (-1)^{j_{a_1} + j_{a_2} + j_{a_3} + j_{a_4}} \frac{\sqrt{[J_{a_3 a_4}]}}{\sqrt{[J]}} \widetilde{v}_{a_4 a_3 a_2 a_1}^{J_{a_3 a_4}}. \tag{D.37}$$

Eq. (D.32) is

$$\langle a_1(a_2^{-1} a_3^{-1} : J_{a_2 a_3}) : J | \widetilde{H} | a_4(a_5^{-1} a_6^{-1} : J_{a_5 a_6}) : J\rangle$$

$$= A(a_2 a_3) \frac{\delta_{J_{a_2 a_3} J_{a_5 a_6}} \delta_{a_2 a_5} \delta_{a_3 a_6}}{\Delta_{a_2 a_3}^2} \widetilde{h}_{a_1 a_4} - A(a_2 a_3) A(a_5 a_6) \frac{\delta_{J_{a_2 a_3} J_{a_5 a_6}} \delta_{a_1 a_4} \delta_{a_3 a_6}}{\Delta_{a_2 a_3} \Delta_{a_5 a_6}} \widetilde{h}_{a_2 a_5} + \delta_{J_{a_2 a_3} J_{a_5 a_6}} \delta_{a_1 a_4} \widetilde{v}_{a_2 a_3 a_5 a_6}^{J_{a_2 a_3}}$$

$$+ A(a_2 a_3) A(a_5 a_6) \sum_{IK} \frac{(-1)^{j_{a_1} + j_{a_2} + j_{a_4} + j_{a_5}} \delta_{a_3 a_6}}{\Delta_{a_2 a_3} \Delta_{a_5 a_6}} [I][K] \sqrt{[J_{a_2 a_3}][J_{a_5 a_6}]} \begin{Bmatrix} j_{a_2} & j_{a_3} & J_{a_2 a_3} \\ J & j_{a_1} & K \end{Bmatrix}$$

$$\times \begin{Bmatrix} j_{a_5} & j_{a_6} & J_{a_5 a_6} \\ J & j_{a_4} & K \end{Bmatrix} \begin{Bmatrix} j_{a_1} & j_{a_5} & I \\ j_{a_4} & j_{a_2} & K \end{Bmatrix} \widetilde{v}_{a_1 a_5 a_4 a_2}^{I}. \tag{D.38}$$

Appendix E

Details for the Other Observables

In this thesis, we calculate, in addition to the energy, the observables such as the expectation values of radii operators. In Appendix E, the equations used in the actual calculations are summarized.

E.1 Cluster Expansion of Original Operators

Here, the cluster expansion of the initial operator used in the numerical calculations is shown. First, we consider the point-nucleon radius. The definition of the squared point-nucleon radius operator is

$$r_{\mathrm{m}}^2 = \frac{1}{A} \sum_{i=1}^{A} (\mathbf{r}_i - \mathbf{R}_{\mathrm{CM}})^2. \tag{E.1}$$

Here, $\mathbf{r}_i$ and $\mathbf{R}_{\mathrm{CM}}$ are the coordinate vectors of ith nucleon and CM of nucleus. By using

$$\mathbf{R}_{\mathrm{CM}} = \frac{1}{A} \sum_{i=1}^{A} \mathbf{r}_i, \tag{E.2}$$

Eq. (E.1) can be decomposed into

$$r_{\mathrm{m}}^2 = \frac{1}{A}\left(1 - \frac{1}{A}\right) \sum_{i=1}^{A} \mathbf{r}_i^2 - \frac{2}{A^2} \sum_{i<j}^{A} \mathbf{r}_i \cdot \mathbf{r}_j. \tag{E.3}$$

Comparing to Eq. (3.59), r_{m}^2 can be rewritten as

$$r_{\mathrm{m}}^2 = \sum_{i=1}^{A} r_{\mathrm{m},i}^2 + \sum_{i<j}^{A} r_{\mathrm{m},ij}^2, \tag{E.4}$$

with the one- and two-body parts,

$$r_{\mathrm{m},i}^2 = \frac{1}{A}\left(1 - \frac{1}{A}\right)\mathbf{r}_i^2, \quad r_{\mathrm{m},ij}^2 = -\frac{2}{A^2}\mathbf{r}_i \cdot \mathbf{r}_j. \tag{E.5}$$

Second, the definition of the squared point-proton radius operator is

$$r_p^2 = \frac{1}{Z} \sum_{i=1}^{A} \left(\frac{1 + \tau_{3,i}}{2}\right)(\mathbf{r}_i - \mathbf{R}_{\mathrm{CM}})^2. \tag{E.6}$$

Here, $\tau_{3,i}$ is the third component of the isospin for the ith nucleon. Similarly to r_{m}^2 case, r_p^2 can be decomposed into

$$r_p^2 = \sum_{i=1}^{A} r_{p,i}^2 + \sum_{i<j}^{A} r_{p,ij}^2, \tag{E.7}$$

with

$$r_{p,i}^2 = \left[\frac{1}{Z}\left(1 - \frac{2}{A}\right)\left(\frac{1 + \tau_{3,i}}{2}\right) + \frac{1}{A^2}\right]\mathbf{r}_i^2, \tag{E.8}$$

$$r_{p,ij}^2 = \left[-\frac{4}{AZ}\left(\frac{1 + \tau_{3,i}}{2}\right)\left(\frac{1 + \tau_{3,j}}{2}\right) - \frac{2}{AZ}\left(\frac{1 + \tau_{3,i}}{2}\right)\left(\frac{1 - \tau_{3,j}}{2}\right) + \frac{2}{A^2}\right]\mathbf{r}_i \cdot \mathbf{r}_j. \tag{E.9}$$

Almost same decomposition can be done for the squared point-neutron radius operator r_n^2:

$$r_n^2 = \sum_{i=1}^{A} r_{n,i}^2 + \sum_{i<j}^{A} r_{n,ij}^2, \tag{E.10}$$

with

$$r_{n,i}^2 = \left[\frac{1}{N}\left(1 - \frac{2}{A}\right)\left(\frac{1 - \tau_{3,i}}{2}\right) + \frac{1}{A^2}\right]\mathbf{r}_i^2, \tag{E.11}$$

$$r_{n,ij}^2 = \left[-\frac{4}{AN}\left(\frac{1 - \tau_{3,i}}{2}\right)\left(\frac{1 - \tau_{3,j}}{2}\right) - \frac{2}{AN}\left(\frac{1 - \tau_{3,i}}{2}\right)\left(\frac{1 + \tau_{3,j}}{2}\right) + \frac{2}{A^2}\right]\mathbf{r}_i \cdot \mathbf{r}_j. \tag{E.12}$$

Next, we consider the CM Hamiltonian:

$$H_{\mathrm{CM}} = \frac{\mathbf{P}_{\mathrm{CM}}^2}{2Am} + \frac{1}{2}Am\omega^2\mathbf{R}_{\mathrm{CM}}^2. \tag{E.13}$$

The H_{CM} can be decomposed into

$$H_{\mathrm{CM}} = \sum_{i=1}^{A} h_{\mathrm{CM},i} + \sum_{i<j}^{A} h_{\mathrm{CM},ij}, \tag{E.14}$$

with

$$h_{\mathrm{CM},i} = \frac{1}{A}\left(\frac{\mathbf{p}_i^2}{2m} + \frac{1}{2}m\omega^2\mathbf{r}_i^2\right), \quad h_{\mathrm{CM},ij} = \frac{1}{A}\left(\frac{\mathbf{p}_i \cdot \mathbf{p}_j}{m} + m\omega^2\mathbf{r}_i \cdot \mathbf{r}_j\right). \tag{E.15}$$

E.2 Translationally Invariant Density

In this work, we assume that the nucleus is spherical and calculate the angle-averaged density

$$\rho(r) = \frac{1}{\int d\hat{\mathbf{r}}}\int d\hat{\mathbf{r}}\rho(\mathbf{r})$$

$$= \frac{1}{4\pi}\sum_{ab}\widetilde{n}_{ab}R_{n_al_a}^*(r)R_{n_bl_b}(r)\delta_{l_al_b}\delta_{j_aj_b}\delta_{m_am_b}. \tag{E.16}$$

Here, $\widetilde{n}_{ab}$ is density matrix calculated in the UMOA. Since our ground-state $|\Psi\rangle$ includes the CM motion, density $\rho(r)$ also includes the contributions from the CM motion. As found in Ref [102], if $|\Phi\rangle$ can be factorized into the translationally invariant state $|\Psi_{\text{ti}}\rangle$ and CM state $|\Psi_{\text{CM}}\rangle$,

$$|\Psi\rangle = |\Psi_{\text{ti}}\rangle \otimes |\Psi_{\text{CM}}\rangle, \tag{E.17}$$

the angle-averaged translationally invariant density, $\rho_{\text{ti}}(r)$, can be introduced as

$$\rho_{\text{ti}}(r) = \frac{1}{2\pi^2} \int_0^\infty dp\, p^2 \frac{\sin(pr)}{pr} F(p). \tag{E.18}$$

Here, $F(p)$ are the angle-averaged Fourier transformed translationally invariant density (form factor) defined by

$$F(p) = \frac{\int_0^\infty dr\, r \sin(pr)\rho(r)}{\int_0^\infty dr\, r \sin(pr)\rho_{\text{CM}}(r)}. \tag{E.19}$$

As discussed in the CCM, the CM motion can be factorized by the Gaussian with the proper frequency $\widetilde{\omega}$ for the ground state [103]. We confirmed that such a factorization is also valid in the UMOA.

Appendix F

Table of Numerical Results

Here, we tabulate the calculated ground-state energies and radii for the shell closed nuclei from ^{4}He to ^{218}Pb. The calculation results are obtained with the chiral N^{3}LO NN interaction [10] softened by SRG transformation with $\lambda_{\mathrm{SRG}} = 1.88$ fm^{-1}, 2 fm^{-1}, 2.24 fm^{-1}. In addition to the point-proton radii $\langle r_p^2 \rangle^{1/2}$, point-neutron radii $\langle r_n^2 \rangle^{1/2}$, and point-nucleon radii $\langle r_m^2 \rangle^{1/2}$, we exhibit the charge radii calculated by

$$r_{\mathrm{ch}} = \sqrt{\langle r_p^2 \rangle + R_p^2 + \frac{N}{Z} R_n^2}, \tag{F.1}$$

and

$$\Delta r_{np} = \langle r_n^2 \rangle^{1/2} - \langle r_p^2 \rangle^{1/2}. \tag{F.2}$$

As for the finite size correction in the charge radius, we employ $R_p^2 = 0.832$ fm^2 [72] and $R_n^2 = -0.115$ fm^2 [73].

Table F.1: Ground-state energies per nucleon $E_{\mathrm{g.s.}}/A$, point-proton radii $\langle r_p^2 \rangle^{1/2}$, point-neutron radii $\langle r_n^2 \rangle^{1/2}$, point-nucleon radii $\langle r_m^2 \rangle^{1/2}$, charge radii r_{ch}, and $\Delta r_{np} = \langle r_n^2 \rangle^{1/2} - \langle r_p^2 \rangle^{1/2}$ for sub-shell closures at $e_{\max} = 12$ and $\hbar\omega = 20$ MeV. The interaction is chiral N^{3}LO NN interaction softened by SRG transformation evolved to $\lambda_{\mathrm{SRG}} = 1.88$ fm^{-1}. The number in parenthesis means the error and is estimated by the difference between $e_{\max} = 10$ and $e_{\max} = 12$ results.

nucleus	$E_{\mathrm{g.s.}}/A$ (MeV)	$\langle r_p^2 \rangle^{1/2}$ (fm)	$\langle r_n^2 \rangle^{1/2}$ (fm)	$\langle r_m^2 \rangle^{1/2}$ (fm)	r_{ch} (fm)	Δr_{np} (fm)
^{4}He	-6.98	1.414	1.408	1.411	1.648	-0.006
^{14}O	-8.41	2.059	1.935	2.007	2.233	-0.124
^{16}O	-10.49	2.029	2.012	2.020	2.198	-0.017
^{22}O	-10.13	2.010	2.294	2.195	2.161	0.285
^{24}O	-10.16	2.011	2.381(1)	2.264	2.156	0.369(1)
^{34}Ca	-12.08	2.423	2.233	2.347	2.573	-0.190
^{36}Ca	-13.56	2.397	2.272	2.342	2.546	-0.124
^{40}Ca	-15.39	2.395	2.366	2.380	2.540	-0.029

Table F.1 continued:

nucleus	$E_{\text{g.s.}}/A$ (MeV)	$\langle r_p^2 \rangle^{1/2}$ (fm)	$\langle r_n^2 \rangle^{1/2}$ (fm)	$\langle r_m^2 \rangle^{1/2}$ (fm)	r_{ch} (fm)	Δr_{np} (fm)
^{48}Ca	-16.10	2.363	2.506	2.448	2.501	0.143
^{52}Ca	-16.33	2.363	2.590	2.505	2.496	0.227
^{54}Ca	-16.28(1)	2.370	2.641	2.544	2.501	0.271(1)
^{60}Ca	-15.51(1)	2.422	2.766(1)	2.656(1)	2.544	0.344(2)
^{48}Ni	-14.21	2.563	2.353	2.477	2.705	-0.210
^{56}Ni	-16.66(1)	2.511	2.477(1)	2.494	2.650	-0.034
^{60}Ni	-17.53(1)	2.503(1)	2.541(1)	2.523(1)	2.639(1)	0.039
^{62}Ni	-17.80(1)	2.507(1)	2.578	2.546(1)	2.641(1)	0.071
^{68}Ni	-18.27(1)	2.541(1)	2.680	2.624	2.670(1)	0.139
^{78}Ni	-17.70(1)	2.543(1)	2.791(1)	2.704(1)	2.663(1)	0.248
^{80}Zr	-19.43(1)	2.740(1)	2.695(1)	2.718(1)	2.868	-0.045
^{90}Zr	-20.59(1)	2.710(1)	2.781(1)	2.749(1)	2.834(1)	0.071
^{96}Zr	-20.99(2)	2.709(1)	2.849(2)	2.791(2)	2.830(1)	0.140
^{98}Zr	-21.08(2)	2.709(2)	2.874(1)	2.808(2)	2.830(1)	0.164
^{102}Zr	-20.99(2)	2.723(2)	2.933(1)	2.852(1)	2.840(1)	0.210
^{110}Zr	-20.44(2)	2.771(1)	3.035(1)	2.942(1)	2.882(1)	0.264
^{122}Zr	-19.78(2)	2.774(2)	3.107(2)	3.002(2)	2.880(2)	0.332
^{100}Sn	-20.58(2)	2.812(2)	2.765(2)	2.788(2)	2.936(2)	-0.047
^{106}Sn	-21.43(2)	2.807(2)	2.824(2)	2.816(2)	2.929(2)	0.017
^{108}Sn	-21.64(2)	2.807(2)	2.845(2)	2.828(2)	2.929(2)	0.038
^{112}Sn	-21.88(2)	2.818(2)	2.893(2)	2.860(2)	2.938(2)	0.075
^{120}Sn	-22.16(2)	2.857(2)	2.982(2)	2.931(2)	2.972(2)	0.126
^{132}Sn	-22.09(3)	2.854(2)	3.055(3)	2.980(3)	2.965(2)	0.201
^{184}Pb	-24.77(5)	3.143(4)	3.205(5)	3.177(5)	3.251(4)	0.062(1)
^{194}Pb	-25.00(5)	3.182(3)	3.283(5)	3.241(4)	3.286(3)	0.102(1)
^{208}Pb	-25.28(6)	3.177(4)	3.336(6)	3.274(5)	3.278(4)	0.160(1)
^{218}Pb	-25.24(7)	3.179(5)	3.390(7)	3.312(6)	3.279(4)	0.210(2)

Table F.2: Same as the Table F.1 except for the interaction. The interaction is chiral N³LO *NN* interaction softened by SRG transformation evolved to $\lambda_{\mathrm{SRG}} = 2$ fm^{-1}.

nucleus	$E_{\mathrm{g.s.}}/A$ (MeV)	$\langle r_p^2 \rangle^{1/2}$ (fm)	$\langle r_n^2 \rangle^{1/2}$ (fm)	$\langle r_{\mathrm{m}}^2 \rangle^{1/2}$ (fm)	r_{ch} (fm)	Δr_{np} (fm)
^{4}He	-6.93	1.411	1.406	1.408	1.646	-0.006
^{14}O	-8.15	2.063	1.938	2.010	2.236	-0.125
^{16}O	-10.17	2.034	2.017	2.026	2.203	-0.017
^{22}O	-9.76	2.015	2.299	2.200	2.166	0.283
^{24}O	-9.77	2.019	2.388	2.272	2.163	0.370(1)
^{34}Ca	-11.52	2.434(1)	2.242(1)	2.357(1)	2.583	-0.191
^{36}Ca	-12.95	2.408(1)	2.283(1)	2.353(1)	2.557	-0.125
^{40}Ca	-14.71	2.407(1)	2.378(1)	2.393(1)	2.552(1)	-0.030
^{48}Ca	-15.37(1)	2.375(1)	2.517(1)	2.459(1)	2.513(1)	0.142
^{52}Ca	-15.55(1)	2.377(1)	2.604	2.519	2.510(1)	0.227
^{54}Ca	-15.48(1)	2.385(1)	2.656	2.559	2.515(1)	0.271(1)
^{60}Ca	-14.71(1)	2.439(1)	2.784(1)	2.674	2.560(1)	0.344(2)
^{48}Ni	-13.49(1)	2.575	2.365(1)	2.490	2.717	-0.210(1)
^{56}Ni	-15.83(2)	2.523(1)	2.489(1)	2.506(1)	2.662(1)	-0.035
^{60}Ni	-16.64(2)	2.517(2)	2.555(1)	2.537(2)	2.652(1)	0.038
^{62}Ni	-16.90(2)	2.522(2)	2.593(1)	2.561(2)	2.655(2)	0.071
^{68}Ni	-17.34(2)	2.558(2)	2.697(1)	2.640(1)	2.685(2)	0.139
^{78}Ni	-16.74(3)	2.560(2)	2.808(2)	2.721(2)	2.679(2)	0.248
^{80}Zr	-18.37(2)	2.760(1)	2.715(2)	2.738(2)	2.887(1)	-0.046
^{90}Zr	-19.47(3)	2.730(2)	2.800(3)	2.769(2)	2.853(2)	0.070
^{96}Zr	-19.83(4)	2.730(3)	2.870(3)	2.813(3)	2.851(2)	0.140
^{98}Zr	-19.90(4)	2.732(3)	2.896(3)	2.830(3)	2.851(3)	0.164
^{102}Zr	-19.81(4)	2.746(3)	2.957(2)	2.876(3)	2.863(3)	0.211
^{110}Zr	-19.26(4)	2.796(3)	3.060(2)	2.967(2)	2.906(2)	0.264
^{122}Zr	-18.59(5)	2.800(3)	3.132(3)	3.027(3)	2.904(3)	0.333
^{100}Sn	-19.39(4)	2.832(3)	2.785(3)	2.809(3)	2.956(3)	-0.048
^{106}Sn	-20.18(5)	2.829(3)	2.845(4)	2.837(4)	2.950(3)	0.016
^{108}Sn	-20.37(5)	2.830(3)	2.868(4)	2.850(4)	2.951(3)	0.038
^{112}Sn	-20.59(5)	2.842(4)	2.917(4)	2.884(4)	2.961(3)	0.076
^{120}Sn	-20.86(5)	2.882(3)	3.008(4)	2.956(4)	2.996(3)	0.126
^{132}Sn	-20.76(6)	2.880(4)	3.080(5)	3.006(5)	2.989(4)	0.201
^{184}Pb	-23.12(9)	3.178(5)	3.241(7)	3.213(6)	3.285(5)	0.062(1)
^{194}Pb	-23.35(10)	3.218(5)	3.320(7)	3.277(6)	3.321(5)	0.102(1)
^{208}Pb	-23.59(11)	3.214(5)	3.374(8)	3.312(7)	3.314(5)	0.160(2)

Table F.2 continued:

nucleus	$E_{\text{g.s.}}/A$ (MeV)	$\langle r_p^2\rangle^{1/2}$ (fm)	$\langle r_n^2\rangle^{1/2}$ (fm)	$\langle r_m^2\rangle^{1/2}$ (fm)	r_{ch} (fm)	Δr_{np} (fm)
^{218}Pb	-23.52(12)	3.218(6)	3.430(9)	3.352(8)	3.316(6)	0.212(3)

Table F.3: Same as the Table F.1 except for the interaction. The interaction is chiral N^{3}LO *NN* interaction softened by SRG transformation evolved to $\lambda_{\text{SRG}} = 2.24$ fm^{-1}.

nucleus	$E_{\text{g.s.}}/A$ (MeV)	$\langle r_p^2\rangle^{1/2}$ (fm)	$\langle r_n^2\rangle^{1/2}$ (fm)	$\langle r_m^2\rangle^{1/2}$ (fm)	r_{ch} (fm)	Δr_{np} (fm)
^{4}He	-6.81	1.413	1.407	1.410	1.647	-0.006
^{14}O	-7.65(1)	2.080(1)	1.954(2)	2.027(1)	2.252(1)	-0.126
^{16}O	-9.55(1)	2.054(2)	2.037(2)	2.046(2)	2.222(1)	-0.017
^{22}O	-9.05(2)	2.038(2)	2.322(1)	2.223(2)	2.187(2)	0.284
^{24}O	-9.00(2)	2.045(2)	2.417	2.300(1)	2.187(2)	0.373(1)
^{34}Ca	-10.45(3)	2.467(3)	2.273(3)	2.389(3)	2.615(3)	-0.194
^{36}Ca	-11.76(3)	2.443(3)	2.316(3)	2.387(3)	2.590(3)	-0.127
^{40}Ca	-13.40(4)	2.445(3)	2.414(3)	2.429(3)	2.587(3)	-0.031
^{48}Ca	-13.92(5)	2.414(4)	2.556(3)	2.498(4)	2.549(3)	0.142
^{52}Ca	-14.03(6)	2.419(4)	2.648(2)	2.562(3)	2.550(3)	0.229(1)
^{54}Ca	-13.94(6)	2.429(4)	2.703(1)	2.605(2)	2.556(3)	0.274(2)
^{60}Ca	-13.20(6)	2.486(3)	2.833	2.722(1)	2.604(3)	0.347(3)
^{48}Ni	-12.09(5)	2.616(2)	2.403(3)	2.529(3)	2.755(2)	-0.213(1)
^{56}Ni	-14.18(7)	2.566(4)	2.530(4)	2.548(4)	2.702(4)	-0.036
^{60}Ni	-14.89(7)	2.563(4)	2.601(4)	2.583(4)	2.696(4)	0.038
^{62}Ni	-15.10(7)	2.569(5)	2.641(4)	2.609(4)	2.700(4)	0.073
^{68}Ni	-15.52(8)	2.607(4)	2.746(4)	2.690(4)	2.732(4)	0.140
^{78}Ni	-14.85(10)	2.611(5)	2.861(5)	2.774(5)	2.728(5)	0.250
^{80}Zr	-16.33(9)	2.816(4)	2.769(5)	2.793(5)	2.941(4)	-0.047
^{90}Zr	-17.27(11)	2.787(5)	2.857(6)	2.826(6)	2.908(5)	0.070
^{96}Zr	-17.55(12)	2.791(6)	2.932(6)	2.874(6)	2.909(6)	0.141
^{98}Zr	-17.59(12)	2.794(6)	2.960(6)	2.894(6)	2.911(6)	0.166
^{102}Zr	-17.49(12)	2.810(6)	3.024(6)	2.942(6)	2.924(6)	0.214
^{110}Zr	-16.97(13)	2.862(6)	3.129(6)	3.034(6)	2.970(5)	0.267
^{122}Zr	-16.26(15)	2.868(6)	3.204(7)	3.098(7)	2.970(6)	0.336(1)
^{100}Sn	-17.03(13)	2.893(6)	2.844(7)	2.868(7)	3.014(6)	-0.049

Table F.3 continued:

nucleus	$E_{\text{g.s.}}/A$ (MeV)	$\langle r_p^2 \rangle^{1/2}$ (fm)	$\langle r_n^2 \rangle^{1/2}$ (fm)	$\langle r_m^2 \rangle^{1/2}$ (fm)	r_{ch} (fm)	Δr_{np} (fm)
^{106}Sn	-17.70(14)	2.893(7)	2.909(7)	2.901(7)	3.012(7)	0.016
^{108}Sn	-17.87(14)	2.896(7)	2.934(7)	2.916(7)	3.014(7)	0.038
^{112}Sn	-18.06(14)	2.910(7)	2.986(7)	2.952(7)	3.026(7)	0.077
^{120}Sn	-18.32(15)	2.950(7)	3.077(8)	3.025(7)	3.062(7)	0.127
^{132}Sn	-18.13(17)	2.951(7)	3.154(9)	3.078(9)	3.058(7)	0.203(1)
^{184}Pb	-19.88(24)	3.271(8)	3.335(10)	3.306(9)	3.375(8)	0.064(1)
^{194}Pb	-20.13(25)	3.311(7)	3.414(10)	3.371(9)	3.411(7)	0.104(2)
^{208}Pb	-20.26(28)	3.309(8)	3.472(12)	3.409(10)	3.407(8)	0.163(3)
^{218}Pb	-20.14(29)	3.318(8)	3.534(13)	3.454(11)	3.413(8)	0.217(4)

Appendix G

Matrix Elements for Three-body Basis States

Here, we show the antisymmetrization of the three-body state and derivations of the matrix element with the three-body state. We begin with the definition of the three-body state. Let the states $|a), |b), \cdots$ be the harmonic oscillator (h.o.) wave functions. The non-antisymmetrized three-body state is defined as

$$|abc) := |a) \otimes |b) \otimes |c), \tag{G.1}$$

in the M-scheme. In this appendix, we denote the non-antisymmetrized and antisymmetrized states as $|\cdots)$ and $|\cdots\rangle$, respectively. By summing up the third component of the angular momentum, the non-antisymmetrized three-body state is

$$|abc: J_{ab}J) = \sum_{m_a m_b m_c} C^{j_a j_b J_{ab}}_{m_a m_b M_{ab}} C^{J_{ab} j_c J}_{M_{ab} m_c M} |abc), \tag{G.2}$$

where $C^{j_1 j_2 j_3}_{m_1 m_2 m_3}$ is the Clebsch-Cordan coefficient. In Eq. (G.2), the total angular momentum J is constructed via J_{ab}.

Before discussing to the antisymmetrization of the three-body state, we note the useful recoupling formulae:

$$C^{j_a j_b J_1}_{m_\alpha m_\beta M_1} C^{j_c j_d J_1}_{m_\gamma m_\delta M_1} = \sum_{J_2} (-1)^{4j_a + 2j_b + 2j_c + J_1 - 3J_2 - m_\alpha + m_\delta} [J_1] \begin{Bmatrix} j_a & j_b & J_1 \\ j_d & j_c & J_2 \end{Bmatrix} C^{j_a j_c J_2}_{m_\alpha - m_\gamma M_2} C^{j_b j_d J_2}_{-m_\beta m_\delta M_2}, \tag{G.3}$$

$$C^{j_a j_b J_1}_{m_\alpha m_\beta M_1} C^{j_c j_d J_1}_{m_\gamma m_\delta M_1} = \sum_{J_2} (-1)^{4j_a + 2j_b - j_c + j_d + 2J_1 - 3J_2 - m_\alpha + m_\gamma} [J_1] \begin{Bmatrix} j_a & j_b & J_1 \\ j_c & j_d & J_2 \end{Bmatrix} C^{j_a j_d J_2}_{m_\alpha - m_\delta M_2} C^{j_b j_c J_2}_{-m_\beta m_\gamma M_2}, \tag{G.4}$$

$$C^{j_b j_c J_{bc}}_{m_\beta m_\gamma M_{bc}} C^{J_{bc} j_a J}_{M_{bc} m_\alpha M} = -(-1)^{j_b + j_c + J_{bc}} \sum_{J_{ab}} \sqrt{[J_{ab}][J_{bc}]} \begin{Bmatrix} j_a & j_b & J_{ab} \\ j_c & J & J_{bc} \end{Bmatrix} C^{j_a j_b J_{ab}}_{m_\alpha m_\beta M_{ab}} C^{J_{ab} j_c J}_{m_{ab} m_\gamma M}, \tag{G.5}$$

$$C^{j_c j_a J_{ca}}_{m_\gamma m_\alpha M_{ca}} C^{J_{ca} j_b J}_{M_{ca} m_\beta M} = -\sum_{J_{ab}} (-1)^{j_a + j_b + J_{ab}} \sqrt{[J_{ab}][J_{bc}]} \begin{Bmatrix} j_a & j_b & J_{ab} \\ J & j_c & J_{ca} \end{Bmatrix} C^{j_a j_b J_{ab}}_{m_\alpha m_\beta M_{ab}} C^{J_{ab} j_c J}_{m_{ab} m_\gamma M}. \tag{G.6}$$

G.1   Antisymmetrization of Three-Body State

Suppose the antisymmetrization of state (G.1) (or (G.2)) is done by acting the three-body antisymmetrizer $\mathcal{A}$. The $\mathcal{A}$ can be written down as

$$\mathcal{A} = \frac{1}{6}(1 - \mathcal{T}_{12} + \mathcal{T}_{31}\mathcal{T}_{12} - \mathcal{T}_{23} + \mathcal{T}_{23}\mathcal{T}_{12} - \mathcal{T}_{31}), \tag{G.7}$$

with the two-body exchange operator $\mathcal{T}_{12}$ satisfying

$$\mathcal{T}_{12}|ab) = \mathcal{T}_{21}|ab) = |ba). \tag{G.8}$$

By employing $\mathcal{A}$, in M-scheme, the antisymmetrized three-body state is

$$|abc\rangle = \mathcal{A}|abc) = \frac{1}{6}\left(|abc) + |bca) + |cab) - |bac) - |acb) - |cba)\right). \tag{G.9}$$

To obtain the antisymmetrized three-body system in the J-scheme, it is easy to consider $\mathcal{A}|abc\colon J_{ab}J)$. After the simple algebra, we have

$$
\begin{aligned}
|abc\colon J_{ab}J\rangle = \Big[&|abc\colon J_{ab}J) - (-1)^{j_a+j_b-J_{ab}}|bac\colon J_{ab}J) \\
&- \sum_{J_{bc}} (-1)^{j_b+j_c+J_{bc}} \sqrt{[J_{ab}][J_{bc}]} \begin{Bmatrix} j_a & j_b & J_{ab} \\ j_c & J & J_{bc} \end{Bmatrix} |bca\colon J_{bc}J) \\
&+ \sum_{J_{bc}} \sqrt{[J_{ab}][J_{bc}]} \begin{Bmatrix} j_a & j_b & J_{ab} \\ j_c & J & J_{bc} \end{Bmatrix} |cba\colon J_{bc}J) \\
&- \sum_{J_{ca}} (-1)^{j_a+j_b-J_{ab}} \sqrt{[J_{ab}][J_{ca}]} \begin{Bmatrix} j_a & j_b & J_{ab} \\ J & j_c & J_{ca} \end{Bmatrix} |cab\colon J_{ca}J) \\
&- \sum_{J_{ca}} (-1)^{j_b+j_c+J_{ab}+J_{ca}} \sqrt{[J_{ab}][J_{ca}]} \begin{Bmatrix} j_a & j_b & J_{ab} \\ J & j_c & J_{ca} \end{Bmatrix} |cab\colon J_{ca}J) \Big]. \tag{G.10}
\end{aligned}
$$

Since the state (G.10) is not normalized and orthogonal, the state (G.10) is not useful in the UMOA calculation. When one calculates the three-body correlation operator $S^{(3)}$ based on the discussion given in Appendix B, the use of the non-orthogonal basis set cannot be directly applied on the effective-interaction theory. Instead of the state (G.10), we can use the normalized and antisymmetirzed three-body states determined by diagonalization of $\mathcal{A}$ [104]. The matrix element of $\mathcal{A}$ is

$$
\begin{aligned}
(a_1a_2a_3\colon J_{a_1a_2}J|\mathcal{A}|a_4a_5a_6\colon J_{a_4a_5}J') &= \sum_{\{m\}} C^{j_{a_1} j_{a_2} J_{a_1a_2}}_{m_{a_1} m_{a_2} M_{a_1a_2}} C^{J_{a_1a_2} j_{a_3} J}_{M_{a_1a_2} m_{a_3} M} C^{j_{a_4} j_{a_5} J_{a_4a_5}}_{m_{a_4} m_{a_5} M_{a_4a_5}} C^{J_{a_4a_5} j_{a_6} J'}_{M_{a_4a_5} m_{a_6} M'} (a_1a_2a_3|\mathcal{A}|a_4a_5a_6) \\
&= \frac{1}{6}\Big[\delta_{a_1a_4}\delta_{a_2a_5}\delta_{a_3a_6}\delta_{J_{a_1a_2}J_{a_4a_5}} \\
&\quad - (-1)^{j_{a_1}+j_{a_2}-J_{a_1a_2}} \delta_{a_1a_5}\delta_{a_2a_4}\delta_{a_3a_6}\delta_{J_{a_1a_2}J_{a_4a_5}} \\
&\quad - (-1)^{j_{a_2}+j_{a_3}+J_{a_4a_5}} \sqrt{[J_{a_1a_2}][J_{a_4a_5}]} \begin{Bmatrix} j_{a_1} & j_{a_2} & J_{a_1a_2} \\ j_{a_3} & J & J_{a_4a_5} \end{Bmatrix} \delta_{a_1a_6}\delta_{a_2a_4}\delta_{a_3a_5}
\end{aligned}
$$

$$+ \sqrt{[J_{a_1 a_2}][J_{a_4 a_5}]} \begin{Bmatrix} j_{a_1} & j_{a_2} & J_{a_1 a_2} \\ j_{a_3} & J & J_{a_4 a_5} \end{Bmatrix} \delta_{a_1 a_6} \delta_{a_2 a_5} \delta_{a_3 a_4}$$

$$- (-1)^{j_{a_1} + j_{a_2} + J_{a_1 a_2}} \sqrt{[J_{a_1 a_2}][J_{a_4 a_5}]} \begin{Bmatrix} j_{a_1} & j_{a_2} & J_{a_1 a_2} \\ J & j_{a_3} & J_{a_4 a_5} \end{Bmatrix} \delta_{a_1 a_5} \delta_{a_2 a_6} \delta_{a_3 a_4}$$

$$\left. - (-1)^{j_{a_2} + j_{a_3} + J_{a_1 a_2} + J_{a_4 a_5}} \sqrt{[J_{a_1 a_2}][J_{a_4 a_5}]} \begin{Bmatrix} j_{a_1} & j_{a_2} & J_{a_1 a_2} \\ J & j_{a_3} & J_{a_4 a_5} \end{Bmatrix} \delta_{a_1 a_4} \delta_{a_2 a_6} \delta_{a_3 a_5} \right] \delta_{J J'}. \quad \text{(G.11)}$$

Since $\mathcal{A}$ can be regarded as the projection operator onto the antisymmetrized three-body Fock space, $\mathcal{A}^2 |abc\rangle = \mathcal{A}|abc\rangle$, eigenvalues of $\mathcal{A}$ are 0 or 1. The eigenvectors with eigenvalues equal 0 belong to non-three-fermion Fock space and the eigenvectors with eigenvalues equal 1 are what we are interested in. Let $|abc: iJ\rangle$ be the eigenvector of $\mathcal{A}$. Here, i is alternative quantum number to the intermediate angular momentum. Using $\mathbf{1} = \sum |abc: J_{ab}J)(abc: J_{ab}J|$, we have

$$|abc: iJ\rangle = \sum_{a'b'c'J_{a'b'}} |a'b'c': J_{a'b'}J)(a'b'c': J_{a'b'}J|abc: iJ\rangle = \sum_{J_{ab}} P(abc) c^i_{abcJ_{ab}} |abc: J_{ab}J), \quad \text{(G.12)}$$

with the diagonalization coefficient $c^i_{abcJ_{ab}}$. The $P(abc)$ is defined by $P(abc)f(abc) = f(abc) + f(bca) + f(cab) + f(bac) + f(acb) + f(cba)$. Moreover, using $\mathcal{A} = \sum |abc: iJ\rangle\langle abc: iJ|$, the three-body state represented with the intermediate angular momentum is

$$|abc: J_{ab}J\rangle = \sqrt{3!}\mathcal{A}|abc: J_{ab}J) = \sqrt{3!} \sum_{a'b'c'i} |a'b'c': iJ\rangle\langle a'b'c': iJ|abc: J_{ab}J)$$

$$= \sqrt{3!} \sum_i c^{i*}_{abcJ_{ab}} |abc: iJ\rangle. \quad \text{(G.13)}$$

Inversely, the three-body state represented by the label i is

$$|abc: iJ\rangle = \mathcal{A}|abc: iJ\rangle = \sum_{J_{ab}} P(abc) c^i_{abcJ_{ab}} \mathcal{A}|abc: J_{ab}J)$$

$$= \frac{1}{\sqrt{3!}} \sum_{J_{ab}} P(abc) c^i_{abcJ_{ab}} |abc: J_{ab}J\rangle. \quad \text{(G.14)}$$

G.2 Matrix Element in Three-Body State

In UMOA calculations, we need the matrix elements of one- and two-body operators in the three-body state. Here, the how to calculate the matrix elements,

$$\langle a_1 a_2 a_3: iJ|O^{(1)}|a_4 a_5 a_6: i'J\rangle, \quad \text{(G.15)}$$

$$\langle a_1 a_2 a_3: iJ|O^{(2)}|a_4 a_5 a_6: i'J\rangle, \quad \text{(G.16)}$$

$$\langle a_1 a_2 a_3: J_{a_1 a_2} J|O^{(1)}|a_4 a_5 a_6: J_{a_4 a_5} J\rangle, \quad \text{(G.17)}$$

$$\langle a_1 a_2 a_3: J_{a_1 a_2} J|O^{(2)}|a_4 a_5 a_6: J_{a_4 a_5} J\rangle, \quad \text{(G.18)}$$

are shown. Note that $O^{(1)}$ and $O^{(2)}$ are the one- and two-body operator, respectively. The matrix elements with i-representation basis are summarized:

$$\langle a_1 a_2 a_3 : iJ | O^{(1)} | a_4 a_5 a_6 : i'J \rangle$$

$$= 3 \sum_{J_{a_1 a_2} J_{a_4 a_5}} P(a_1 a_2 a_3) P(a_4 a_5 a_6) c^{i*}_{a_1 a_2 a_3 J_{a_1 a_2}} c^{i'}_{a_4 a_5 a_6 J_{a_4 a_5}} o_{a_1 a_4} \delta_{a_2 a_5} \delta_{a_3 a_6}, \qquad \text{(G.19)}$$

and

$$\langle a_1 a_2 a_3 : iJ | O^{(2)} | a_4 a_5 a_6 : i'J \rangle$$

$$= \frac{3}{2} \sum_{J_{a_1 a_2} J_{a_4 a_5}} P(a_1 a_2 a_3) P(a_4 a_5 a_6) c^{i*}_{a_1 a_2 a_3 J_{a_1 a_2}} c^{i'}_{a_4 a_5 a_6 J_{a_4 a_5}} \delta_{J_{a_1 a_2} J_{a_4 a_5}} \delta_{a_3 a_6} \Delta_{a_1 a_2} \Delta_{a_4 a_5} o^{J_{a_1 a_2}}_{a_1 a_2 a_4 a_5}. \qquad \text{(G.20)}$$

Here, the following notations

$$o_{a_1 a_2} = \langle a_1 | o_1 | a_2 \rangle, \quad o^J_{a_1 a_2 a_3 a_4} = \langle a_1 a_2 : J | o_{12} | a_3 a_4 : J \rangle, \quad \Delta_{a_1 a_2} = \sqrt{1 + \delta_{a_1 a_2}}, \qquad \text{(G.21)}$$

are used. Although, the actual calculations are done with i-representation basis set, we note the matrix elements Eq. (G.17) and (G.18). Eq. (G.17) is

$$\langle a_1 a_2 a_3 : J_{12} J | O^{(1)} | a_4 a_5 a_6 : J_{45} J \rangle$$

$$= o_{a_1 a_4} \delta_{a_2 a_5} \delta_{a_3 a_6} \delta_{J_{12} J_{45}}$$

$$- (-1)^{j_2 + j_3 + J_{12} + J_{45}} \sqrt{[J_{a_1 a_2}][J_{a_4 a_5}]} \begin{Bmatrix} j_{a_1} & j_{a_2} & J_{12} \\ J & j_{a_3} & J_{45} \end{Bmatrix} o_{a_1 a_4} \delta_{a_2 a_6} \delta_{a_3 a_5}$$

$$- (-1)^{j_2 + j_3 + J_{45}} \sqrt{[J_{a_1 a_2}][J_{a_4 a_5}]} \begin{Bmatrix} j_{a_1} & j_{a_2} & J_{12} \\ j_{a_3} & J & J_{45} \end{Bmatrix} o_{a_1 a_6} \delta_{a_2 a_4} \delta_{a_3 a_5}$$

$$+ \sqrt{[J_{a_1 a_2}][J_{a_4 a_5}]} \begin{Bmatrix} j_{a_1} & j_{a_2} & J_{12} \\ j_{a_3} & J & J_{45} \end{Bmatrix} o_{a_1 a_6} \delta_{a_2 a_5} \delta_{a_3 a_4}$$

$$- (-1)^{j_{a_1} + j_{a_2} + J_{12}} \sqrt{[J_{a_1 a_2}][J_{a_4 a_5}]} \begin{Bmatrix} j_{a_1} & j_{a_2} & J_{12} \\ J & j_{a_3} & J_{45} \end{Bmatrix} o_{a_1 a_5} \delta_{a_2 a_6} \delta_{a_3 a_4}$$

$$- (-1)^{j_{a_1} + j_{a_2} - J_{12}} \delta_{J_{12} J_{45}} o_{a_1 a_5} \delta_{a_2 a_4} \delta_{a_3 a_6}$$

$$- (-1)^{j_{a_1} + j_{a_2} + J_{12}} \sqrt{[J_{a_1 a_2}][J_{a_4 a_5}]} \begin{Bmatrix} j_{a_1} & j_{a_2} & J_{12} \\ J & j_{a_3} & J_{45} \end{Bmatrix} o_{a_3 a_4} \delta_{a_1 a_5} \delta_{a_2 a_6}$$

$$+ \sqrt{[J_{a_1 a_2}][J_{a_4 a_5}]} \begin{Bmatrix} j_{a_1} & j_{a_2} & J_{12} \\ j_{a_3} & J & J_{45} \end{Bmatrix} o_{a_3 a_4} \delta_{a_1 a_6} \delta_{a_2 a_5}$$

$$+ o_{a_3 a_6} \delta_{a_1 a_4} \delta_{a_2 a_5} \delta_{J_{12} J_{45}}$$

$$- (-1)^{j_{a_1} + j_{a_2} - J_{12}} o_{a_3 a_6} \delta_{a_1 a_5} \delta_{a_2 a_4} \delta_{J_{12} J_{45}}$$

$$- (-1)^{j_2 + j_3 + J_{45}} \sqrt{[J_{a_1 a_2}][J_{a_4 a_5}]} \begin{Bmatrix} j_{a_1} & j_{a_2} & J_{12} \\ j_{a_3} & J & J_{45} \end{Bmatrix} o_{a_3 a_5} \delta_{a_1 a_6} \delta_{a_2 a_4}$$

$$- (-1)^{j_2+j_3+J_{12}+J_{45}} \sqrt{[J_{a_1a_2}][J_{a_4a_5}]} \left\{ \begin{array}{ccc} j_{a_1} & j_{a_2} & J_{12} \\ J & j_{a_3} & J_{45} \end{array} \right\} o_{a_3a_5}\delta_{a_1a_4}\delta_{a_2a_6}$$

$$- (-1)^{j_2+j_3+J_{45}} \sqrt{[J_{a_1a_2}][J_{a_4a_5}]} \left\{ \begin{array}{ccc} j_{a_1} & j_{a_2} & J_{12} \\ j_{a_3} & J & J_{45} \end{array} \right\} o_{a_2a_4}\delta_{a_1a_6}\delta_{a_3a_5}$$

$$- (-1)^{j_{a_1}+j_{a_2}-J_{12}}\delta_{J_{12}J_{45}}o_{a_2a_4}\delta_{a_1a_5}\delta_{a_3a_6}$$

$$- (-1)^{j_{a_1}+j_{a_2}+J_{12}} \sqrt{[J_{a_1a_2}][J_{a_4a_5}]} \left\{ \begin{array}{ccc} j_{a_1} & j_{a_2} & J_{12} \\ J & j_{a_3} & J_{45} \end{array} \right\} o_{a_2a_6}\delta_{a_1a_5}\delta_{a_3a_4}$$

$$- (-1)^{j_2+j_3+J_{12}+J_{45}} \sqrt{[J_{a_1a_2}][J_{a_4a_5}]} \left\{ \begin{array}{ccc} j_{a_1} & j_{a_2} & J_{12} \\ J & j_{a_3} & J_{45} \end{array} \right\} o_{a_2a_6}\delta_{a_1a_4}\delta_{a_3a_5}$$

$$+ o_{a_2a_5}\delta_{a_1a_4}\delta_{a_3a_6}\delta_{J_{12}J_{45}}$$

$$+ \sqrt{[J_{a_1a_2}][J_{a_4a_5}]} \left\{ \begin{array}{ccc} j_{a_1} & j_{a_2} & J_{12} \\ j_{a_3} & J & J_{45} \end{array} \right\} o_{a_2a_5}\delta_{a_1a_6}\delta_{a_3a_4}. \tag{G.22}$$

Eq. (G.18) is

$$\langle a_1a_2a_3\colon J_{12}J|O^{(2)}|a_4a_5a_6\colon J_{45}J\rangle$$

$$= \Delta_{a_1a_2}\Delta_{a_4a_5}\delta_{J_{12}J_{45}}\delta_{a_3a_6}o^{J_{12}}_{a_1a_2a_4a_5}$$

$$- (-1)^{j_{a_5}+j_{a_6}+J_{12}}\Delta_{a_1a_2}\Delta_{a_5a_6} \sqrt{[J_{a_1a_2}][J_{a_4a_5}]} \left\{ \begin{array}{ccc} j_{a_3} & j_{a_5} & J_{45} \\ j_{a_6} & J & J_{12} \end{array} \right\} o^{J_{12}}_{a_1a_2a_5a_6}\delta_{a_3a_4}$$

$$- (-1)^{j_{a_3}+j_{a_4}+J_{45}}\Delta_{a_1a_2}\Delta_{a_4a_6} \sqrt{[J_{a_1a_2}][J_{a_4a_5}]} \left\{ \begin{array}{ccc} j_{a_6} & j_{a_4} & J_{12} \\ j_{a_3} & J & J_{45} \end{array} \right\} o^{J_{12}}_{a_1a_2a_6a_4}\delta_{a_3a_5}$$

$$- (-1)^{j_{a_1}+j_{a_2}+J_{12}}\Delta_{a_3a_1}\Delta_{a_4a_5} \sqrt{[J_{a_1a_2}][J_{a_4a_5}]} \left\{ \begin{array}{ccc} j_{a_3} & j_{a_1} & J_{45} \\ j_{a_2} & J & J_{12} \end{array} \right\} o^{J_{45}}_{a_3a_1a_4a_5}\delta_{a_2a_6}$$

$$+ \sum_K (-1)^{j_{a_1}+j_{a_2}+j_{a_5}+j_{a_6}+J_{12}+K}\Delta_{a_3a_1}\Delta_{a_5a_6} \sqrt{[J_{a_1a_2}][J_{a_4a_5}]}[K]$$

$$\times \left\{ \begin{array}{ccc} j_{a_3} & j_{a_1} & K \\ j_{a_2} & J & J_{12} \end{array} \right\} \left\{ \begin{array}{ccc} j_{a_2} & j_{a_5} & J_{45} \\ j_{a_6} & J & K \end{array} \right\} o^{K}_{a_3a_1a_5a_6}\delta_{a_2a_4}$$

$$- \sum_K (-1)^{j_{a_1}+j_{a_4}+J_{12}+J_{45}}\Delta_{a_3a_1}\Delta_{a_6a_4} \sqrt{[J_{a_1a_2}][J_{a_4a_5}]}[K]$$

$$\times \left\{ \begin{array}{ccc} j_{a_3} & j_{a_1} & K \\ j_{a_2} & J & J_{12} \end{array} \right\} \left\{ \begin{array}{ccc} j_{a_6} & j_{a_4} & K \\ j_{a_2} & J & J_{45} \end{array} \right\} o^{K}_{a_3a_1a_6a_4}\delta_{a_2a_5}$$

$$- (-1)^{j_{a_2}+j_{a_3}+J_{45}}\Delta_{a_2a_3}\Delta_{a_4a_5} \sqrt{[J_{a_1a_2}][J_{a_4a_5}]} \left\{ \begin{array}{ccc} j_{a_1} & j_{a_2} & J_{12} \\ j_{a_3} & J & J_{45} \end{array} \right\} o^{J_{45}}_{a_2a_3a_4a_5}\delta_{a_1a_6}$$

$$+ \sum_K (-1)^{j_{a_2}+j_{a_3}+j_{a_5}+j_{a_6}}\Delta_{a_2a_3}\Delta_{a_5a_6} \sqrt{[J_{a_1a_2}][J_{a_4a_5}]}[K]$$

$$\times \left\{ \begin{array}{ccc} j_{a_1} & j_{a_2} & J_{12} \\ j_{a_3} & J & K \end{array} \right\} \left\{ \begin{array}{ccc} j_{a_1} & j_{a_5} & J_{45} \\ j_{a_6} & J & K \end{array} \right\} o^{K}_{a_2a_3a_5a_6}\delta_{a_1a_4}$$

$$+ \sum_K (-1)^{j_{a_1}+j_{a_2}+j_{a_3}+j_{a_4}+J_{45}+K} \Delta_{a_2 a_3} \Delta_{a_6 a_4} \sqrt{[J_{a_1 a_2}][J_{a_4 a_5}]} [K]$$

$$\times \begin{Bmatrix} j_{a_1} & j_{a_2} & J_{12} \\ j_{a_3} & J & K \end{Bmatrix} \begin{Bmatrix} j_{a_6} & j_{a_4} & K \\ j_{a_1} & J & J_{45} \end{Bmatrix} o^K_{a_2 a_3 a_6 a_4} \delta_{a_1 a_5}. \tag{G.23}$$

References

[1] I. Tanihata, H. Hamagaki, O. Hashimoto, Y. Shida, N. Yoshikawa, K. Sugimoto, O. Yamakawa, T. Kobayashi, and N. Takahashi, *Measurements of Interaction Cross Sections and Nuclear Radii in the Light p-Shell Region*, Phys. Rev. Lett. **55**, 2676 (1985).

[2] T. Otsuka, T. Suzuki, R. Fujimoto, H. Grawe, and Y. Akaishi, *Evolution of Nuclear Shells due to the Tensor Force*, Phys. Rev. Lett. **95**, 232502 (2005).

[3] H. Yukawa, *On the Interaction of Elementary Particles*, Proc. Phys. Math. Soc. Jap. **17**, 48 (1935).

[4] P. Cziffra, M. H. MacGregor, M. J. Moravcsik, and H. P. Stapp, *Modified Analysis of Nucleon-Nucleon Scattering. I. Theory and p-p Scattering at 310 MeV*, Phys. Rev. **114**, 880 (1959).

[5] G. Breit, M. H. Hull, K. E. Lassila, and K. D. Pyatt, *Phase-Parameter Representation of Proton-Proton Scattering from 9.7 to 345 MeV*, Phys. Rev. **120**, 2227 (1960).

[6] J. Iwadare, S. Otsuki, R. Tamagaki, and W. Watari, *Verification of Pion Theory of Nuclear Forces*, Prog. Theor. Phys. **6**, 581 (1956).

[7] *Nuclear Forces. I: Nuclear Forces in Dynamical Region*, Prog. Theor. Phys. Suppl. **39** (1967).

[8] R. B. Wiringa, V. G. J. Stoks, and R. Schiavilla, *Accurate nucleon-nucleon potential with charge-independent breaking*, Phys. Rev. C **51**, 38 (1995).

[9] R. Machleidt, *High-precision, charge-dependent Bonn nucleon-nucleon potential*, Phys. Rev. C **63**, 024001 (2001).

[10] D. R. Entem, and R. Machliedt, *Accurate charge-dependent nucleon-nucleon potential at forth order of chiral perturbation theory*, Phys. Rev. C **68**, 041001 (2003).

[11] E. Epelbaum, W. Glöchle, and U. G. Meißner, *The two-nucleon system at next-to-next-to-next-to-leading order*, Nucl. Phys. **A747**, 362 (2005).

[12] S. Pieper and R. B. Wiringa, *QUANTUM MONTE CARLO CALCULATIONS OF LIGHT NU-CLEI*, Ann. Rev. Nucl. Part. Sci. **51**, 53 (2001).

[13] T. Otsuka, T. Suzuki, J. D. Holt, A. Schwenk, and Y. Akaishi, *Three-Body Forces and the Limit of Oxygen Isotopes*, Phys. Rev. Lett. **105**, 032501 (2010).

[14] K. A. Brückner, C. A. Levison, and H. M. Mahmoud, *Two-Body Forces and Nuclear Saturation. I. Central Forces*, Phys. Rev. **95**, 217 (1954).

[15] B. D. Day, *Elements of the Brueckner-Goldstone Theory of Nuclear Matter*, Rev. Mod. Phys. **39**, 719 (1967).

[16] S. K. Bogner, R. J. Furnstahl, and A. Schwenk, *From low-momentum interactions to nuclear structure*, Prog. Part. Nucl. Phys. **65**, 94 (2010).

[17] L. D. Faddeev, *SCATTERING THEORY FOR A THREE-PARTICLE SYSTEM*, Sov. Phys. JETP. **12**, 1014 (1961).

[18] O. A. Yakubovsky, *One the Interal equation in the theory o N particle scattering*, Sov. J. Nucl. Phys. **5**, 937 (1967).

[19] B. R. Barrett, P. Navrátil, and J. P. Vary, *Ab initio no core shell model*, Prog. Part. Nucl. Phys. **69**, 131 (2013) and references therein.

[20] J. Carlson, S. Gandolfi, F. Pederiva, S. C. Pieper, R. Schiavilla, K. E. Schmidt, and R. B. Wiringa, *Quantum Monte Carlo methods for nuclear physics*, Rev. Mod. Phys. **87**, 1067 (2015) and references therein.

[21] D. Lee, *Lattice simulations for few- and many-body systems*, Prog. Part. Nucl. Phys. **63**, 117 (2009) and references therein.

[22] P. Navrátil, S. Quaglioni, G. Hupin, C. Romero-Redondo, and A. Calci, *Unified ab initio approaches to nuclear structure and reactions*, Phys. Scipta **91** no.5, 054606 (2016).

[23] M. Wang, G. Audi, A. H. Wapstra, F. G. Kondev, M. MacCormick, X. Xu, and B. Pfeiffer, *The Ame2012 atomic mass evaluation*, Chin. Phys. C **36**, 1603 (2012).

[24] G. Hagen, T. Papenbrock, M. Hjorth-Jensen, and D. J. Dean, *Coupled-Cluster computations of atomic nuclei*, Rept. Prog. Phys. **77**, 096302 (2014).

[25] W. H. Dickhoff and C. Barbieri, *Self-consistent Green's function method for nuclei and nuclear matter*, Prog. Part. Nucl. Phys. **52**, 377 (2004) and references therein.

[26] H. Hergert, S. K. Bogner, T. D. Morris, A. Schwenk, and K. Tsukiyama, *The In-Medium Similarity Renormalization Group: A novel ab initio method for nuclei*, Phys. Rept. **621**, 165 (2016) and references therein.

[27] K. Suzuki and R. Okamoto, *Effective Interaction Theory and Unitary-Model-Operator Approach to Nuclear Saturation Problem*, Prog. Theor. Phys. **92**, 1045 (1994).

[28] S. Binder, J. Langhammer, A. Calci, and R. Roth, *Ab initio Path to Heavy Nuclei*, Phys. Lett. B **736**, 119 (2014).

[29] G. Hagen, M. Hjorth-Jensen, G. R. Jensen, R. Machleidt, and T. Papenbrock, *Continuum Effects and Three-Nucleon Forces in Neutron-Rich Oxygen Isotopes*, Phys. Rev. Lett. **108**, 242501 (2012).

[30] A. Cipollone, C. Barbieri, and P. Navrátil, *Isotopic Chains Around Oxygen from Evolved Chiral Two- and Three-Nucleon Interactions*, Phys. Rev. Lett. **111**, 062501 (2013).

[31] H. Hergert, S. Binder, A. Calci, J. Langhammer, and R. Roth, *Ab initio Calculations of Even Oxygen Isotopes with Chiral Two-Plus=three-Nucleon Interactions*, Phys. Rev. Lett. **110**, 242501 (2013).

[32] K. Hebeler, J. D. Holt, J. Menéndez, and A. Schwenk, *Nuclear Forces and Their Impact on Neutron-Rich Nuclei and Neutron-Rich Matter*, Ann. Rev. Nucl. Part. Sci. **65**, 457 (2015).

[33] V. Somà, A. Cipollone, C. Barbieri, P. Navátil, and T. Duguet, *Chiral two- and three-nucleon forces along medium-mass isotope chains*, Phys. Rev. C **89**, 061301 (2014).

[34] H. Hergert, S. K. Bogner, T. D. Morris, S. Binder, A. Calci, J. Langhammer, and R. Roth, *Ab initio multireference in-medium similarity renormalization group calculations of even calcium and nickel isotopes*, Phys. Rev. C **90**, 041302 (2014).

[35] J. DA. Providência and C. M. Shakin, *Some Aspect of Short-Range Correlations in Nuclei*, Ann. Phys. **30**, 95 (1964).

[36] C. M. Shakin and Y. R. Waghmare, *Unitary-Model-Operator Approach to Nuclear-Structure Physics. I*, Phys. Rev. **161**, 1006 (1967); *Unitary-Model-Operator Approach to Nuclear-Structure Physics. II*, Phys. Rev. **161**, 1015 (1967).

[37] K. Suzuki and R. Okamoto, *Unitary-Model-Operator Approach to Nuclear Many-Body Problem. I*, Prog. Theor. Phys. **75**, 1388 (1986); *Unitary-Model-Operator Approach to Nuclear Many-Body Problem. II*, Prog. Theor. Phys. **76**, 127 (1986).

[38] H. Kumagai, K. Suzuki, and R. Okamoto, *Ground-state Properties of ^{40}Ca in Unitary-Model-Operator Approach with Realistic Nucleon-Nucleon Potentials*, Prog. Theor. Phys. **97**, 1023 (1997).

[39] S. Fujii, R. Okamoto, and K. Suzuki, *Charge-dependent calculations of single-particle energies in nuclei around ^{16}O with Realistic Nucleon-Nucleon Potentials*, Phys. Rev. C **69**, 034328 (2004).

[40] S. Fujii, R. Okamoto, and K. Suzuki, *Ground-State and Single-Particle Energies of Nuclei around ^{16}O, ^{40}Ca, and ^{56}Ni from Realistic Nucleon-Nucleon Forces*, Phys. Rev. Lett. **103**, 182501 (2009).

[41] G. Hagen, et al., *Neutron and weak-charge distributions of the ^{48}Ca nucleus*, Nature Phys. **12** no.2, 186 (2015).

[42] T. Miyagi, T. Abe, R. Okamoto, and T. Otsuka, *Ground-state energies and charge radii of ^4He, ^{16}O, ^{40}Ca, ^{56}Ni, in the unitary-model-operator approach*, Prog. Theor. Exp. Phys. (2015) 041D01.

[43] T. Miyagi, T. Abe, R. Okamoto, and T. Otsuka, *Many-Body Calculations for Medium-Mass Nuclei by the Unitary Transformation Method*, JPS Conf. Proc. **6**, 030037 (2015).

[44] N. Ishii, S. Aoki, and T. Hatsuda, *Nuclear Force from Lattice QCD*, Phys. Rev. Lett. **99**, 022001 (2007).

[45] V. G. J. Stoks, R. A. M. Klomp, M. C. .M. Rentmeester, and J. J. de Swart, *Partial-wave analysis of all nucleon-nucleon scattering data below 350 MeV*, Phys. Rev. C **48**, 792 (1993).

[46] K. A. .Wendt, R. J. Furnstahl, and S. Ramanan, *Local projection of low-momentum potentials*, Phys. Rev. C **86**, 014003 (2012).

[47] A. Gezerlis, I. Tews, E. Epelbaum, M. Freunek, S. Gandolfi, K. Hebeler, A. Nogga, and A. Schwenk, *Local chiral effective field theory interactions and quantum Monte Carlo applications*, Phys. Rev. C **90**, 054323 (2014).

[48] P. Navrátil and E. Caurier, *Nuclear structure with accurate chiral perturbation theory nucleon-nucleon potential: Application to ^6Li and ^{10}B*, Phys. Rev. C **69**, 014311 (2004).

[49] S. Okubo, *Diagonalization of Hamiltonian and Tamm-Dancoff Equation*, Prog. Theor. Phys. **12**, 5 (1954).

[50] S. Y. Lee and K. Suzuki, *The effective interaction of two nucleons in the s-d shell*, Phys. Lett. B **91**, 173 (1980).

[51] K. Suzuki and S. Y. Lee, *Convergent Theory for Effective Interaction in Nuclei*, Prog. Theor. Phys. **64**, 2091 (1980).

[52] A. Nogga, H. Kamada, W. Glöckle, and B. R. Barrett, *The α particle based on modern nuclear forces*, Phys. Rev. C **65**, 054003 (2002).

[53] P. Navrátil, G. P. Kamuntavičius, and B. R. Barrett, *Few-nucleon systems in translationally invariant harmonic oscillator basis*, Phys. Rev. C **61**, 044001 (2000).

[54] S. K. Bogner, T. T. S. Kuo, and A. Schwenk, *Model-independent low momentum nucleon interaction from phase shift equivalence*, Phys. Rep. **386**, 1 (2003).

[55] S. Fujii, E. Epelbaum, H. Kamada, R. Okamoto, K. Suzuki, and W. Glöckle, *Low-momentum nucleon-nucleon interaction and its application to few-nucleon systems*, Phys. Rev. C **70**, 024003 (2004).

[56] E. D. Jurgenson, P. Navrátil, and R. J. Furnstahl, *Evolution of Nuclear Many-Body Forces with the Similarity Renormalization Group*, Phys. Rev. Lett. **103**, 082501 (2009).

[57] E. D. Jurgenson, P. Navrátil, and R. J. Furnstahl, *Evolving nuclear many-body forces with the similarity renormalization group*, Phys. Rev. C **83**, 034301 (2011).

[58] S. K. Bogner, R. J. Furnstahl, and R. J. Perry, *Similarity renormalization group for nucleon-nucleon interactions*, Phys. Rev. C **75**, 061001 (2007).

[59] F. Wegner, *Flow equations for Hamiltonian*, Ann. Phys. (Leipzig) **3**, 77 (1994).

[60] K. Suzuki, R. Okamoto, and H. Kumagai, *Nuclear ground-state properties and nuclear forces in the unitary-model-operator approach: Application to ^{16}O*, Phys. Rev. C **36**, 804 (1987).

[61] K. Suzuki, *Theory of Many-Fermion System on Unitary-Transformation Method*, Prog. Thoer. Phys. **79**, 330, (1988); Errata **79**, 1249 (1988).

[62] K. Suzuki, *Reformulation of Coupled-Cluster Theory for Many-Fermion System on Similarity-Transformation Theory*, Prog. Theor. Phys. **87**, 937 (1992).

[63] M. Hjorth-Jensen, T. T. S. Kuo, and E. Osnes, *Realistic Effective Interactions For Nuclear Systems*, Phys. Rep. **261**, 125 (1995).

[64] C. W. Wong, *Application of the reaction matrix theory (I). The calculation of nuclear reaction matrix elements*, Nucl. Phys. **A91**, 399 (1967).

[65] R. D. Lawson, *Theory of the Nuclear Shell Model*, (Clarendon Press, Oxford, 1980).

[66] D. H. Glöckner and R. D. Lawson, *Spurious Center-of-Mass Motion*, Phys. Lett. B **53**, 313 (1974).

[67] M. Kohno and R. Okamoto, ^{4}*He energies and radii calculated by the coupled-cluster method with a many-body average potential*, Phys. Rev. C **86**, 014317 (2012).

[68] E. Schiller, H. Müther, and P. Czerski, *Pauli exclusion operator and binding energy of nuclear matter*, Phys. Rev. C **59**, 2934 (1999); *Erratum: Pauli exclusion operator and binding energy of nuclear matter*, Phys. Rev. C **60**, 059901 (1999).

[69] K. Suzuki, R. Okamoto, M. Kohno, and S. Nagata, *Exact treatment of the Pauli exclusion operator in the nuclear matter calculation*, Nucl. Phys. **A665**, 92 (2000).

[70] G. Baardsen, A. Ekström, G. Hagen, and M. Hjorth-Jensen, *Coupled-cluster studies of infinite nuclear matter*, Phys. Rev. C **88**, 054312 (2013).

[71] J. L. Friar and J. W. Negele, *Theoretical and experimental determination of nuclear charge distributions*, Adv. Nucle. Phys. **8**, 219 (1975).

[72] D. Borisyuk, *Proton charge and magnetic rms radii from the elastic ep scattering data*, Nucl. Phys. **A843**, 59 (2010).

[73] I. Angeli and K. P. Marinova, *Table of experimental nuclear ground state charge radii: An update*, At. Data Nucl. Data Tables **99**, 69 (2013).

[74] P. Ring and P. Schuck, *The Nuclear Many-Body Problem*, (Springer, Berlin, 1980), 3rd ed.

[75] C. Barbieri, A. Cipollone, V. Somà, T. Duguet, and P. Navrátil, *Toward the Ab-initio Description of Medium Mass Nuclei*, arXiv:1211.3315.

[76] R. Fritz, H. Müther, and R. Machleidt, *Dirac effects in the Hartree-Fock description of finite nuclei employing realistic forces*, Phys. Rev. Lett. **71**, 46 (1993).

[77] G. Hagen, D. J. Dean, M. Hjorth-Jensen, T. Papenbrock, and A. Schwenk, *Benchmark calculations for ^3H, ^4He, ^{16}O, and ^{40}Ca with ab initio coupled-cluster theory*, Phys. Rev. C **76**, 044305 (2007).

[78] A. Nogga, S. K. Bogner, and A. Schwenk, *Low-momentum interaction in few-nucleon systems*, Phys. Rev. C **70**, 061002(R) (2004).

[79] R. Roth, J. Langhammer, A. Calci, S. Binder, and P. Navratil, *Similarity-Transformed Chiral NN+3N Interactions for the Ab initio Description of ^{12}C and ^{16}O*, Phys. Rev. Lett. **107**, 072501 (2011).

[80] G. D. Alkhazov et al., *Nuclear Matter Distributions in ^6He and ^8He from Small Angle p-He Scattering in Inverse Kinematics at Intermediate Energy*, Phys. Rev. Lett. **78**, 2313 (1997).

[81] R. Roth, S. Binder, K. Vobig, A. Calci, J. Langhammer, and P. Navrátil, *Medium-Mass Nuclei with Normal-Ordered Chiral NN + 3N Interactions*, Phys. Rev. Lett. **109**, 052501 (2012).

[82] K. Tsukiyama, S. K. Bogner, and A. Schwenk, *In-Medium Similarity Renormalization Group for Nuclei*, Phys. Rev. Lett. **106**, 222502 (211).

[83] H. Hergert, S. K. Bogner, S. Binder, A. Calci, J. Langhammer, R. Roth, and A. Schwenk, *In-medium similarity renormalization group with chiral two- plus three-nucleon interactions*, Phys. Rev. C **87**, 034307 (2013).

[84] C. R. Hoffman et al., *Determination of the N = 16 Shell Closure at the Oxygen Drip Line*, Phys. Rev. Lett. **100**, 152502 (2008).

[85] E. Lunderberg et al., *Evidence for the Ground-State Resonance of ^{26}O*, Phys. Rev. Lett. **108**, 142503 (2012).

[86] H. Sakurai et al., *Evidence for particle stability of ^{31}F and particle instability of ^{25}N and ^{28}O*, Phys. Lett. B **448**, 180 (1990).

[87] T. Duguet, H. Hergert, J. D. Holt, and V. Somà, *Nonobservable nature of the nuclear shell structure: Meaning, illustrations, and consequences*, Phys. Rev. C **92**, 034313 (2015).

[88] F. Ajzenberg-Selove, *Energy levels of light nuclei A = 13 − 15*, Nucl. Phys. A **523**, 1 (1991).

[89] D. R. Tilley, H. R. Weller, and C. M. Cheves, *Energy levels of light nuclei A = 16 − 17*, Nucl. Phys. A **564**, 1, (1993).

[90] S. K. Bogner, A. Schwenk, R. J. Furnstahl, A. Nogga, *Is nuclear matter perturbative with low-momentum interactions?*, Nucl. Phys. **A763**, 59 (2005).

[91] A. Trzcinńska, J. Jastrzębski, P. Lubiński, F. .J. Hartmann, R. Schmidt, T. von Egidy, and B. Kłos, *Neutron Density Distributions Deduced from Antiprotonic Atoms*, Phys. Rev. Lett. **87**, 082501 (2001).

[92] J. Jastrzębski, A. Trzciński, B. Kłos, F. J. Hartmann, T. von Egidy, and S. Wycech, *NEUTRON DENSITY DISTRIBUTIONS FROM ANTIPROTONIC ATOMS COMPARED WITH HADRON SCATTERING DATA*, Int. J. Mod. Phys. E **13**, 343 (2004).

[93] B. A. Brown, *Neutron Radii in Nuclei and the Neutron Equation of State*, Phys. Rev. Lett. **85**, 5296 (2000).

[94] R. J. Furnstahl, *Neutron radii in mean-field models*, Nucl. Phys. **A706**, 85 (2002).

[95] X. Roca-Maza, M. Centelles, X. Viñas, and M. Warda, *Neutron Skin of ^{208}Pb, Nuclear Symmetry Energy, and the Parity Radius Experiment*, Phys. Rev. Lett. **106**, 252501 (2011).

[96] M. Moshinsky, *Transformation brackets for harmonic oscillator functions*, Nucl. Phys. **13**, 104 (1959).

[97] I. Shavitt and L. T. Redmon, *Quasidegenerate perturbation theories. A canonical van Vleck formalism and its relationship to other approaches*, J. Chem. Phys. **73**, 5711 (1980).

[98] P. Westhaus, *Connections between Perturbation Theory and the Unitary Transformation Methods of Deriving Effective Hamiltonian*, Int. J. Quantum Chem. **20**, 1243 (1981).

[99]   K. Suzuki, *Construction of Hermitian Effective Interaction in Nuclei*, Prog. Theor. Phys. **68**, 246 (1982).

[100] K. Suzuki and R. Okamoto, *Degenerate Perturbation Theory in Quantum Mechanics*, Prog. Theor. Phys. **70**, 493 (1983).

[101] T. T. S. Kuo et al., *Hermitian effective interactions derived from the Paris and Bonn potentials*, Nucl. Phys. **A560**, 621 (1993).

[102] C. Cockrell, J. P. Vary, and P. Maris, *Lithium isotopes within the ab initio no-core full configuration approach*, Phys. Rev. C **86**, 034325 (2012).

[103] G. Hagen, T. Papenbrock, and D. J.Dean, *Solution of the Center-Of-Mass Problem in Nuclear Structure Calculations*, Phys. Rev. Lett. **103**, 062503 (2009).

[104] K. Takada, M. Sato, and S. Yasumoto, *A New Formulation of a Many-Level Shell Model*, Prog. Theor. Phys. **104**, 173 (2000).